



**The physiological role of autoprolysis of the
Adhesion GPCR Latrophilin/dCIRL**

***Die physiologische Bedeutung der Autoproteolyse
des Adhäsions-GPCR Latrophilin/dCIRL***

Doctoral thesis for a medical doctoral degree
at the Graduate School of Life Sciences,
Julius-Maximilians-Universität Würzburg,
Section Neuroscience

submitted by

Matthias Nieberler

from

Veitshöchheim

Würzburg, 2018



Submitted on: April 18th, 2018

Members of the Thesis Committee:

Chairperson: Prof. Dr. Philip Tovote

Primary Supervisor: Prof. Dr. Tobias Langenhan, D.Phil. (Oxon)

Supervisor (Second): Prof. Dr. Robert Kittel

Supervisor (Third): Assoc. Prof. Dr. Elena Seiradake

Supervisor (Fourth): Prof. Dr. Anna-Leena Sirén

Date of Public Defence: July 26th, 2018

Date of Receipt of Certificates:

Research presented in this thesis was conducted in the following facilities:

Department of Neurophysiology, Institute of Physiology, University of Würzburg

Department of Biotechnology and Biophysics, University of Würzburg

Department of Biochemistry, University of Oxford

Table of Contents

1. Summary.....	1
2. Zusammenfassung.....	2
3. Introduction	4
3.1 Adhesion class G protein-coupled receptors	4
3.1.1 Structural characteristics of aGPCRs	4
3.1.2 Autoproteolytic cleavage at the GPS	7
3.2 Latrophilin as a prototypic aGPCR.....	10
3.2.1 Structure	10
3.2.2 Function.....	13
3.3 <i>Drosophila melanogaster</i> as study object for neurosciences	17
3.4 Aim of this study.....	18
4. Materials and Methods.....	20
4.1 Molecular biology	20
4.1.1 Materials	20
4.1.2 Reactions and protocols	20
4.1.3 <i>dCirl</i> transgenes.....	22
4.2 Cell culture.....	22
4.2.1 Materials and handling of HEK293 cells	22
4.2.2 Transfection.....	23
4.2.3 Protein harvest	23
4.3 Protein biochemistry	23
4.3.1 Materials	23
4.3.2 SDS-PAGE	24
4.3.2 Western blot	24
4.3.3 Protein purification and processing.....	24
4.3.4 Protein deglycosylation assays.....	25
4.4 <i>Drosophila melanogaster</i>	26
4.4.1 Fly cultivation.....	26
4.4.2 Transgenesis of <i>Drosophila</i>	26

4.4.3 The GAL4/UAS system.....	27
4.4.4 Behavioral assays.....	28
4.4.5 Isolation of genomic DNA	29
4.4.6 Protein extraction from animals	29
4.4.7 Immunohistochemistry and antibodies.....	29
4.5 Microscopic techniques.....	32
4.5.1 Confocal microscopy	32
4.5.2 Structured illumination microscopy	32
4.5.3 Image processing	33
4.6 Biophysical methods	33
4.6.1 Circular Dichroism Spectrophotometry	33
4.6.2 Dynamic Light Scattering.....	34
4.6.3 Size Exclusion Chromatography/Multi-Angle Light Scattering	34
5. Results.....	36
5.1 Generation of a genomic <i>dCirl</i> cloning toolkit.....	36
5.2 Localization of <i>dCirl</i> expression in <i>Drosophila</i> larvae.....	37
5.2.1 <i>dCirl^{N-RFP/C-Flag}</i> is expressed in <i>Drosophila</i>	37
5.2.2 Behavioral phenotypes are rescued in <i>dCirl^{N-RFP/C-Flag}</i>	39
5.2.3 <i>dCirl</i> is broadly expressed in different neuronal tissues.....	40
5.2.4 The expression profile of <i>dCirl</i> is exclusively neuronal	44
5.3 Analysis of dCIRL autoproteolysis	47
5.3.1 dCIRL ^{H>A} and dCIRL ^{T>A} contain a mutated GPS	47
5.3.2 GPS autoproteolysis is disabled in dCIRL ^{H>A} and dCIRL ^{T>A}	48
5.3.3 Receptor cleavage is dispensable for dCIRL function	50
5.3.4 dCIRL trafficking does not rely on GPS autoproteolysis	51
5.4 Structural analysis of extracellular dCIRL motifs.....	55
5.4.1 The IRH region of dCIRL is heavily glycosylated.....	55
5.4.2 dCIRL-IRH follows the random coil model	58
5.4.3 The IRH is a large and elongated region in dCIRL's NTF.....	60
6. Discussion.....	64
6.1 dCIRL function in <i>Drosophila</i> 's central nervous system	64
6.2 Tethered agonism and versatile signaling modes for Latrophilin	66

6.3 Physiological function of GPS cleavage.....	69
6.4 Role of the IRH region in dCIRL's mechanosensitive function.....	72
7. References.....	75
8. Appendix.....	94
8.1 Abbreviations.....	94
8.2 List of Figures.....	97
8.3 Publications.....	98
8.4 Acknowledgements.....	99
8.5 Curriculum vitae.....	100
8.6 Affidavit.....	102

1. Summary

G protein-coupled receptors of the Adhesion family (aGPCRs) comprise the second largest group within the GPCR realm with over 30 mammalian homologs. They contain a unique structure with unusually large extracellular domains (ECDs) holding many structural folds known to mediate cell-cell and cell-matrix interactions. Furthermore, aGPCRs undergo autoproteolytic cleavage at the GPCR proteolysis site (GPS), an integral portion of the GPCR autoproteolysis inducing (GAIN) domain. Thus far, it is largely unknown if and how self-cleavage affects aGPCR activation and signaling and how these signals may shape the physiological function of cells. Latrophilin, alternatively termed the calcium-independent receptor of α -latrotoxin (CIRL) constitutes a highly conserved, prototypic aGPCR and has been assigned roles in various biological processes such as synaptic development and maturation or the regulation of neurotransmitter release. The *Drosophila melanogaster* homolog dCIRL is found in numerous sensory neurons including the mechanosensory larval pentascolopodial chordotonal organs (CHOs), which rely on dCIRL function in order to sense mechanical cues and to modulate the mechanogating properties of present ionotropic receptors.

This study reveals further insight into the broad distribution of *dCirl* expression throughout the larval central nervous system, at the neuromuscular junction (NMJ), as well as subcellular localization of dCIRL in distal dendrites and cilia of chordotonal neurons. Furthermore, targeted mutagenesis which disabled GPS cleavage of dCIRL left intracellular trafficking in larval CHOs unaffected and proved autoproteolysis is not required for dCIRL function *in vivo*. However, substitution of a threonine residue, intrinsic to a putative tethered agonist called *Stachel* that has previously been documented for several other aGPCRs, abrogated receptor function. Conclusively, while this uncovered the presence of *Stachel* in dCIRL, it leaves the question about the biological relevance of the predetermined breaking point at the GPS unanswered. In an independent approach, the structure of the "Inter-RBL-HRM" (IRH) region, the region linking the N-terminal Rhamnose-binding lectin-like (RBL) and the hormone receptor motif (HRM) domains of dCIRL, was analyzed. Results suggest random protein folding, excessive glycosylation, and a drastic expansion of the size of IRH. Therefore, the IRH might represent a molecular spacer ensuring a certain ECD dimension, which in turn may be a prerequisite for proper receptor function. Taken together, the results of this study are consistent with dCIRL's mechanosensitive faculty and its role as a molecular sensor that translates mechanical cues into metabotropic signals through a yet undefined *Stachel*-dependent mechanism.

2. Zusammenfassung

G-Protein-gekoppelte Rezeptoren der Adhäsions-Klasse (aGPCRs) bilden mit über 30 Homologen in Säugern die zweitgrößte Gruppe innerhalb des GPCR-Reichs. Sie teilen eine einzigartige Morphologie mit einer ungewöhnlich großen extrazellulären Domäne (ECD), welche meist vielfältige Strukturen enthält, die Zell-Zell- und Zell-Matrix-Interaktionen vermitteln. Weiterhin unterziehen sich aGPCRs einer autoproteolytischen Spaltung an der GPCR proteolysis site (GPS), die einen integralen Bestandteil der GPCR autoproteolysis inducing (GAIN) Domäne darstellt. Bisher ist weitestgehend unbekannt, ob und wie die Selbstspaltung Aktivierung und Signaltransduktion von aGPCRs beeinflusst und wie diese Signale die physiologische Zellfunktion modulieren.

Latrophilin, oder auch der Kalzium-unabhängige Rezeptor für α -Latrotoxin (CIRL), stellt einen evolutiv stark konservierten, prototypischen aGPCR dar und spielt eine Rolle in verschiedenen biologischen Prozessen, darunter die Entwicklung und Reifung von Synapsen, sowie die Regulation der Neurotransmitterausschüttung. Zusätzlich ist dCIRL, das Latrophilinhomolog von *Drosophila melanogaster*, an der Wahrnehmung mechanischer Reize beteiligt und moduliert die Mechanosensitivität larvaler Chordotonalorgane (CHOs), indem es das mechanisch gesteuerte Verhalten vorliegender ionotroper Rezeptoren verändert.

Die vorliegende Arbeit enthüllt weitere Erkenntnisse zur umfassenden Expression von *dCirl* im larvalen Zentralnervensystem, an der motorischen Endplatte (NMJ), und stellt erstmals dessen subzelluläre Lokalisation in distalen Dendriten und Zilien von Chordotonalneuronen dar. Außerdem zeigen Mutationsstudien mit ausgeschalteter Autoproteolyse an der GPS, dass diese für den intrazellulären Transport und die Rolle von dCIRL in larvalen CHOs *in vivo* von untergeordneter Bedeutung ist. Die Mutation eines Threonins, welches integraler Bestandteil eines möglichen gebundenen Agonisten *Stachel*, der kürzlich für einige andere aGPCRs beschrieben wurde, ist, verschlechtert jedoch drastisch die Rezeptorfunktion. Während dies die Existenz *Stachels* in dCIRL aufdeckt, bleibt die Frage nach der biologischen Bedeutung der vorgegebenen Bruchstelle an der GPS unbeantwortet. Zusätzlich wurde die Struktur der „Inter-RBL-HRM“ (IRH) Region von dCIRL, die die N-terminale Rhamnose-binding lectin-like (RBL) und die hormone receptor motif (HRM) Domänen verbindet, analysiert. Die Ergebnisse legen eine zufällige Proteinfaltung, starke Glykosylierung sowie riesige strukturelle Ausmaße von IRH nahe. Daher könnte die IRH einen molekularen Abstandhalter für dCIRL darstellen, der eine bestimmte Länge der ECD sicherstellt, was wiederum eine Voraussetzung für die Rezeptorfunktion sein könnte.

Zusammen betrachtet sind die Ergebnisse dieser Arbeit vereinbar mit der mechanoszeptiven Funktion von dCIRL und dessen Rolle als molekularer Sensor, der mechanische Reize mit Hilfe eines bisher unbekanntes *Stachel*-abhängigen Mechanismus in metabotrope Signale umwandelt.

3. Introduction

3.1 Adhesion class G protein-coupled receptors

G protein-coupled receptors (GPCRs) are metabotropic receptors that represent the largest of all protein superfamilies with approximately 800 different members (Pierce et al., 2002; Fredriksson et al., 2003). They exhibit enormous functional diversity and activation profiles mediated through a myriad of endogenous ligands including (glyco)peptides, biogenic amines, cations and lipids (Fredriksson et al., 2003). Furthermore, GPCRs play a fundamental role in the sensation of exogenous stimuli such as light, smell and taste (Heng et al., 2013). Their impact on modern medicine is beyond comparison as approximately 40% of all clinically approved drugs target GPCRs to mediate their effects (Heng et al., 2013). Groundbreaking research on GPCRs and G protein-mediated signaling has contributed to understanding the principles of eukaryotic living, and has been awarded several Nobel Prizes.

According to the GRAFS classification, GPCRs are grouped into five families: Glutamates, Rhodopsins, Adhesions, Frizzled/Taste2, and Secretins, with the Adhesions forming the second largest group among GPCRs (Fredriksson et al., 2003; Lagerström and Schiöth, 2008). However, compared to other GPCRs, structural and functional aspects as well as knowledge about the signaling modes of adhesion GPCRs (aGPCRs) is rather scarce. The Adhesion family is furthermore accompanied by a lack of cognate ligands, rendering most aGPCRs orphan receptors (Langenhan et al., 2013).

Several mutations in human aGPCRs have been linked to human pathologies such as the Usher syndrome (Weston et al., 2004; Reiners et al., 2005), bilateral frontoparietal polymicrogyria BFPP (Piao et al., 2004) or neural tube defects (Allache et al., 2012; Robinson et al., 2012). Additionally, aGPCRs have been assigned crucial functions in most organ systems (Hamann et al., 2015), and have been associated with many forms of cancer (Aust et al., 1997; Xu et al., 2010; Ward et al., 2011; Aust et al., 2016) rendering them an important study subject for future investigations.

3.1.1 Structural characteristics of aGPCRs

GPCRs in general are structured similarly in that they are organized in modular domains. They usually consist of an extracellular domain (ECD), seven transmembrane-spanning helices (7TM) anchoring the protein in the cell membrane, and an intracellular domain (ICD).

These basic structural principles are matched by aGPCRs as well. However, there are unique characteristics that set aGPCRs apart from other GPCR families: first,

their ECDs are often extraordinary in size and complexity, like for example the ECD of the Very large G protein-coupled receptor 1 (VLGR-1), which includes more than 5000 amino acids (Hamann et al., 2015). The ECDs of aGPCRs usually contain different functional domains and motifs with adhesive properties, which facilitate cell-cell and cell-matrix interactions (Hamann et al., 1996; Hamann et al., 1998; Paavola et al., 2014; Hamann et al., 2015; Jackson et al., 2015). Furthermore, the arrangement of these structural adhesive folds has provided the basis to classify the 33 mammalian aGPCR homologs into nine distinct subfamilies depicted in **Figure 1**.

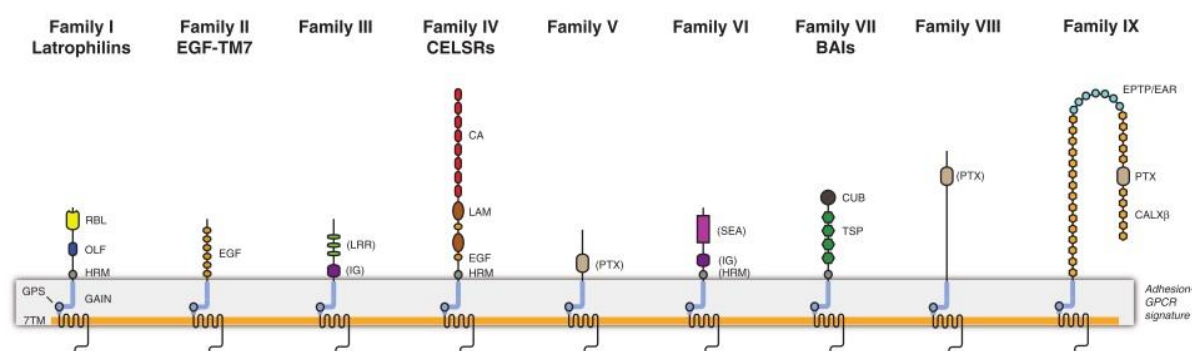


Figure 1. Adhesion GPCR families. The 33 mammalian aGPCR homologs can be divided into nine families (I-IX) according to the allocation of adhesive folds within their extracellular domains (ECDs). All aGPCRs possess a 7TM domain, which display high sequence similarities across different subfamilies. The hallmark structure of aGPCRs is the juxtamembrane GAIN domain present in all aGPCR families. Families I (Letrophilins) and IV (CELSRs) are also found in invertebrates such as *Drosophila melanogaster*, whereas the other families are predominantly expressed in vertebrates (Langenhan et al., 2013).

Second, aGPCRs constitute one of only two receptor families known to possess a GPCR autoproteolysis inducing (GAIN) domain. This evolutionarily highly conserved structural fold localizes to the C-terminus of the ECD and includes a GPCR proteolysis site (GPS) that catalyzes autoproteolytic cleavage of the receptor during protein maturation (V. Krasnoperov et al., 2002b; Lin et al., 2004). The GAIN domain has been shown to be sufficient and required for the self-catalytic cleavage (Arac et al., 2012). The resulting N-terminal and C-terminal fragments (NTF and CTF) remain non-covalently linked, so that aGPCRs form heterodimeric receptor complexes that are presented at the cell surface (**Figure 2**). Although most, but not all identified aGPCR homologs undergo autoproteolytic processing, the GAIN domain is present in nearly all members of this family, posing the question about the functional relevance of receptor cleavage. Due to its significance for this study, the GPS-mediated

autoproteolysis of aGPCRs and its implication in biological functions of the receptors will be further delineated in 3.1.2 (page 7).

Only recently, a third characteristic feature of the aGPCR class has been identified: the extracellular end of the CTF contains an agonistic sequence, the *Stachel* sequence, which is believed to promote aGPCR activation through an unknown intramolecular interaction with the 7TM domain upon structural changes in the NTF (Liebscher et al., 2014b; Stoveken et al., 2015). The *Stachel* consists of around 15 amino acids and has been shown to exist in several aGPCRs including GPR126 and GPR133 (Liebscher et al., 2014b), GPR56 and GPR110 (Stoveken et al., 2015), GPR114 (Wilde et al., 2016), GPR64 (Demberg et al., 2015) and LAT-1 (Müller et al., 2015), a nematode Latrophilin homolog. The frequency of occurrence of the *Stachel* in several aGPCRs from different subfamilies implies a general activation mechanism employed by the entire aGPCR family. Even *in vitro* cross-activation utilizing synthetic peptides derived from endogenous agonist sequences of other aGPCRs was demonstrated in some cases, which supports this hypothesis (Demberg et al., 2017).

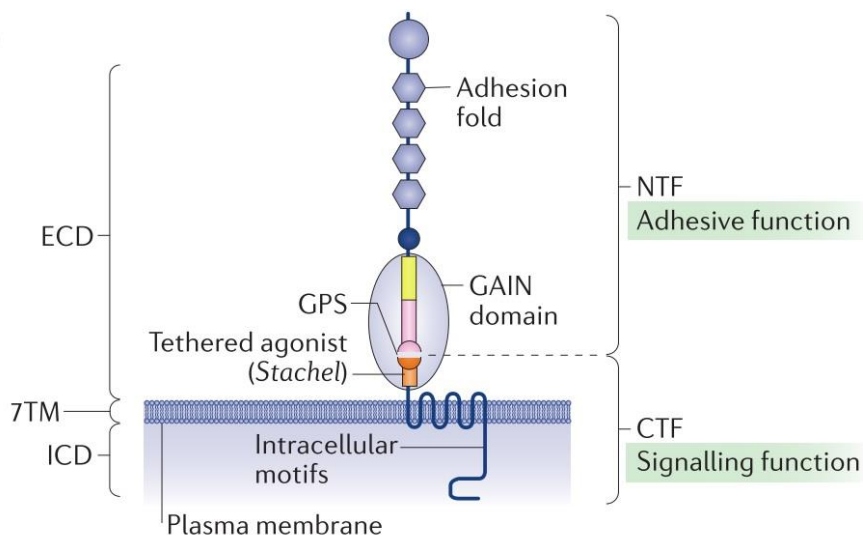


Figure 2. Molecular architecture of aGPCRs. Similar to canonical GPCRs, aGPCRs can be structured into extracellular domain (ECD), 7TM domain and intracellular domain (ICD). The ECD can be remarkably large and consists of adhesion folds facilitating cell-cell and cell-matrix interactions. Further, the ECD contains a juxtamembrane GPCR autoproteolysis inducing (GAIN) domain, which, promotes cleavage of aGPCRs at the GPCR proteolysis site (GPS), a highly conserved fold that itself is part of the GAIN domain. Resulting from this autoproteolytic reaction, the N-terminal and C-terminal fragments (NTF and CTF) subsequently stay non-covalently associated forming heterodimeric aGPCR complexes. The *Stachel* sequence is a recently identified linker of about 15 amino acids, which connects the GPS cleavage site to the 7TM domain. For several aGPCR homologs, the *Stachel* has been shown to stimulate metabotropic activity and thus act as a tethered agonist (Langenhan et al., 2016).

However, the mode through which the tethered agonist stimulates metabotropic activity of aGPCRs remains unclear. According to the first aGPCR GAIN domain crystal structure, the *Stachel* is anchored within this domain via numerous hydrophobic interactions (Arac et al., 2012). Therefore, the question arises how the *Stachel* sequence is exposed or how the conformation of the GAIN domain changes in order to allow interactions of the *Stachel*. A possible explanation could originate from GPS autoproteolysis, which may comprise a hinge allowing the *Stachel* to interact with the 7TM domain under certain conditions, like for example upon mechanical strain conferred through adhesive interaction. Alternatively, the entire NTF could be removed from the CTF, which leaves a liberated *Stachel* behind (Liebscher et al., 2014b; Liebscher et al., 2015). How the tethered agonist acts at the molecular scale and how its function impacts receptor physiology is a major controversy within the aGPCR community and still awaits additional experimental evidence.

3.1.2 Autoproteolytic cleavage at the GPS

Autoproteolytic modification of aGPCRs is a long known, yet poorly understood phenomenon. It was first discovered for CD97, a family II aGPCR involved in immunological processes, before the GPS motif was known (Gray et al., 1996).

Later on, similar studies on C1RL, a Latrophilin homolog, identified the GPS as the location where the cleavage takes place (V. G. Krasnoperov et al., 1997; V. Krasnoperov et al., 1999). The GPS motif consists of approximately 50 residues and is evolutionarily highly conserved. It is absolutely necessary, but insufficient to mediate proteolytic cleavage on its own (Chang et al., 2003). As no exogenous proteases are involved, the GPS contains a catalytic triad of particular amino acids, usually His, Leu/Ile and Ser/Thr ($H^{-2} L/I^{-1} \downarrow S/T^{+1}$), with proteolysis occurring between Leu/Ile and Ser/Thr (Lin et al., 2010; Nieberler et al., 2016). The ER located reaction (**Figure 3**) is initiated by the withdrawal of a proton from the hydroxyl group of the Ser/Thr (+1) through the His (-2). This is followed by a *cis*-nucleophilic attack on the carbonyl group of the Leu/Ile (-1), generating a tetrahedral intermediate and subsequently an ester intermediate. Finally, the ester bond is hydrolyzed creating two distinct peptide chains, the NTF and the CTF (Lin et al., 2004).

After proteolytic cleavage, the two protomers remain non-covalently linked, mainly through hydrophobic side-chain interactions, to generate heterodimeric aGPCR complexes (V. Krasnoperov et al., 1999; V. Krasnoperov et al., 2002b).

The structural background for this non-covalent association was found in an extracellular domain much larger than the GPS motif, the GPCR autoproteolysis inducing (GAIN) domain. The approximately 320 residues comprising GAIN domain can be

divided into subdomain A, consisting of alpha-helices, and subdomain B, predominantly consisting of beta-sheets and integrating the GPS motif. The GAIN domain provides an essential environment for the autoproteolytic reaction, which occurs tightly embedded within its structure, and renders dissociation of NTF and CTF energetically highly unfavorable (Arac et al., 2012; Prömel et al., 2013). In contrast to the GPS, the evolutionarily ancient GAIN domain suffices to promote the cleavage reaction on its own (Arac et al., 2012; Arac et al., 2016). The GAIN domain is not exclusive to aGPCRs, but also present in Polycystin-1 (PKD1) and its homologs, facilitating autoproteolysis in a similar manner (Ponting et al., 1999).

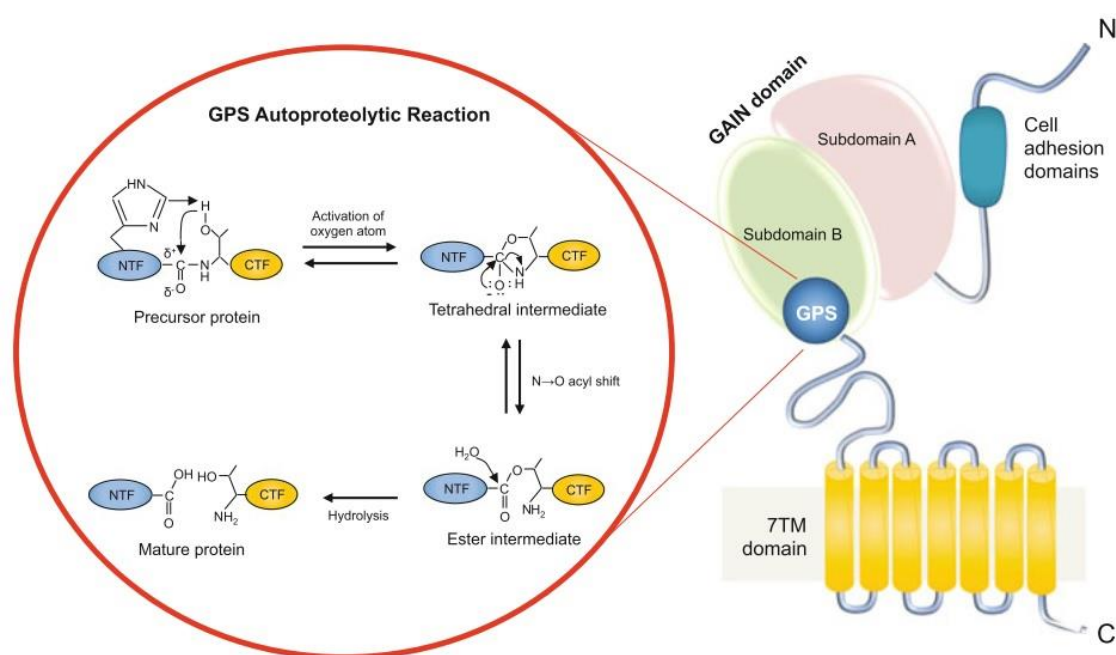


Figure 3. Mechanism of the autoproteolytic reaction at the GPS. The juxtamembrane GAIN domain can be divided into subdomain A and subdomain B, with the latter one comprising the GPS motif. The proposed cleavage reaction is initiated by the withdrawal of a proton from the hydroxyl group of the Ser/Thr (+1) through the His (-2). This is followed by a *cis*-nucleophilic attack on the carbonyl group of the Leu/Ile (-1), producing a tetrahedral intermediate and subsequently an ester intermediate. Finally, the ester bond is hydrolyzed generating two split peptide chains, the NTF and the CTF (Nieberler et al., 2016).

The efficiency of GPS autoproteolysis is not always complete: for several receptors, a coexistence of cleaved and uncleaved variants has been detected *in vivo* (Qian et al., 2002; Iguchi et al., 2008). It is believed that proteolytic processing can be regulated depending on the expressing cell type or the cellular environment, for example through N-glycosylation (Wei et al., 2007; Hsiao et al., 2009; Arac et al., 2012) or intracellular phosphorylation pathways (Deyev and Petrenko, 2010).

Even though from a chemical point of view the autoproteolytic reaction at the GPS is well understood, its role for receptor viability and function as well as its impact on cellular physiology remains concealed. While cleavage seems crucial for membrane trafficking of some aGPCRs (Liebscher et al., 2014b), it was shown to be dispensable for others (Chang et al., 2003; Lin et al., 2004; Bohnkamp and Schöneberg, 2011). Studies on Latrophilin homologs even provided conflicting results (V. Krasnoperov et al., 2002b; Arac et al., 2012; Prömel et al., 2012).

Another model suggests independent functions of the two cleaved fragments: for GPR126 function during heart development, only the NTF is absolutely necessary, while the CTF seems not required. Even a paracrine signaling mode through NTF shedding has been proposed (Waller-Evans et al., 2010; Patra et al., 2013). On the contrary, removal of the NTF has also been reported to increase metabotropic aGPCR activity (Okajima et al., 2010; Paavola et al., 2011), consistent with the hypothesis of *Stachel* being released upon NTF shedding.

The “split personality” model describes the formation of heterodimeric receptor chimeras, which can be dynamically composed by NTF and CTF fragments of different aGPCRs at the cell surface (Volynski et al., 2004; Silva et al., 2009; Huang et al., 2012). However, with the crystallization of the GAIN domain, it became obvious that this rigid structure does not allow dissociation of NTF and CTF without denaturation of the protein (Silva and Ushkaryov, 2010; Arac et al., 2012). Thus, to what extent chimeric aGPCR complexes might contribute to the biological function of the receptors still awaits to be clarified.

In a clinical context, several GAIN domain mutations have been linked to human pathologies, underlining its exceptional role in receptor function (Piao et al., 2004; Kan et al., 2010). For instance, mutation studies with uncleavable Polycystin-1 in mice revealed abnormal renal development and reduced life expectancy due to renal insufficiency (Qian et al., 2002; Wei et al., 2007; Yu et al., 2007), which represents the pathomechanism for one of the most common genetic diseases worldwide, the autosomal dominant polycystic kidney disease (ADPKD).

Another very recent publication presents patients with a severe form of vibratory urticaria, which originates in a single point mutation within the GPS of the aGPCR EMR2 (Boyden et al., 2016). This mutation is suggested to destabilize the non-covalent interaction between cleaved NTF and CTF, which as a consequence is completely disrupted upon minimal mechanical stress. The loss of the NTF then results in a pathological histamine release from mast cells, which is responsible for urticaria-specific symptoms.

Apart from these findings, a common role of the GAIN domain and its autocatalytic activity in the aGPCR class remains yet to be established.

3.2 Latrophilin as a prototypic aGPCR

Latrophilins (family I) belong to the oldest members of the aGPCR class. Their receptor architecture is highly conserved over a large phylogenetic distance reaching from early invertebrates to humans (Fredriksson and Schiöth, 2005; Nordström et al., 2009). Therefore, Latrophilins are considered prototype aGPCRs and rank among the best investigated aGPCRs.

The vertebrate genome contains three Latrophilins, *LPHN1-3* (Matsushita et al., 1999), encoding receptors Latrophilin-1, -2, and -3 (**Figure 4**). The invertebrates *C. elegans* and *Drosophila melanogaster* encode two homologs (LAT-1 and LAT-2), and one homolog, dCIRL, the calcium-independent receptor of α -latrotoxin, respectively.

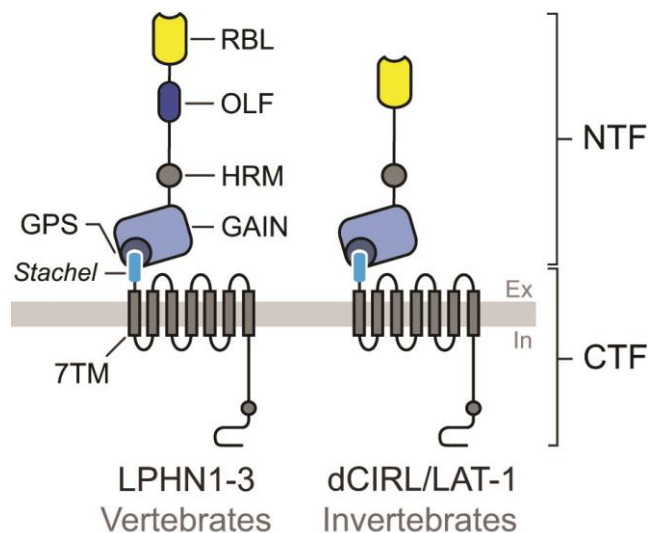


Figure 4. Latrophilin and its homologs. The receptor layout of Latrophilins is highly conserved: the three mammalian homologs Latrophilin-1, -2, and -3 differ from invertebrate Latrophilins mainly in the existence of the extracellular OLF domain. Domains (N–C): RBL (rhamnose-binding lectin-like), OLF (olfactomedin-like), HRM (hormone receptor motif), GAIN (GPCR autoproteolysis inducing), GPS (GPCR proteolysis site), 7TM (seven transmembrane). Adapted from Scholz et al., 2015.

3.2.1 Structure

Latrophilin follows the structural principles of the aGPCR family (**Figure 4**): it consists of a large extracellular tail that contains several structural folds, which have been analyzed using crystallography (Vakonakis et al., 2008; Arac et al., 2012; Jackson et al., 2015), a 7TM region and an intracellular C-terminal region, which is only scarcely investigated. As most aGPCRs, Latrophilins undergo GAIN domain-

mediated autoproteolytic processing at the GPS (V. G. Krasnoperov et al., 1997). The following section delineates the structural and functional features of the individual domains or segments of Latrophilin from the N- to the C-terminus.

The rhamnose-binding lectin-like (RBL) domain is a cysteine-rich lectin fold mainly known from sea urchin and catfish eggs (Ozeki et al., 1991; Hosono et al., 1999). The murine Latrophilin-1 RBL adopts a unique alpha/beta fold with two long structured loops that are essential for monosaccharide recognition (Vakonakis et al., 2008). Although the preferably bound monosaccharide rhamnose is rare under endogenous conditions (Tymiak et al., 1993), the RBL domain is required for LAT-1 receptor function *in vivo* (Prömel et al., 2012). An additional non-carbohydrate ligand was suggested but has not been identified yet (Vakonakis et al., 2008). Interestingly, an RBL domain was also found in the GAIN domain-containing receptor Polycystin-1, though with a yet unknown ligand (A. Li et al., 2003).

The Olfactomedin-like (OLF) domain is located C-terminal to the RBL domain and is present only in vertebrate Latrophilins, but not in invertebrate homologs (Snyder et al., 1991). The OLF domain can be found predominantly in neuronal tissues, with possible implication in numerous physiological processes such as synaptic transmission (Boucard et al., 2012; Nakaya et al., 2013), regulation of axon growth (Nakaya et al., 2012), vascular remodeling (Shi et al., 2017), and sensory organ functions (Sultana et al., 2014). An X-ray crystallographic model of the murine Latrophilin-3 OLF domain is shown in **Figure 5A**. It reveals a five-bladed beta-propeller, with each blade consisting of a four-stranded beta-sheet (Jackson et al., 2015). The five blades are arranged in an anticlockwise direction around the center of the molecule, which holds a sodium and a calcium ion. Blades II and III of the OLF propeller hold a conserved binding site for fibronectin leucine-rich repeat transmembrane proteins (FLRTs), which are major regulators of cortical and synapse development (Maretto et al., 2008; O'Sullivan et al., 2012; Leyva-Diaz et al., 2014). They fulfill a dual function, as they promote both cell adhesion and cell repulsion (Seiradake et al., 2014; Jackson et al., 2015). Additionally, the OLF domain has been shown to promote mediate binding of another ligand, neurexin-1 β (Boucard et al., 2012). However, why the OLF domain is not present in invertebrate Latrophilins such as dCIRL, even though it appears to execute essential tasks for receptor function, seems inscrutable and requires further investigation.

The hormone receptor motif (HRM) is, as its name suggests, initially recognized in a variety of hormone receptors from secretin class GPCRs (Harmar, 2001). It spans 60-70 amino acids and contains several conserved sulfurous residues, which form internal disulfide bridges (Silva and Ushkaryov, 2010; Arac et al., 2012). Intriguingly, the HRM domain is present in over a third of all mammalian aGPCRs (Langenhan et

al., 2013), but seems dispensable for receptor function, as shown for LAT-1. Furthermore, no ligand-binding activity was discovered for HRM (Prömel et al., 2012). This is consistent with findings from other GPCRs (Grace et al., 2004) and not surprising as the putative hormone binding site is occupied by the GAIN domain and therefore not accessible (Arac et al., 2012).

Immediately adjacent to the HRM domain, the GAIN domain constitutes a highly complex structure in the extracellular juxtamembrane region. The GAIN domain (**Figure 5B**) can be divided into two subdomains. Subdomain A is constructed of six alpha-helices, while subdomain B consists of a twisted beta-sandwich including 13 beta-strands and 2 small alpha-helices (Arac et al., 2012). The GPS motif is integrated into subdomain B and resides within the last five beta-strands. A more detailed characterization of the GAIN domain and its role in GPS autoproteolysis are presented in 3.1.2 (page 7).

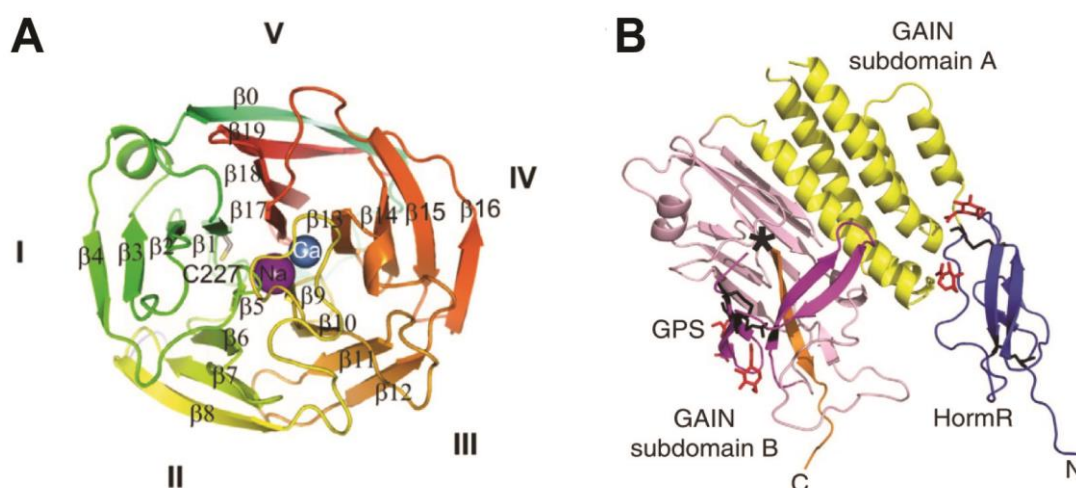


Figure 5. Crystal structure of vertebrate Latrophilin domains. (A) The OLF domain of Latrophilin-3 folds into a five-bladed beta-propeller presented here from a view along the pseudo-5-fold symmetry axis. Individual beta sheets are numbered (I-V) and beta-strands are labeled (0-19). Predicted sodium and calcium ions in the center of the molecule are shown as purple and blue spheres, respectively (Jackson et al., 2015). (B) The crystal structure of the Latrophilin-1 HRM/GAIN domains reveals two GAIN subdomains (subdomain A in yellow, subdomain B in light pink). The HRM domain is shown in blue, the GPS motif in magenta. The beta-sheet which holds the cleavage site is colored orange. Disulfide bonds and carbohydrates are shown as black and red sticks, respectively (Arac et al., 2012).

The 7TM region of Latrophilin is comparatively little investigated. Compared to the extracellular domains the 7TM is less conserved, and no extracellular ligand binding sites similar to those of canonical GPCRs have been identified yet. However, the

7TM domain is engaged in G protein activation and metabotropic responses through its interaction with the tethered agonist *Stachel* (Liebscher et al., 2014b).

The ICD is the least conserved of all Latrophilin domains (Silva and Ushkaryov, 2010). The intracellular stretch of GPCRs usually includes binding sites for G proteins and other signal molecules. Although no such structural correlate was identified, current pharmacological studies suggest $G\alpha_s$ signaling for LAT-1 (Winkler and Prömel, 2016), and a $G\alpha_i$ signaling mechanism for dCIRL (Scholz et al., 2017). Earlier, affinity chromatography had unveiled Latrophilin-1 coupling to $G\alpha_o$ and $G\alpha_{q/11}$ (Lelianova et al., 1997; Rahman et al., 1999; Serova et al., 2008). This diversity of signaling mechanisms might indicate a pleiotropy of intracellular effects or the capacity for biased signaling (Langenhan et al., 2013; Kishore and Hall, 2016). In addition, there are numerous phosphorylation sites (Silva and Ushkaryov, 2010) and a PDZ binding site (Kreienkamp et al., 2000) suggesting even more possible intracellular interactions.

3.2.2 Function

Latrophilin was initially described as calcium-independent receptor of α -latrotoxin (CIRL), because of its ability to bind α -latrotoxin (α -LTX), an ingredient of the venom cocktail released by the black widow spider (Davletov et al., 1996; V. G. Krasnoperov et al., 1996). Application of α -LTX triggers massive exocytosis of synaptic vesicles at the neuromuscular junction (Matteoli et al., 1988), which is why Latrophilin was assumed to be involved in the exocytotic activity of these cells. Further studies revealed tetramerization of α -LTX in order to form membrane pores to enhance secretion (Orlova et al., 2000). However, investigation of the effect of α -LTX on endogenous Latrophilin mostly provided unsatisfactory results, as α -LTX shows high affinity to additional receptors, such as neurexins or protein-tyrosine phosphatase σ (Ushkaryov et al., 1992; V. Krasnoperov et al., 2002a).

Apart from α -LTX, several endogenous ligands have been described for Latrophilin, which renders it one of the few deorphanized members of the aGPCR class (Langenhan et al., 2013). In most cases, this interaction has been shown on a biochemical level, leaving its functional relevance unclear. Endogenous Latrophilin ligands include the afore-mentioned FLRTs, which transsynaptically interact with Latrophilin-3 and govern synapse development and maturation (O'Sullivan et al., 2012; O'Sullivan et al., 2014; Seiradake et al., 2014). A similar role was proposed for the high-affinity interaction between Latrophilin-1 and lasso, a splice variant of teneurin-2, which is capable of inducing presynaptic calcium signals and thus may have an effect on neurotransmitter release and synaptic function (Silva et al., 2011;

Boucard et al., 2014; Vysokov et al., 2016). In addition, Latrophilin-1 forms intercellular complexes with neurexin-1 β , regulated by alternative splicing (Boucard et al., 2012). Interestingly, neurexin-1 β represents another receptor for α -LTX, however, its role in Latrophilin function remains to be elucidated.

Latrophilin-2 has recently been shown to mediate target recognition in the assembly of synapses between entorhinal and hippocampal regions (Anderson et al., 2017). *In vivo* experiments with knock-out mice unveiled altered learning and memory, probably due to a deficit in dendritic spines, suggesting that Latrophilin-2 may control synapse numbers in the entorhinal-hippocampal circuit (Anderson et al., 2017).

Other *in vivo* studies on Latrophilins have been scarce, however invertebrate model organisms provided first insights into the functional principles of Latrophilin: the *C. elegans* homolog LAT-1, for example, has been demonstrated to play an essential role in the establishment of tissue polarity during embryogenesis (Langenhan et al., 2009). While the majority of homozygous *lat-1* mutants arrest in early larval stages, individual animals escape the arrest, but produce offspring with increased embryonic lethality and morphogenetic defects during different developmental stages. These phenotypes are the result of *lat-1*-dependent alteration in blastomere orientation during early development and aberrant anterior-posterior alignment of cell division planes after the 12-cell state (Langenhan et al., 2009; Langenhan and Russ, 2010). Furthermore, *lat-1* mutants show a defect in the male germline responsible for impaired sperm development or sperm function (Prömel et al., 2012).

Employing these two phenotypes, a systematic investigation of the LAT-1 domains via transgene complementation (structure-function analysis) revealed the dispensability of the HRM domain and necessity of the RBL domain as well as the GPS motif for proper LAT-1 function. Surprisingly, not GPS autoproteolysis itself, but rather the structural integrity of the GPS is required to rescue the lethality and fertility phenotype. As ICD-deficient animals sufficed to rescue the reproduction, but not the tissue polarity defect, two independent signaling modes were assumed for these two LAT-1 governed processes in *C. elegans* (Prömel et al., 2012).

The endogenous function of the *Drosophila* homolog dCIRL was long considered the least investigated among the Latrophilins. However, recently, dCIRL has been shown to partake in the physiology of certain mechanosensory neurons (Scholz et al., 2015). *dCirl*^{KO} mutant third instar larvae display altered locomotion behavior signified by increased pausing and excessive head swinging instead of linear forward locomotion seen in wildtype larvae (**Figure 6A**). *dCirl* was found to be expressed in larval pentascolopodial chordotonal organs (lch5; CHOs), which are sensory structures that govern the perception of multiple mechanical stimuli such as proprioception, gentle touch, sound and vibration (Keil, 1997; Eberl, 1999; Eberl et al., 2000;

M. J. Kernan, 2007). In larvae, CHOs are embedded in the muscular body wall (**Figure 6B**) and are restrained by muscle on one side and the cuticle on the other side. Each CHO contains five monociliated bipolar neurons (chordotonal neurons) that display genetic and functional parallels with inner hair cells of the mammalian auditory system (Nadrowski et al., 2008). A schematic depiction of a third instar larval CHO is shown in **Figure 6C**. Beside the five chordotonal neurons, each organ contains a variety of support cells, which are essential for CHO function: mechanical input leads to deflection or movement of the cilium, whose tip is fixed to the dendritic cap, a part of the cap cell. This is believed to induce the opening of mechanosensitive ion channels, for example the TRP channel subunits NOMPC or inactive (IAV) located in the distal and proximal cilium, respectively (Gong et al., 2004; Cheng et al., 2010). Electrophysiological recordings of the electrical activity of the chordotonal neurons during mechanical stimulation revealed reduced action current frequencies of *dCirl* mutants compared to wildtypic controls (**Figure 6D**). Furthermore, *dCirl* was shown to genetically interact with TRP channel subunits indicating its capacity to adjust the mechanogating properties of these ionotropic receptors in order to shape the mechanosensory profile of these neurons (Scholz et al., 2015). At the same time other aGPCR members have been shown to be involved in mechanical contexts, which led to the notion that mechanosensitivity may be a general property of the aGPCR family (Scholz et al., 2016).

Apart from these investigations on a molecular level, there have also been several studies about Latrophilins in a clinical context.

Latrophilin-3 has been statistically linked to attention deficit hyperactivity disorder (ADHD), a common psychiatric disorder with very high heritability (Arcos-Burgos et al., 2010; Martinez et al., 2011). Consistently, functional studies showed Latrophilin-3 expression in key brain regions that are causally related to attention and activity (Arcos-Burgos et al., 2010). Furthermore, common non-coding variants of Latrophilin-3 have been identified, which predispose individuals to ADHD (Martinez et al., 2016). In addition, patients carrying these Latrophilin-3 polymorphisms share a statistically higher response to medical treatment with methylphenidate (Bruxel et al., 2015). The corresponding zebrafish ortholog, *lphn3.1*, was indicated a key regulator in the development of the dopaminergic circuitry in the ventral diencephalon. Loss of *lphn3.1* leads to ADHD-like behavior and can be rescued by methylphenidate (Lange et al., 2012). Similar phenotypes consistent with ADHD have been observed in mice and *Drosophila melanogaster* (Orsini et al., 2016; van der Voet et al., 2016). In non-neuronal tissues, Latrophilin-1 has been reported to mediate airway function in association with asthma (Faiz et al., 2017). Latrophilin-1 expression is upregulated in smooth muscle cells of asthmatics' lung tissue *in vivo* and *in vitro*, and was

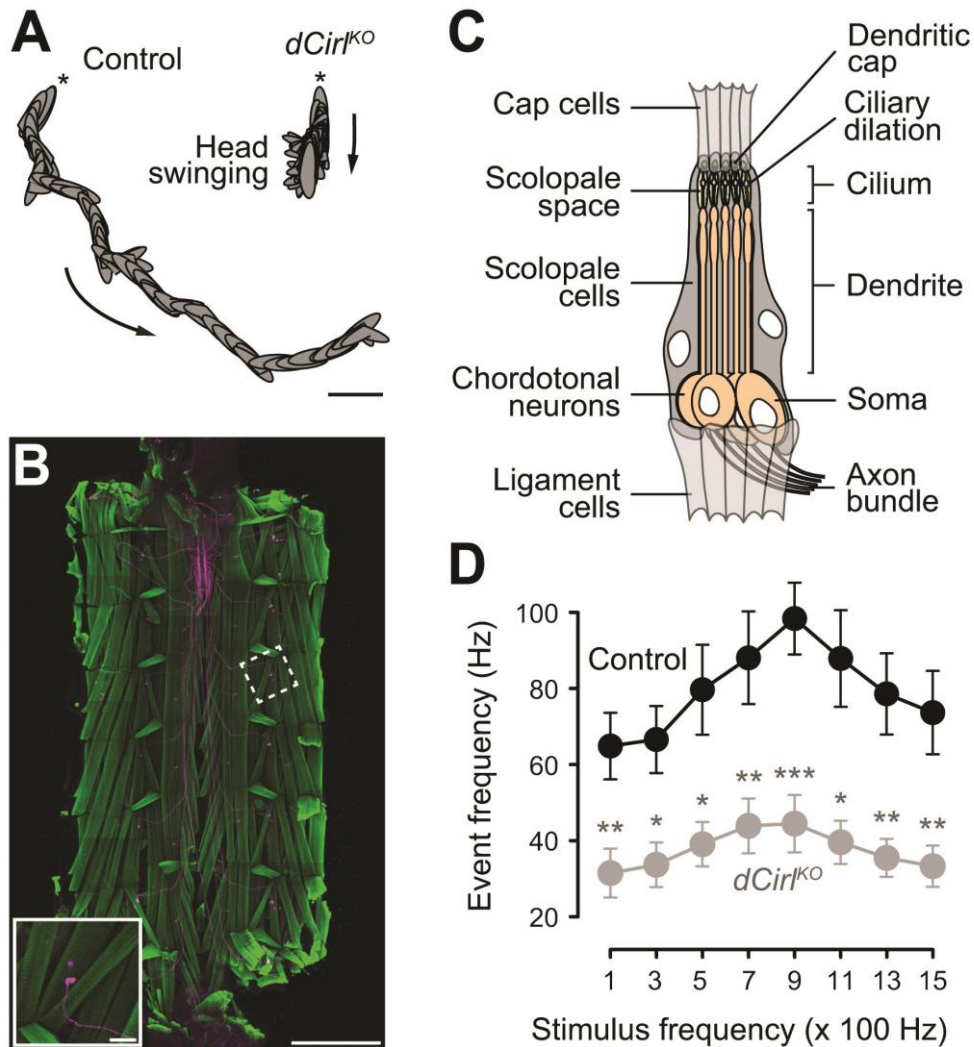


Figure 6. dCIRL function in *Drosophila* chordotonal organs. (A) Loss of *dCirl* results in increased pausing and excessive head swing behavior of third instar *Drosophila* larvae. Reconstruction of crawling paths of 36s. Scale bar 5 mm. (B) Each hemisegment of the larval muscular body wall (stained in green using phalloidin) contains a pentascolopidial chordotonal organ (CHO). The mechanosensory neurons and their projections are shown in magenta. Collage of high-resolution confocal images. Scale bar 0.5 mm (inset 50 μ m). (C) Schematic depiction of a third instar larval pentascolopidial CHO consisting of five bipolar neurons ensheathed by a number of support cells, a structure that allows the perception of proprioception, sound and vibration. (D) *dCirl* shapes the physiological response to mechanical stimulation in CHOs. The diagram shows the action current frequencies recorded from CHO axons as a function of the frequency of the vibration stimulus delivered to the cap cells. Figures 6A,C,D adapted from Scholz et al., 2015.

suggested to play a role in airway contraction. Given the well-established methods to pharmaceutically target GPCRs in general, Latrophilin-1 could comprise a promising novel target for therapeutic intervention of asthma in the future.

Finally, Latrophilins have been proposed as biomarkers for several forms of malignant tumors, including acute myeloid leukemia (Sumbayev et al., 2016), gastrointes-

tinal cancer (Jeon et al., 2016), and glioblastoma (Towner et al., 2013; Ziegler et al., 2017). How these very recent findings can be utilized for diagnosis and treatment will have yet to be demonstrated.

3.3 *Drosophila melanogaster* as study object for neurosciences

Drosophila melanogaster, the common fruit fly, was first described by Johann W. Meigen in 1830. However, it was only in the beginning of the 20th century when its advantages were used for basic genetic investigations. Since then, the fruit fly has been a study object for pioneering researchers all over the world and led to groundbreaking findings, particularly in the field of neurosciences (Bellen et al., 2010).

The life cycle of *Drosophila* is depicted in **Figure 7**. It starts with female flies laying up to 100 fertilized eggs per day, from which larvae will hatch about 24 hours later.

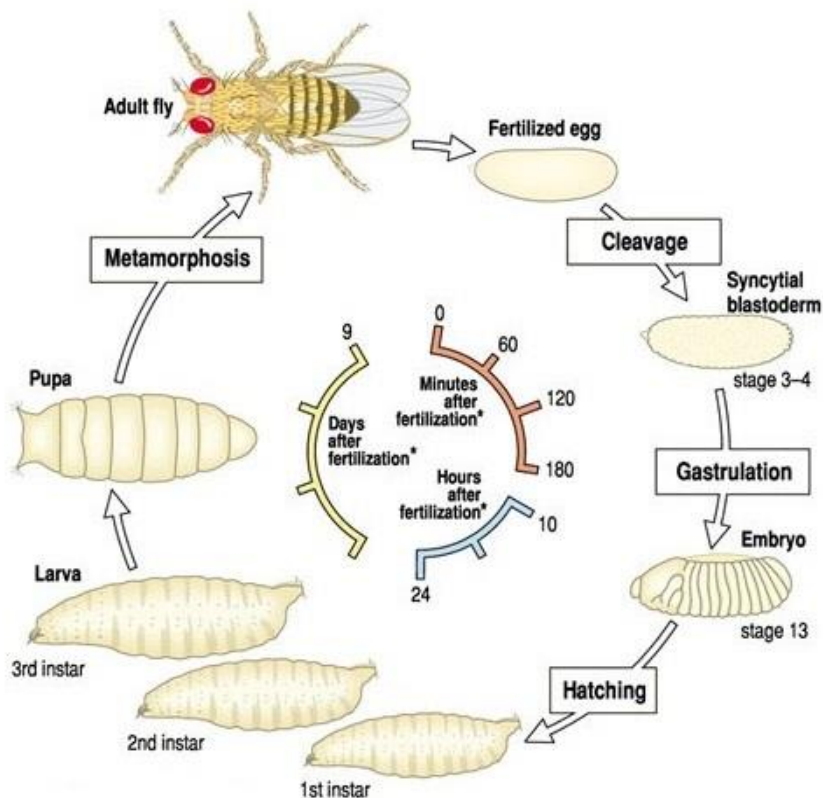


Figure 7. *Drosophila* life cycle. At 25° C and under optimal conditions, the *Drosophila* life cycle lasts nine days. About 24 hours after egg laying, first instar larvae hatch. They pass three larval stages and form pupae after five days. The adult fly ecloses after remaining in this metamorphic stage for four more days, resulting in a generation time of nine days (Wolpert and Tickle, 2011).

They pass three larval stages lasting one, one and two days, with substantial growth and a moulting process in between each stage. After the third larval stage, the larvae pupate and undergo drastic morphological and physiological changes, and after four more days, adult flies eclose after metamorphosis. Within twelve hours the flies become fertile, and the cycle starts anew (Ashburner et al., 2005; Ashburner and Roote, 2007; Wolpert and Tickle, 2011).

The short generation times allow quick production of high numbers of transgenic flies, which is a major factor for *Drosophila*'s popularity as an experimental animal model. Further advantages include its cost efficiency, its small size and the easy conditions to cultivate even large numbers of flies. The genome of *Drosophila melanogaster* has been one of the first to be sequenced completely (Adams et al., 2000), and up to now a substantial number of genes has been investigated using mutation studies, handing researchers an encyclopedic knowledge to benefit from. The fruit fly contains only four chromosome pairs, compared to 23 in humans and 20 in mice, which allows a simplified, straightforward analysis of genes and their products despite a high correlation to mammalian genomes (Bellen et al., 2010). Finally, a vast variety of genetic tools and techniques has been established for *Drosophila*, e.g. binary expression systems such as GAL4/UAS (see 4.4.3), RNA interference (Dietzl et al., 2007), or CRISPR/Cas9 (Deltcheva et al., 2011).

3.4 Aim of this study

Although aGPCR research has been on the rise for several years, direct visualization of aGPCR molecules *in vivo* proved difficult thus far. With this overall goal, this study was initiated to interrogate the cellular and subcellular localization pattern of dCIRL in *Drosophila melanogaster*. Employing genomic engineering techniques, the *dCirl* mutant was used to create transgenic fly lines to directly visualize endogenously expressed dCIRL employing confocal and super-resolution microscopy *in vivo*.

Moreover, the role of GPS autoproteolysis for dCIRL function in chordotonal neurons was investigated. Genomic mutation studies together with biochemical, behavioral and immunohistochemical analysis helped to understand how the autoproteolytic cleavage at the GPS affects dCIRL function and how it might impinge on aGPCR signaling.

In cooperation with the Department of Biochemistry of the University of Oxford, the structure of dCIRL's ECD was analyzed. With the OLF domain playing a key role in ligand binding in mammalian Latrophilins, its absence in dCIRL challenges the significance of known extracellular interactors that are capable to induce dCIRL signal-

ing. To gain further insights into the structural properties of dCIRL's NTF, numerous biophysical techniques were utilized to draw a connection between the protein structure of the NTF and the proposed signaling mechanism of dCIRL/Latrophilin.

4. Materials and Methods

4.1 Molecular biology

4.1.1 Materials

All chemicals and reagents used for molecular biological cloning were, if not stated otherwise, either purchased from Sigma-Aldrich (Taufkirchen, Germany), Merck (Darmstadt, Germany) or Roth (Karlsruhe, Germany).

4.1.2 Reactions and protocols

Polymerase Chain Reaction

Polymerase Chain Reaction (PCR) is a technique used for amplification of specific linear DNA fragments using oligonucleotide DNA primers (produced by Eurofins Genomics, Ebersberg, Germany).

The following DNA polymerases were used: AccuStar DNA Polymerase (Eurogentec, Cologne, Germany), *Taq* Polymerase Master Mix Kit (Qiagen, Hilden, Germany), Q5 High Fidelity DNA Polymerase (New England Biolabs, Frankfurt, Germany) and Cloned Pfu DNA Polymerase (Agilent, Waldbronn, Germany).

DNA restriction digest

Type II restriction endonucleases were purchased from New England Biolabs (Frankfurt, Germany). Restriction digest of DNA plasmids or PCR fragments was performed for a minimum duration of three hours at 37°C in the provided buffers.

Gel electrophoresis and DNA purification

Linear DNA fragments resulting from PCRs or restriction digests were separated according to their size by gel electrophoresis in customized electrophoresis units applying 0.5-2% agarose gels (agarose from Biozym, Hessisch Oldendorf, Germany). Subsequently, the DNA was extracted from the gel and purified using either QIAEX II Gel Extraction Kit or QIAquick Gel Extraction Kit (both Qiagen, Hilden, Germany). Procedures were performed according to provided protocols.

Ligation

Prior to ligation of prepared DNA fragments, the backbone-containing fragment was dephosphorylated using Antarctic Phosphatase (Roche, Mannheim, Germany). The following ligation itself was performed at 16°C overnight using T4 DNA Ligase (Roche, Mannheim, Germany).

Transformation in competent bacterial cells

Amplification of plasmid DNA was established using chemically competent *E. coli* cells of the genotype *recA1 endA1 gyrA96 thi-1 hsdR17 supE44 relA1 lac [F' proAB lac^q ZΔM15 Tn10 (Tet^r)]*.

Preparation of plasmid DNA

For DNA extraction from *E. coli* cells NucleoSpin Plasmid Mini or NucleoBond Plasmid Midi Kits (Macherey-Nagel, Düren, Germany) were used. The underlying technique is based on loading the bacterial cell lysate on a silica membrane column with plasmid DNA binding to the column. After several washing steps, purified plasmid DNA can be eluted from the column.

High-level DNA amplification and purification for transfection in HEK293T cells was performed with PureLink HiPure Plasmid DNA Gigaprep Kit (Life Technologies, Paisley, United Kingdom). All procedures were carried out according to provided protocols.

DNA sequencing

Sequencing of plasmid DNA was provided by Eurofins Genomics (Ebersberg, Germany) applying the Sanger method (Sanger et al., 1977).

Site-directed mutagenesis

Site-directed DNA mutagenesis was performed using an adapted protocol based on the QuikChange® Site-Directed Mutagenesis Protocol provided by Agilent (Waldbronn, Germany). After generation of customized complementary DNA primers, which faced outward and contained the mutation, an inverse PCR was started using Cloned Pfu DNA Polymerase. Subsequently, the PCR reagent was digested with *DpnI* in order to degrade the methylated template DNA and then used for transformation in competent *E. coli* cells (see above).

4.1.3 *dCirl* transgenes

The following *dCirl* constructs were generated for experiments presented in this thesis:

Name	Genotype	Backbone	Primers used (5'-3')
pMN4	<i>dCirl</i> ^{N-RFP/C-Flag}	pTL393	mn_3F, mn_4R
pMN9	<i>dCirl</i> ^{T>A}	pTL370	mn_12F, mn_13R
pMN10	<i>dCirl</i> ^{N-RFP/C-Flag/T>A}	pMN4	mn_12F, mn_13R
pMN34	<i>dCirl</i> cloning platform	pMN4	/
pMN36	<i>dCirl</i> -IRH	pTL452	mn_49F, mn_50R
pMN38	<i>dCirl</i> ^{N-RFP/C-Flag/H>A}	pMN34	mn_38F, mn_39R
pMN44	<i>dCirl</i> ^{H>A}	pMN42	mn_38F, mn_39R

mn_3F: TAACCGGTGCTGCTGCAGCTGCCTCCTCCGAGGAC

mn_4R: ATACCGGTAGCCGCTGCAGCGGCGCCGGTGGAGTG

mn_12F: CAGTTGCAACCACCTGGCAAACCTTTGCCATACT

mn_13R: AGTATGGCAAAGTTTGCCAGGTGGTTGCAACTG

mn_38F: GCGTCTGCAGTTGCAACGCCCTGACAACTTTGCC

mn_39R: GGCAAAGTTTGTCAGGGCGTTGCAACTGCAGACGC

mn_49F: TCGTCACCGGTGCCCAAACCTTCGACGACGACCAAC

mn_50R: ATCGTGGTACCCTCATCATCGCCTCCGGACATCCC

For the *dCirl* cloning toolkit, the following subclones were generated:

Subclone I	Subclone II	Subclone III	Subclone IV
pMN43 (<i>wt</i>)	pMN21 (<i>wt</i>)	pMN27 (<i>wt</i>)	pMN28 (<i>wt</i>)
pMN22 (+ <i>mRFP</i>)	pMN29 (<i>GPS</i> ^{T>A})	pMN20 (+ <i>3xFlag</i>)	
pMN23 (+ <i>HA/Btx</i>)	pMN25 (<i>GPS</i> ^{H>A})	pMN30 (+ <i>V5</i>)	

4.2 Cell culture

4.2.1 Materials and handling of HEK293 cells

HEK293 is a secondary cell culture line derived from human kidney epithelial cells, which is commonly used in biology and pharmacology. Here, its derivative HEK293T was used. HEK293T cells were kept in 75 cm² cell culture flasks at a controlled atmosphere of 37°C and 5% CO₂. They were grown to a nearly confluent cell layer

and then passaged using trypsin thrice a week. Medium consisted of DMEM and additional 10% FBS, 1% non-essential amino acids and 1% L-Glutamine.

All chemicals, media and components or cell culture containers were, if not stated otherwise, purchased from Sigma-Aldrich (Dorset, United Kingdom).

4.2.2 Transfection

In preparation for large-scale transfection, HEK293T cells were grown in larger 175 cm² flasks in order to increase the amount of cells. After preculturing for three days, the cells were seeded in 2,125 cm² roller bottles, which provide a significantly higher surface for them to attach. Again, cells were grown for three days and then transfected with the prepared plasmid vectors:

For each roller bottle a serum-free transfection cocktail containing 50 ml DMEM, 1% non-essential amino acids and 1% L-Glutamine was prepared. After adding 500 µg DNA and 500 µg PEI, the solution was incubated for ten minutes. PEI is a polycationic polymer with high transfective efficiency and, at the same time, very low cytotoxicity, which makes it a widely used transfection agent (Boussif et al., 1995).

In the meantime, the seeding medium in the roller bottle was replaced by 200 ml transfection medium containing DMEM, 2% FBS, 1% non-essential amino acids and 1% L-Glutamine. After the incubation, the transfection cocktail was given into the medium in the roller bottle and carefully dispensed.

4.2.3 Protein harvest

Four days after transfection, the medium containing the secreted protein was collected from the roller bottles. In order to eliminate remaining cells from the solution, the medium was centrifuged at 7,500 rpm for 20 minutes. The supernatant was then sterile-filtered (Stericup, Merck Millipore, Feltham, United Kingdom) and stored at 4°C.

4.3 Protein biochemistry

4.3.1 Materials

All chemicals used for protein biochemical applications including SDS-PAGE and western blotting were, if not stated otherwise, purchased from Sigma-Aldrich (Taufkirchen, Germany or Dorset, United Kingdom).

4.3.2 SDS-PAGE

For electrophoretic analysis of dCIRL variants derived from transgenic adult *Drosophila*, 4-15% Mini-PROTEAN TGX Precast Protein Gels were applied in a Mini-PROTEAN Tetra Handcast Electrophoresis System (Bio-Rad, Munich, Germany). Samples were denatured at 55-60°C for ten minutes prior to loading on the gel. Running Buffer consisted of 3.03 g Tris base, 14.4 g glycine and 1.0 g SDS in 1 l dH₂O. Electrophoresis was performed at 4°C.

Heterologously expressed *dCirl-IRH* was analyzed using NuPAGE 4-12% Bis-Tris Gels and NuPAGE MOPS SDS Running Buffer (Life Technologies, Paisley, United Kingdom). Protein samples were mixed with 6x SDS Loading Buffer and denatured at 60°C for 10-20 minutes. Protein bands were stained with SimplyBlue SafeStain Coomassie (Life Technologies, Paisley, United Kingdom) overnight.

4.3.2 Western blot

Transfer of protein bands from the polyacrylamide gel to a polyvinylidene fluoride membrane (Immobilon-FL PVDF 0.45 µm, Merck Millipore, Darmstadt, Germany) was performed in a Mini Trans-Blot Cell Unit (Bio-Rad, Munich, Germany) at 4°C. The Blotting Buffer consisted of 3.03 g Tris base, 14.4 g glycine and 200 ml methanol ad 1 l dH₂O.

The blot membrane was blocked from unspecific antibody binding in Odyssey Blocking Buffer (LI-COR Biosciences, Bad Homburg, Germany) diluted 1:8 in 1xTBS. For primary antibody incubation, the blocking solution was replaced by Odyssey Blocking Buffer diluted 1:8 in 1xTBS + 0.1% Tween-20. The following antibodies were added: rabbit-anti-mRFP (1:250; antibodies-online, Aachen, Germany) and mouse-anti-beta-tubulin (1:1,000; DSHB, Iowa City, USA). Primary antibody incubation was performed overnight at 4°C.

After several washing steps, the blot membrane was incubated in a replaced staining solution with secondary antibodies for one hour: IRDye goat-anti-rabbit 680RD and IRDye goat-anti-mouse 800CW (both 1:15,000; LI-COR Biosciences, Bad Homburg, Germany). After washing, fluorescent protein bands were detected using an Odyssey Fc Imaging System (LI-COR Biosciences, Bad Homburg, Germany).

4.3.3 Protein purification and processing

Protein samples for structural analysis of dCIRL-IRH obtained from collecting the supernatant of the transfection medium were diafiltered (Cole-Parmer, London,

United Kingdom) in 20 mM Tris pH 8.0, 150 mM NaCl, 1xPBS until they were concentrated from 3,000 to about 600 ml.

Subsequently, the diafiltered protein solution was loaded to a 5 ml His-Trap HP column (GE Healthcare Life Sciences, Little Chalfont, United Kingdom) at a flow of 5 ml/min. The heterologously expressed protein contained a 6xHistidine-tag, which binds to the nickel sepharose containing column while contaminants simply remain in the buffer. After washing with 20 mM Tris pH 7.5, 300 mM NaCl, 40 mM Imidazole, the protein was eluted from the column using an imidazole-rich buffer (20 mM Tris pH 7.5, 300 mM NaCl, 500 mM Imidazole). Imidazole, whose ring system is present in histidines, displaces the 6xHistidine-tagged protein in the nickel matrix and allows its elution from the column, where it was collected for further processing. As a last step of purification, gel filtration was used to eliminate remaining contaminant proteins. For this purpose, the protein solution obtained from the elution of the His-Trap column was loaded onto an equilibrated HiLoad 16/600 Superdex 200 pg Gel Filtration Column connected to an ÄKTA Protein Purification System (GE Healthcare Life Sciences, Little Chalfont, United Kingdom). This method separates the total volume of different molecules into smaller fractions depending on their Stokes radius, which can be used as a rough indicator for protein dimensions (Erickson, 2009). The column, similar to the His-Trap column, is filled with a highly cross-linked polymer (here dextran) forming pores the proteins have to pass. The smaller the molecules, the more time they spend in these pores. Larger molecules, in contrast, interact less with the gel matrix, are therefore eluted more quickly and thus found in the first eluate fractions. Elution buffer contained 20 mM Tris pH 8.0 and 300 mM NaCl. The relative amount of protein in each fraction could later be estimated using the corresponding UV chromatogram. The correct protein fraction had to be determined by loading samples of the different fractions on an SDS gel and comparing to the calculated molecular weight of the respective protein. For biophysical measurements, fractions with highest purity and concentrations were used.

4.3.4 Protein deglycosylation assays

In order to test glycosylation properties of the heterologously expressed proteins, two different deglycosylating enzymes were used: PNGase F (New England Biolabs, Ipswich, United Kingdom) and Endoglycosidase F (from own expression). Both enzymes release N-linked oligosaccharides, while O-linked oligosaccharides are left unchanged (Maley et al., 1989). Experiments were performed according to the provided protocols.

4.4 *Drosophila melanogaster*

4.4.1 Fly cultivation

Drosophila stocks were held in acrylic glass vials (Klühspies, Retzstadt, Germany) containing solid food medium of the following recipe:

H ₂ O	1 l
Agar	4.5 g
Beet syrup	20 g
Malt	72.2 g
Yeast	16.3 g
Soy flour	9 g
Corn flour	72.2 g
Nipagine (Methyl-4-hydroxybenzoate)	1.45 g
Propionic acid	5.7 g

Nipagine and propionic acid were added due to their fungicidal and pesticidal functions. Cultivation vials were kept at 4°C until needed, but not longer than ten days. For fly keeping, vials were warmed up and kept at 18°C for four weeks, then stocks were transferred to fresh vials. Crossbreeding was performed at 25°C.

4.4.2 Transgenesis of *Drosophila*

Production of transgenic *Drosophila* lines was performed by Best Gene Inc (Chino Hills, USA) using the bacteriophage PhiC31 integrase (Groth, 2004). Transgenic *dCirl* constructs containing a bacterial attachment site (*attB*) were injected into a fly line whose *dCirl* locus had been replaced by a phage attachment site (*attP*) (Scholz et al., 2015). This method ensured site-specific transgenic integration at the original *dCirl* locus. Transgenesis efficiency was verified by co-insertion of a *hsp70-white* selection cassette, which was later removed for application of the animals in experiments (Sternberg and Hamilton, 1981). The following fly lines were used for experiments presented in this thesis:

Name	Genotype
LAT26	$w^{1118} ; dCirl^{108/3A.2} \{attP+ loxP+\} w / CyOGFPw ; +$
LAT54	$w^{1118} ; dCirl^{KO} attP+ loxP- w^+-loxP ; +$
LAT56	$w^{1118} ; dCirl^{KO} attP\{dCirl^{C-RFP} w^+\} loxP ; +$

LAT67	$w^{1118}; dCirl^{KO} attP\{dCirl^{C-Flag} w^+\} loxP; +$
LAT79	$w^{1118}; dCirl^{KO} attP\{dCirl w^+\} loxP / CyOw; +$
LAT84	$w^{1118}; dCirl^{KO} attP\{dCirlp^{GAL4} w^+\} loxP / CyOGFPw; +$
LAT122	$w^{1118}; dCirl^{KO} attP\{dCirl^{N-RFP/C-Flag} w^+\} loxP / CyOGFPw; +$
LAT132	$w^{1118}; dCirl^{KO} attP\{dCirl^{T>A} w^+\} loxP / CyOGFPw; +$
LAT133	$w^{1118}; dCirl^{KO} attP\{dCirl^{N-RFP/C-Flag/T>A} w^+\} loxP / CyOGFPw; +$
LAT157	$w^{1118}; dCirl^{KO} attP\{dCirl^{C-Flag} w\} loxP / CyOGFPw; +$
LAT158	$w^{1118}; dCirl^{KO} attP\{dCirl^{C-RFP} w\} loxP / CyOGFPw; +$
LAT159	$w^{1118}; dCirl^{KO} attP\{dCirl^{N-RFP/C-Flag} w\} loxP / CyOGFPw; +$
LAT163	$w^{1118}; dCirl^{KO} attP\{dCirl w\} loxP / CyOGFPw; +$
LAT174	$w^{1118}; dCirl^{KO} attP\{dCirl^{T>A} w\} loxP / CyOGFPw; +$
LAT176	$w^{1118}; dCirl^{KO} attP\{dCirl^{N-RFP/C-Flag/T>A} w\} loxP / CyOGFPw; +$
LAT255	$w^{1118}; dCirl^{KO} attP\{dCirl^{H>A} w^+\} loxP / CyOw; +$
LAT256	$w^{1118}; dCirl^{KO} attP\{dCirl^{N-RFP/C-Flag/H>A} w^+\} loxP / CyOw; +$
LAT280	$w^{1118}; dCirl^{KO} attP\{dCirl^{H>A} w\} loxP / CyOGFPw; +$
LAT282	$w^{1118}; dCirl^{KO} attP\{dCirl^{N-RFP/C-Flag/H>A} w\} loxP / CyOGFPw; +$

4.4.3 The GAL4/UAS system

The GAL4/UAS system is an example for a binary expression system. It is a common powerful genetic tool used for specific protein expression limited to a certain group of cells or cell types. The system is based on two independently inserted genetic components: a gene encoding the transcription factor GAL4 and the promoter sequence UAS. GAL4 is a transcription factor exclusively existing in yeast, which can be heterologously expressed in *Drosophila*. Expression can be controlled by a specific endogenous promoter (e.g. by the *dCirl* promoter *dCirlp*) or by enhancer-trap lines, which provide exclusive expression in certain tissues (e.g. the motoneuron-specific driver line *ok6-GAL4*). GAL4 will then bind the UAS region in order to promote gene transcription and thus protein biosynthesis of the reporter gene located downstream. As endogenous UAS promoters are inexistent in the *Drosophila* genome, the reporter transgene will be selectively transcribed in cells expressing the GAL4 transcription factor (Brand and Perrimon, 1993).

4.4.4 Behavioral assays

Crawling assay

For the assessment of larval crawling behavior, wandering third instar larvae (up to six at a time) were placed in the centre of a petri dish filled with 1% agarose (Biozym, Hessisch Oldendorf, Germany). Their locomotion paths were immediately video captured for 30 seconds and analyzed using the wrMTrck plugin (J. S. Pedersen, <http://www.phage.dk/plugins/wrmtrck.html>) for ImageJ software (NIH, USA). The covered distance was obtained for each larva individually; paths that were not completely digitally recognized were not included in the data set.

Touch sensitivity assay

This assay was performed to test external touch sensitivity of third instar larvae. A single larva was placed in a petri dish and, as soon as it had started crawling, gently touched at its anterior end with a 0.3 mN von-Frey filament (M. Kernan et al., 1994). The reaction of the larva upon this mechanical stimulus was classified using the following scoring system (Caldwell et al., 2003):

- | | |
|---|--|
| 0 | no response |
| 1 | stopping or brief hesitation |
| 2 | brief retraction, continuation of crawling forward |
| 3 | brief retraction, turn $<90^\circ$ |
| 4 | brief retraction, turn $>90^\circ$ |

Each larva was touched and scored four times, the single values were summed up to a maximum score of 16. Genotypes were blinded prior to the experiments.

Statistical analysis

Data sets of n individuals per genotype were statistically analyzed with non-parametrical Mann-Whitney tests in reference to *dCirr^{Rescue}*, which has been shown to function as control in the presented assays (Scholz et al., 2015). Analysis and plotting were performed using Prism 5 (GraphPad Software, La Jolla, USA). Data are stated as mean \pm SEM; asterisks represent the level of significance: * $p \leq 0.05$, ** $p \leq 0.01$, *** $p \leq 0.001$, ns non-significant.

4.4.5 Isolation of genomic DNA

To isolate genomic DNA from adult *Drosophila*, one to five flies were collected and homogenized manually in 100 µl Squishing Buffer with proteinase K (200 µg/ml; Sigma-Aldrich, Taufkirchen, Germany) using a pipet tip. After incubation at 37°C for 30 minutes, proteinase K was inactivated and the sample was centrifuged at 13,000 rpm for ten minutes. The supernatant containing the genomic DNA was collected separately and stored at 4°C.

4.4.6 Protein extraction from animals

For protein extraction from adult *Drosophila*, five fly heads were used per genotype. The exclusive use of heads was due to the fact that *dCirl* expression levels were believed to be highest in the fly brain and to minimize contaminant protein amounts. After chopping off the heads, they were immediately transferred to a 0.5 ml tube containing 5 µl RIPA buffer (150 mM NaCl, 1% Triton X-100, 0.5% sodium deoxycholate, 0.1% SDS, 50 mM Tris pH 8.0) and a protease inhibitor cocktail (1:1,000; Sigma-Aldrich, Taufkirchen, Germany). In order to support the protease inhibition process and prevent the protein sample from being degraded, the tubes were instantly quick-frozen in liquid nitrogen (Tyczka, Würzburg, Germany) and later thawed on ice. Fly heads were then manually homogenized using a pipette tip. 7.5 µl 4x Protein Loading Buffer (LI-COR Biosciences, Bad Homburg, Germany) and further 14.5 µl RIPA + protease inhibitor cocktail were added and shortly mixed. In a last step, 3 µl 2-Mercaptoethanol (Sigma-Aldrich, Taufkirchen, Germany) were added to support the denaturation and reduction of proteins. The resulting sample was centrifuged at 13,000 rpm for five minutes for removal of the remaining fly head solids. The supernatant was transferred to a fresh tube and stored at -20°C.

4.4.7 Immunohistochemistry and antibodies

Buffer recipes

All chemicals and components for the following buffers were purchased from Sigma-Aldrich (Taufkirchen, Germany), except for PFA (Merck, Darmstadt, Germany).

10xPBS:	NaCl	74 g
	Na ₂ HPO ₄ x 2H ₂ O	12.46 g
	NaH ₂ PO ₄ x H ₂ O	4.14 g
	ad 1 l dH ₂ O, pH adjusted to 7.4	

HL-3:	NaCl	70 mM
	KCl	5 mM
	MgCl ₂	5 mM
	NaHCO ₃	10 mM
	trehalose	5 mM
	sucrose	115 mM
	HEPES	5 mM
	ad 500 ml dH ₂ O, pH adjusted to 7.2	
4% PFA:	paraformaldehyde	8 g ad 15 ml dH ₂ O (55°C)
	2 N NaOH	10 drops
	10xPBS	20 ml
	ad 400 ml dH ₂ O, pH adjusted to 7.4	
x% PBT:	1xPBS + x% Triton X-100	

Preparation of larval nervous system

For immunohistochemical stainings, wandering third instar larvae were collected and shortly washed with dH₂O before placing them in a drop of ice-cold HL-3 on a rubber pad. Using two insect pins, larvae were fixed at their ends and cut on their dorsal side from the posterior to the anterior end using dissection spring scissors. After relief cuts at the two ends of the longitudinal section, the body wall was unfolded and pinned down flat with two insect pins on each side. In a next step, the inner fat body was removed with a forceps in order to expose the muscular system, the central nervous system and its projections into the periphery.

All dissection instruments were purchased from Fine Science Tools (Heidelberg, Germany). Preparations were performed using a binocular reflected light microscope (Zeiss Stemi 2000, Zeiss, Oberkochen, Germany).

Fixation and staining protocols

Dissected larval preparations were fixed in 4% PFA for ten minutes at room temperature. Staining protocols for ventral nerve cords und chordotonal organs highly differed; this is why they will be illustrated separately:

For VNC staining, samples were blocked from unspecific antibody binding in 0.05% PBT + 5% NGS (Dianova, Hamburg, Germany) for 30 minutes at room temperature. After replacement of the PBT/NGS solution, primary antibodies were added and

samples were incubated overnight at 4°C. On the next day, dissections were washed in 0.05% PBT two times shortly and three times for 20 minutes. Secondary antibody incubation was performed in 0.05% + 5% NGS for two hours at room temperature, followed by another washing procedure. Finally, larval preparations were incubated in Vectashield Mounting Medium (Vector Laboratories, Burlingame, USA) overnight at 4°C.

After PFA fixation, CHO dissections were incubated in 0.3% PBT for 30 minutes at room temperature and subsequently blocked in 1% PBT + 5% NGS + 2% BSA overnight at 4°C. On the next day, the blocking solution was replaced, primary antibodies were added and samples incubated overnight at 4°C. After washing in PBS + 0.1% Tween-20 (Sigma-Aldrich, Taufkirchen, Germany) two times shortly and four times for 30 minutes, secondary antibody incubation was performed in PBS + 0.1% Tween + 5% NGS overnight at 4°C. On the fourth day, dissections were washed again in PBS + 0.1% Tween and incubated in Vectashield Mounting Medium overnight at 4°C.

At last, larval fillets were embedded in Vectashield Mounting Medium on an object slide with the interior side facing upward, covered with a cover slip and sealed with nail polish. Object slides were stored at 4°C.

Antibodies

The following antibodies or toxins were used for immunohistochemical stainings of larval dissections:

Antibody	Dilution	Reference
mouse-anti-acetyl. tubulin	1:400	Sigma-Aldrich (Taufkirchen, Germany)
mouse-anti-nc82(BRP)	1:250	Prof. E. Buchner (University of Würzburg)
mouse-anti-DLG	1:500	DSHB (Iowa City, USA)
mouse-anti-EYS	1:250	DSHB (Iowa City, USA)
mouse-anti-FLAG(M2)	1:500	Sigma-Aldrich (Taufkirchen, Germany)
mouse-anti-6xHis	1:500	Life Technologies (Darmstadt, Germany)
mouse-anti-NOMPC	1:250	Prof. M. Göpfert (University of Göttingen)
rabbit-anti-GFP	1:400	Life Technologies (Darmstadt, Germany)
rabbit-anti-mRFP	1:500	antibodies-online (Aachen, Germany)
rabbit-anti-V5	1:500	Sigma-Aldrich (Taufkirchen, Germany)
rat-anti-HA	1:500	Roche (Mannheim, Germany)
goat-anti-mouse-A488	1:250	Life Technologies (Darmstadt, Germany)

goat-anti-mouse-Cy3	1:250	Dianova (Hamburg, Germany)
goat-anti-mouse-Cy5	1:250	Dianova (Hamburg, Germany)
goat-anti-rabbit-Cy3	1:250	Dianova (Hamburg, Germany)
goat-anti-rat-A488	1:250	Life Technologies (Darmstadt, Germany)
goat-anti-HRP-Cy3	1:250	Dianova (Hamburg, Germany)
goat-anti-HRP-Cy5	1:250	Dianova (Hamburg, Germany)
phalloidin-A488	1:500	Cell Signaling Technology (Danvers, USA)

4.5 Microscopic techniques

4.5.1 Confocal microscopy

Microscopic imaging of *Drosophila* preparations constitutes an integral part of this thesis project. Confocal microscopic images were acquired with a Zeiss LSM 5 confocal system (Zeiss, Oberkochen, Germany). For experiments presented in this thesis the following Plan Neofluar objectives were used: 10x/0.3 air objective, 20x/0.5 air objective, 63x/1.25 oil immersion objective (all Zeiss, Oberkochen, Germany). An Argon laser (488 nm) and a Helium-neon laser (543 nm) were used for excitation of the fluorescent dyes Alexa Fluor 488 and Cy3, respectively.

Preparations of different genotypes were imaged using the same microscope and laser settings in order to ensure comparability.

4.5.2 Structured illumination microscopy

Structured illumination microscopy (SIM) is a technique used to overcome limitations in resolution of conventional light microscopy. Its basic principle consists in the patterned illumination of the sample with a high spatial frequency in multiple angles. This way, the emission of individual fluorophores can be temporally separated and allows a resolution of approximately 100 nm, which means at least twofold improvement compared to the resolution of confocal microscopy (Heintzmann and Cremer, 1999; Gustafsson, 2000).

SIM images were obtained with an ELYRA S.1 Super-resolution imaging system connected to an LSM 7 and a Plan Aplanachromat 63x/1.4 oil immersion objective (Zeiss, Oberkochen, Germany). HR Diode 488 nm (100 mW), 561 nm (100 mW) and 642 nm (150 mW) lasers were used for excitation of fluorescent dyes. Acquired confocal images were processed to SIM images with the provided ZEN software. Laser settings were kept constant for total data sets.

4.5.3 Image processing

Raw data obtained from microscopic imaging was processed and analyzed using ImageJ software (NIH, USA). Images are shown as either individual slices or z-projections of stacks in maximum intensity. Background subtraction and reduction of unspecific fluorescent signal was achieved by manipulation of brightness and contrast. Individual images of total data sets were processed identically.

4.6 Biophysical methods

4.6.1 Circular Dichroism Spectrophotometry

Circular dichroism (CD) is the ability of chiral molecules to differently absorb right- and left-handed circularly polarized light. Proteins provide optical activity predominantly through their peptide bonds, which offer characteristic CD spectra at UV wavelengths between 190 and 250 nm (Beychok, 1966).

When light, which is electromagnetic radiation, passes suitable filters, its electric field will start oscillating in sinusoidal waves and the light beam will transform from being linearly polarized to being circularly polarized. When the beam hits optically active molecules, such as nearly all polypeptides, it is further refracted to being elliptically polarized. Ellipticity θ , which has certain characteristics for differently structured proteins, can be detected for UV wavelengths and forms spectra (**Figure 8**)

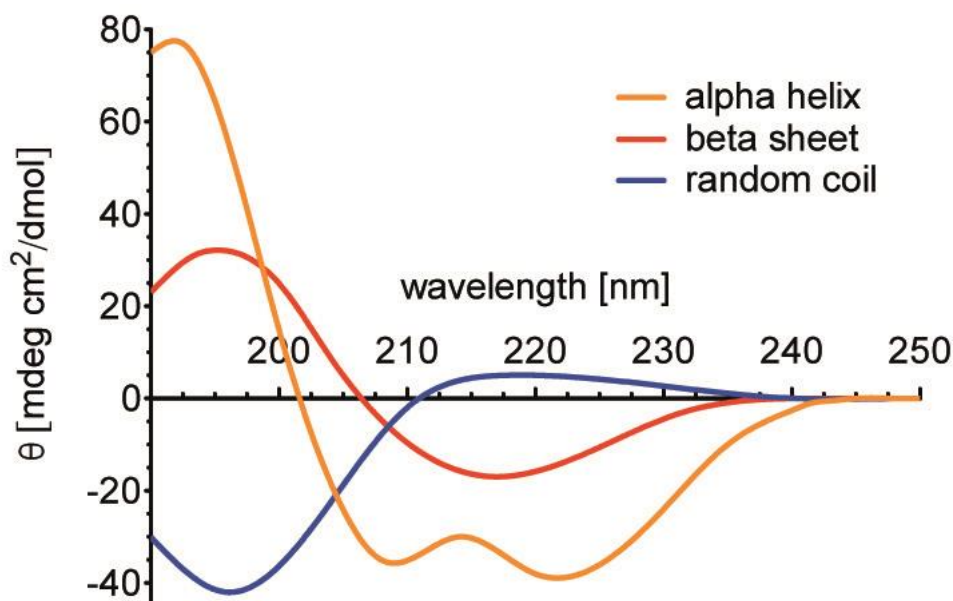


Figure 8. Standard CD spectra. Ellipticity values are displayed as a function of the wavelength of the applied UV light. Spectra are specific for different secondary protein structures. Adapted from Greenfield, 2006.

that allow conclusions about their secondary structure (Greenfield, 2006). For the experiments, a Jasco J-815 Spectropolarimeter (Jasco Inc, Easton, USA) was used. Samples had concentrations of 0.3 mg/ml in a 10 mM phosphate + 20 mM NaCl buffer and were filtered prior to the measurements. Experiments were performed three times and spectra were averaged for presentational reasons.

4.6.2 Dynamic Light Scattering

Dynamic Light Scattering (DLS) is a well-established method which is used for experimental estimation of particle sizes that are smaller than the wavelength of light. According to the Brownian motion theory, molecules diffuse randomly in a solution. When monochromatic light hits the solvated particles, the beam is scattered. The distance of the scattered light to its detector varies with time, as molecules are constantly in motion, where small ones move faster than larger ones. Taking the diffusion coefficient of the buffer into account, the intensity of scattered light fluctuates depending on time (Hassan et al., 2015). Exactly this intensity can be used to draw conclusions from the diffusion characteristics of molecules to their size: DLS data enables calculation of the hydrodynamic radius R_h , which is defined as the theoretical radius of a solid sphere that shows the same diffusion behavior as the solute, and is considered a reliable indicator for the molecule's physical size and shape (Erickson, 2009).

Results were obtained using a Viscotek 802 (Malvern Instruments, Malvern, United Kingdom) with a 660 nm laser. Samples were concentrated to 0.3 mg/ml in 20 mM Tris pH 8.0 + 300 mM NaCl and were filtered before the experiment. Ten runs for ten seconds were performed and the distribution of the molecule sizes in the sample was displayed by the provided software (OmniSIZE 3.0).

4.6.3 Size Exclusion Chromatography/Multi-Angle Light Scattering

Size Exclusion Chromatography connected with Multi-Angle Light Scattering (SEC-MALS) is an elegant method that can be used to address a variety of questions. In general, it is applied for experimental determination of molecular weights and is based on the principle of a gel filtration (see 4.3.3). Subsequent to the elution of the proteins, which have been fractionated based on their dimensions, the eluate is shot with a laser beam, which is scattered and emitted in all directions. UV detectors that are positioned at different angles with respect to the beam record the scatter, which is proportional to the product of concentration and molecular weight of the protein in the sample (Wyatt, 1993). As the concentration itself is dependent on the differential

refractive index (DRI) of the solution, it can be determined with the included DRI detector. The molecular weight is now easily calculated. Another advantage of the existence of both UV and DRI detectors that can be benefitted from is based upon the fact that only peptides absorb UV light, while other components (e.g. carbohydrates or detergents) do not. This way, the share of carbohydrates in the total molecular weight of dCIRL-IRH was estimated (Arakawa and Wen, 2001).

SEC was performed in a Superdex 75 HR10/30 Column (GE Healthcare Life Sciences, Little Chalfont, United Kingdom) linked to a Shimadzu HPLC system comprising LC-20AD pump, SIL-20A Autosampler and SPD20A UV/Vis detector (Shimadzu, Milton Keynes, United Kingdom). MALS equipment included a Wyatt Dawn HELEOS-II 8-angle Scattering Detector and a Wyatt Optilab rEX refractive index monitor (Wyatt Technology, Dernbach, Germany).

Filtered samples had concentrations of 0.6-1.7 mg/ml and were solved in 20 mM Tris pH 8.0 + 300 mM NaCl. LPHN3-OLF was derived from own heterologous expression; Ovalbumin was obtained from a Gel Filtration Calibration Kit (GE Healthcare Life Sciences, Little Chalfont, United Kingdom). Data was analyzed using ASTRA 6.1.1 software provided from Wyatt Technology, conjugate analysis was performed with the respective software tool. A glycosylation of three N-linked carbohydrates was assumed according to sequence predictions for dCIRL-IRH (<http://www.cbs.dtu.dk/services/NetNGlyc/>) and results from deglycosylating assays; the dn/dc value was adjusted to 0.1752 (standard 0.1860).

5. Results

5.1 Generation of a genomic *dCirl* cloning toolkit

Over the last decades, Latrophilins and their invertebrate homologs have been subject of intense research. Different methodical approaches included genomic, biochemical, and structural analyses (V. G. Krasnoperov et al., 1997; Orlova et al., 2000; Serova et al., 2008; Arcos-Burgos et al., 2010; Arac et al., 2012), but often lacked detailed functional aspects of Latrophilins in their native context.

To be able to address this question, advanced molecular biological techniques were used to modify the original *dCirl* allele, e.g. by the insertion of point mutations, immunohistochemical tags, or the alteration of specific domains or allelic regions.

For the purpose of easier and faster cloning strategies, a genomic *dCirl* cloning platform was generated: utilizing specific existing and introduced restriction sites in non-coding regions, the allele was separated into six parts, four of which contained the majority of the protein coding regions (**Figure 9**). These fragments were sub-cloned into individual vectors (subclones I-IV), which then allowed for modification such as the insertion of an mRFP-cassette, a 3xFlag-tag, an HA-tag or the site-directed mutagenesis of *dCirl*'s GPS. For a complete list of generated subclones, see 4.1.3. Subsequent reassembly of the genetically altered fragments was easily achieved using the unique restriction sites again, resulting in the reconstitution of the whole – and now modified – *dCirl* allele.

Furthermore, the vast number of combinations of the different subclones will provide a useful tool for future experiments.

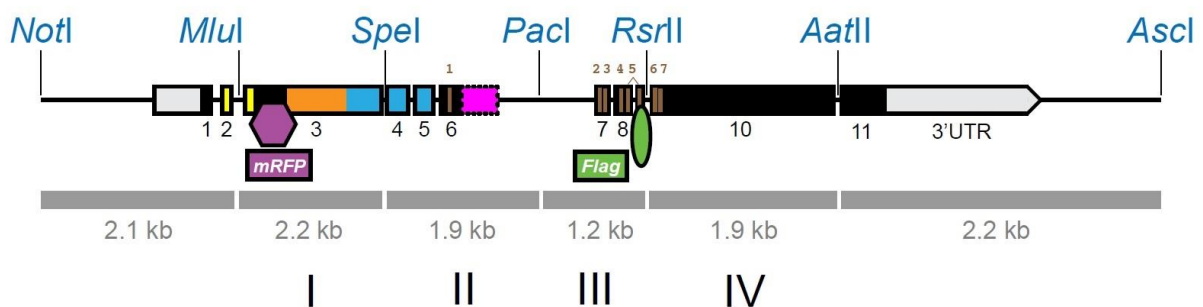


Figure 9. The *dCirl* cloning toolkit allows easier molecular modification. The cartoon shows the allele of *dCirl* separated into six parts by unique restriction sites (indicated in blue). Regions representing the RBL (yellow), HRM (orange), GAIN (light blue), 7TM (brown) domains and the alternative exon region (violet) are depicted. Molecular modification, e.g. through the insertion of immunohistochemical tags or point mutations, can be performed in subclones I-IV. Reinsertion of the altered subclones reconstitutes the whole *dCirl* allele. The cartoon here shows *dCirl*^{N-RFP/C-Flag}, the modified allele described in the following paragraph (see also Figure 10A).

5.2 Localization of *dCirl* expression in *Drosophila* larvae

5.2.1 *dCirl*^{N-RFP/C-Flag} is expressed in *Drosophila*

Direct visualization of Latrophilins in their native context has remained complicated thus far. In order to pursue this challenge, the *Drosophila melanogaster* homolog of Latrophilin, dCIRL, was marked with immunohistochemical tags.

A *dCirl* null allele (*dCirl*^{KO}) generated by a homologous recombination-based approach (Scholz et al., 2015) was used as a basis to reconstitute the native *dCirl* locus through locus-directed knock-in of modified or unmodified DNA fragments. First, the wildtype genomic *dCirl* sequence was integrated to restore the original locus (*dCirl*^{Rescue}), which was reliably used to rescue *dCirl*-specific defects (Scholz et al., 2015) and thus served as a control for this study.

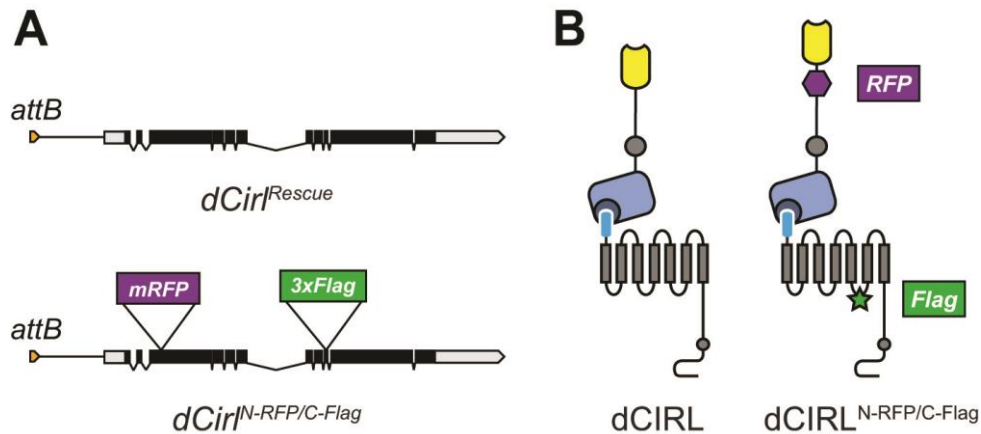


Figure 10. dCIRL^{N-RFP/C-Flag} is marked with immunohistochemical tags. (A) Cartoon of the genomic region of the native (*dCirl*^{Rescue}) and modified *dCirl* locus (*dCirl*^{N-RFP/C-Flag}) in 5'-3'-direction. The upstream located *attB* site is required for locus-directed knock-in. (B) Protein layout of both alleles presented in Figure 10A. RBL (yellow), HRM (gray), GAIN (light blue) domains and GPS motif (dark blue) are depicted. The magenta hexagon and the green star indicate the location of mRFP and Flag tags, respectively.

To visualize endogenous dCIRL, a *dCirl*^{N-RFP/C-Flag} allele was created (**Figure 10A**): on the one hand, a 0.7 kb sequence encoding a monomeric RFP (mRFP) fluorophore was inserted into exon 3 encoding part of the NTF of the receptor. On the other hand, a 0.1 kb sequence containing a 3xFlag tag was inserted into exon 8 encoding the third intracellular loop of the 7TM domain of dCIRL (**Figure 10B**). Positioning of the tags followed several rationales: first, individual tagging of NTF and CTF enables tracking of both fragments in case they become separated and colocalization studies of associated fragments. Second, previous work has shown that

receptor function is not affected by insertion of a 3xFlag tag into the third intracellular loop of *dCirl* (Scholz et al., 2015), which is why this strategy was adopted here. Third, the rather large mRFP fluorophore should not disrupt extracellular domains of dCIRL. The region between the RBL and HRM domains appeared applicable, hence, the mRFP cassette was introduced here, in close proximity to the RBL domain, so that putative unknown domains would not be harmed.

The altered genomic DNA fragment was introduced into the endogenous *dCirl* locus using PhiC31 mediated insertion resulting in the transgenic fly strain *dCirl^{N-RFP/C-Flag}*, which was then analyzed in western blots using an RFP antiserum to detect *dCirl^{N-RFP/C-Flag}* (Figure 11).

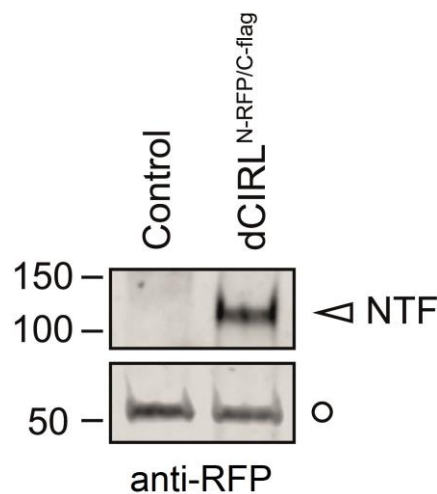


Figure 11. *dCirl^{N-RFP/C-Flag}* is expressed in *Drosophila*. Western blot analysis of adult fly protein extracts from wildtype and tagged *dCIRL^{N-RFP/C-Flag}* variants probed against the N-terminal mRFP tag using polyclonal antiserum. A fragment corresponding to the cleaved NTF of *dCirl^{N-RFP/C-Flag}* flies was found at ~ 106 kDa, while no dCIRL fragments were detected in the unmarked control. Beta-tubulin (~ 55 kDa; open circle) served as loading control.

Probed against the mRFP tag, extracts from fly head homogenates of *dCirl^{N-RFP/C-Flag}* showed a specific protein band at approximately 110 kDa, which was absent in untagged control flies. This fragment corresponds to the cleaved NTF of dCIRL, as the detected mRFP tag is located in the extracellular part of the receptor. Hence, transgenesis of *dCirl^{N-RFP/C-Flag}* was successful and transcription as well as translation of the altered locus was unaffected. Furthermore, no band of ~ 220 kDa, which would correspond to the uncleaved full-length receptor was detected, suggesting that autoproteolytic processing at the GPS of dCIRL is complete or at least highly efficient.

5.2.2 Behavioral phenotypes are rescued in *dCirl*^{N-RFP/C-Flag}

Drosophila larval locomotion relies on patterned muscle contractions that move stereotypically along the body segments (Caldwell et al., 2003). Linear movement is periodically intermitted by periods of head swinging, which are assumed to be required for orientation and decision making. Coordination of all movements is absolutely necessary for proper locomotion, where peripheral sensory input, e.g. from chordotonal organs (CHOs), constitutes one major feedback mechanism (Caldwell et al., 2003).

Removal of *dCirl*, which is expressed in chordotonal neurons, leads to a particular phenotype in *Drosophila* larvae, which is consistent with defective CHO function: *dCirl*^{KO} animals show increased head swinging phases and reduced linear movement resulting in decreased net crawling distances compared to wildtype animals (Scholz et al., 2015). Additionally, they exhibit a diminished sensitivity toward gentle touch in a well-established scoring assay (M. Kernan et al., 1994; Caldwell et al., 2003; Yan et al., 2013).

In order to analyze whether the insertion of the tags impaired dCIRL function, *dCirl*^{N-RFP/C-Flag} larvae were tested for the phenotypes described above. **Figure 12** shows crawling distances of control, *dCirl*^{KO} and *dCirl*^{N-RFP/C-Flag} larvae, used as a means to quantify the locomotive head swinging phenotype. As expected, *dCirl*^{KO} larvae showed a significant reduction of their crawling distance, while *dCirl*^{N-RFP/C-Flag} animals sufficed to rescue the phenotype indicating normal locomotion.

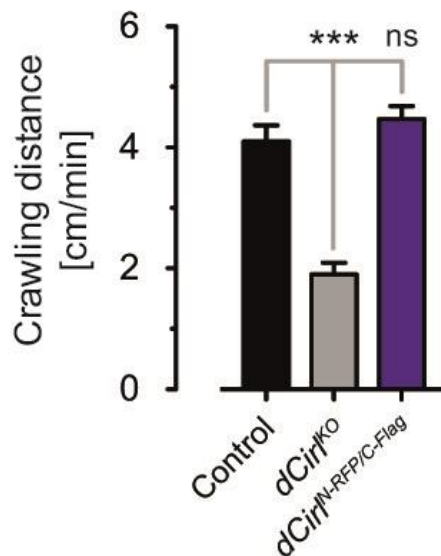


Figure 12. The locomotion phenotype is rescued in *dCirl*^{N-RFP/C-Flag} larvae. Quantification of crawling distances to test the effect of tag insertion on the locomotion of *Drosophila* larvae. n=20 per genotype. Data are presented as mean \pm SEM.

The perception of gentle touch was tested utilizing a touch sensitivity assay, which scores behavioral response of the larvae toward a gentle tactile stimulus at their anterior end (M. Kernan et al., 1994). The averaged results as well as the distribution of individual scores are shown in **Figure 13**. Corroborating previous findings (Scholz et al., 2015), *dCirl*^{KO} larvae exhibited diminished touch sensitivity, whereas the results of *dCirl*^{N-RFP/C-Flag} remained indistinguishable from controls.

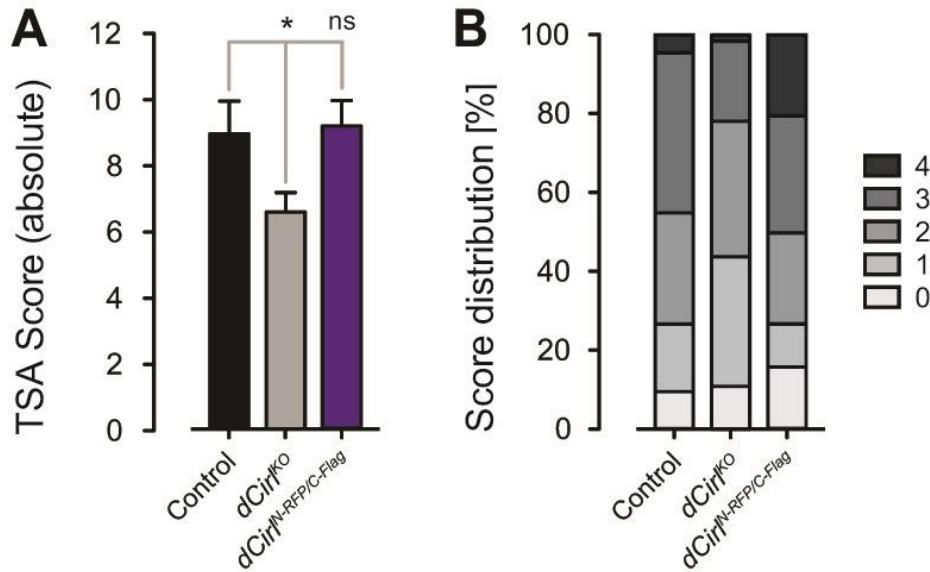


Figure 13. *dCirl*^{N-RFP/C-Flag} larvae exhibit normal sensitivity toward gentle touch. (A) Averaged results of the touch sensitivity of different genotypes displayed as the sum of four-fold scoring (0-4) of individual larvae (for description of the assay and protocol see 4.4.4 on page 28). n=16 per genotype. Data are presented as mean ± SEM. (B) Distribution of individual scores.

Based on behavioral read-outs, insertion of an mRFP and 3xFlag tag into the endogenous *dCirl* sequence seems not to affect receptor function. The locomotion and touch sensitivity phenotypes observed in *dCirl*^{KO} are rescued to control levels in *dCirl*^{N-RFP/C-Flag}, indicating that both receptor and CHO function are intact.

5.2.3 *dCirl* is broadly expressed in different neuronal tissues

It is long known that Latrophilins are expressed in neuronal tissues with implication in synaptic transmission, adhesive interactions and development (Davletov et al., 1996; V. G. Krasnoperov et al., 1997; Boucard et al., 2012; O'Sullivan et al., 2012). Similarly, invertebrate homologs LAT-1 and dCIRL have been assigned neuronal functions (Langenhan et al., 2009; Scholz et al., 2015).

However, visualization of Latrophilin expression patterns has remained challenging thus far. First approaches provided promising results (Gehring, 2014; Scholz, 2015) and provide the platform for the experiments conducted in this study.

Unfortunately, detection of endogenous fluorescence signals of the mRFP tag in $dCIRL^{N-RFP/C-Flag}$ failed, which may indicate low expression levels of dCIRL compatible with findings in *C. elegans* LAT-1 (Langenhan et al., 2009). The utilization of antibodies amplified the mRFP and Flag-based signals, which then became detectable in confocal laser microscopy. In third instar larvae, endogenous $dCirI^{N-RFP/C-Flag}$ was broadly expressed throughout the ventral nerve cord (VNC; **Figure 14**), a prominent structure of the central nervous system (CNS). The dCIRL staining was most prominent in the neuropile of a synapse-rich region in the central VNC, as well as in somata of neurons located laterally within the cortex. A magnified view of $dCIRL^{N-RFP/C-Flag}$ suggests its localization to the plasma membrane (**Figure 14B**), consistent with previous studies (Gehring, 2014).

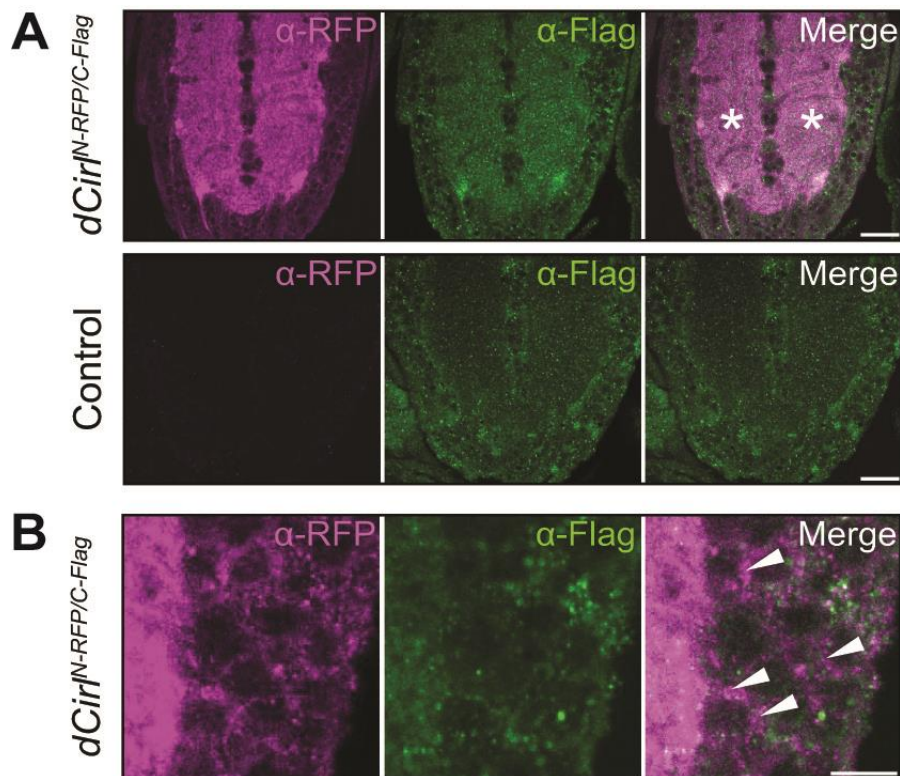


Figure 14. *dCirI* is expressed throughout the larval ventral nerve cord. (A) Maximal projections of confocal images of larval ventral nerve cords (VNCs) from different genotypes. mRFP and Flag signals are shown in magenta and green, respectively, and indicate $dCIRL^{N-RFP/C-Flag}$ location in the central neuropile (marked with asterisks) and in the somata of the VNC. Note the unspecific signal of anti-Flag staining in the control animal. Scale bar 20 μ m. (B) Magnification of Figure 14A suggests membrane targeting (arrowheads). Scale bar 10 μ m.

In contrast, the anti-Flag staining appeared unspecific rendering interpretations obsolete, which is why anti-Flag-based stainings were omitted for subsequent experiments.

Although *dCirl* has been shown to modulate the morphology of larval neuromuscular junctions (NMJs), the presence of dCIRL has not been observed yet (Scholz, 2015). One reasonable explanation is based on low expression levels, as observed for numerous aGPCRs. Structured illumination microscopy (SIM), a commonly used super-resolution imaging technique, now revealed low signals of dCIRL^{N-RFP/C-Flag} in synaptic boutons of NMJs (**Figure 15**) implying that at least a portion of the receptors could be trafficked from VNC-located somata into the axonal projections of motoneurons. The NMJ constitutes a highly specialized glutamatergic synapse (Jan and Jan, 1976), which is why *dCIRL* expression here seems consistent with the prominent signals found in synapse-rich areas of the VNC suggesting synaptic localization of dCIRL.

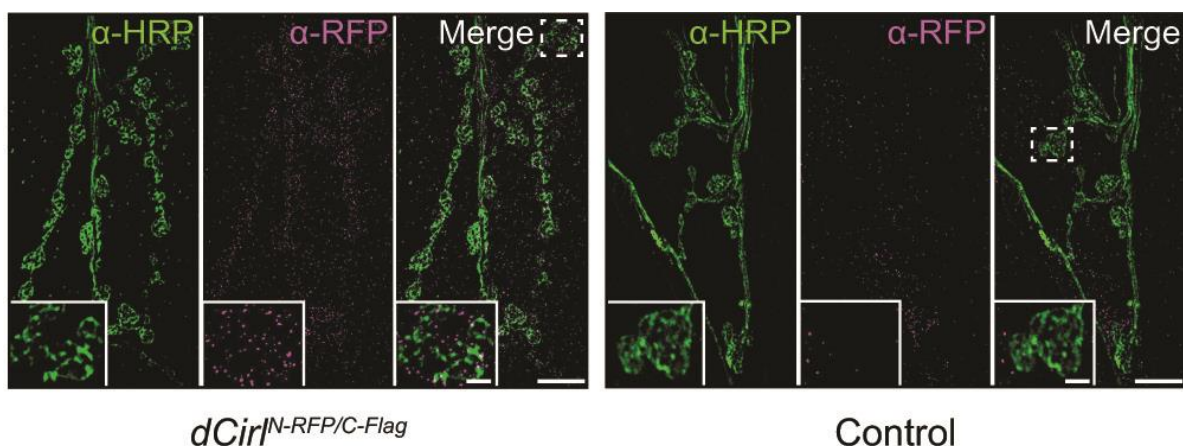


Figure 15. *dCirl* is expressed in neuromuscular junctions. Maximal projections of SIM images from neuromuscular junctions (NMJs) of muscle pair 6/7. mRFP signal is shown in magenta, counterstaining against HRP is indicated in green. dCIRL^{N-RFP/C-Flag} localizes to synaptic boutons, though expression levels appear very low. Dashed rectangles indicate the area magnified in the inset. Scale bar 10 μm (insets 2 μm).

dCirl expression is not restricted to the CNS, but was also found in a set of mechanosensory neurons – the chordotonal neurons – of larval pentascolopodial organs (Scholz et al., 2015), which are part of the peripheral nervous system (PNS). Chordotonal neurons are compound sensors ensheathed by numerous support cells (M. J. Kernan, 2007), which is why the identification of single cells or subcellular compartments using standard light microscopy proved difficult thus far. As depicted in **Figure 16A**, confocal microscopy revealed dCIRL^{N-RFP/C-Flag} localization at the level

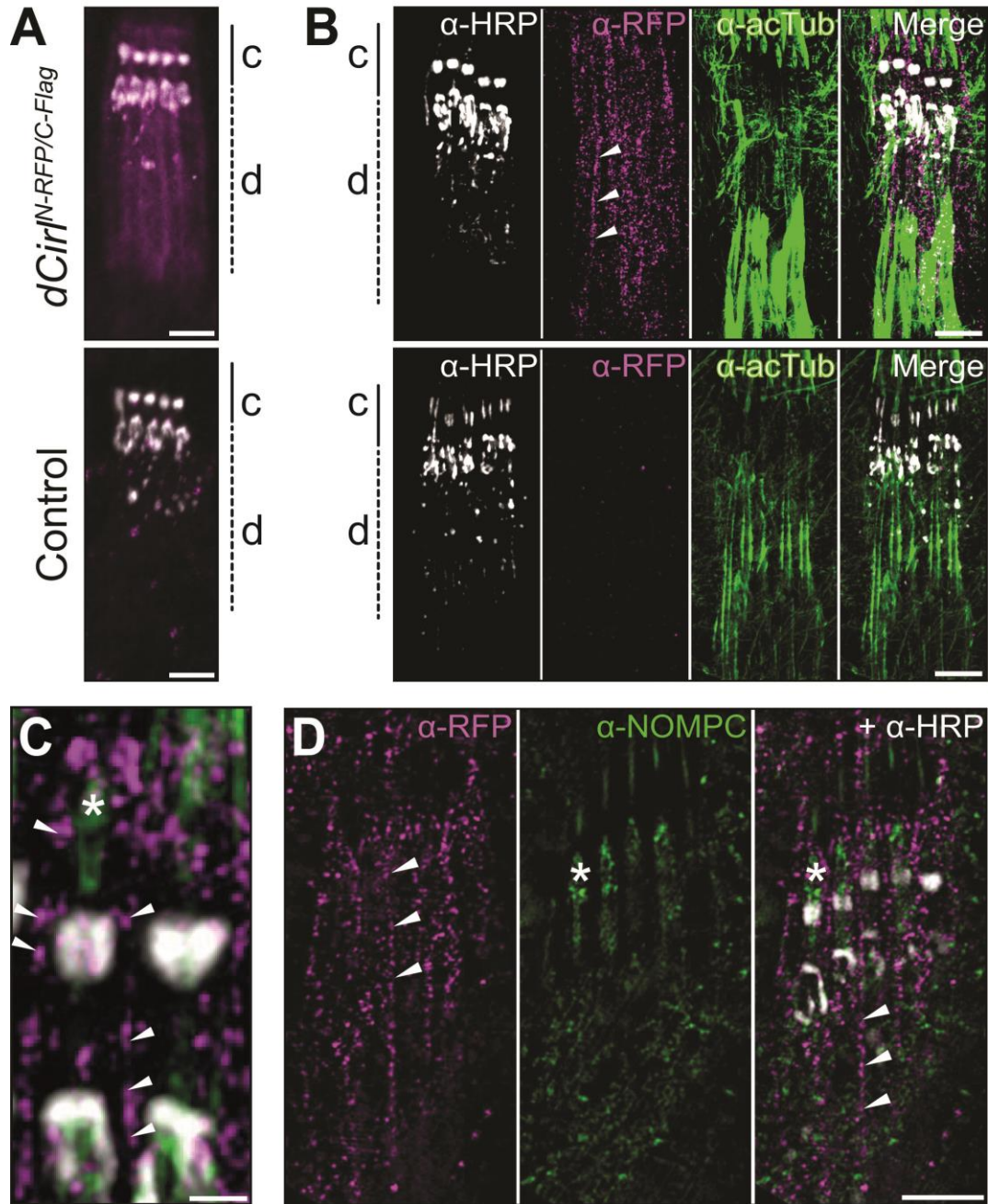


Figure 16. dCIRL localizes to ciliary and dendritic compartments of chordotonal neurons. (A) Maximal projections of confocal images of larval chordotonal organs (CHOs). mRFP signal in magenta, counterstaining using anti-HRP is shown in white. *dCIRL^{N-RFP/C-Flag}* localizes to ciliary (indicated with “c”) and dendritic (“d”) compartments of CHOs. Scale bar 5 μm. (B) Maximal projections of SIM images of CHOs from *dCIRL^{N-RFP/C-Flag}*. mRFP stained in magenta, counterstaining using anti-HRP and acetylated tubulin are shown in white and green, respectively. Scale bar 5 μm. (C) Magnified image shows detailed view of *dCIRL^{N-RFP/C-Flag}* expression in the ciliary compartment (arrowheads). The ciliary dilation is indicated in green (asterisk). Note that SIM resolves the HRP-labeled canal through which the cilium passes. Scale bar 1 μm. (D) Maximal projections of SIM images of *dCIRL^{N-RFP/C-Flag}*, which localizes in close proximity to the TRP channel NOMPC. mRFP stained in magenta, NOMPC in green, HRP-counterstaining in white. Scale bar 5 μm.

of dendritic and ciliary compartments of CHOs. However, the exact location of the signal remained concealed due to limitations in resolution. For this reason, another set of images was obtained using SIM (**Figure 16B,C**). This super-resolution technique uncovered scarce, patchy *dCirl*^{N-RFP/C-Flag} expression at the membrane of distal dendrites and cilia of chordotonal neurons.

Several TRP channel subunits, e.g. NOMPC or IAV, which have been suggested to be involved in the signal pathway downstream of dCIRL (Scholz et al., 2015), are located in these subcellular compartments. However, while microscopy argues against colocalization of dCIRL and NOMPC (**Figure 16D**), these findings are in line with the fact that the aGPCR dCIRL is functionally involved in the modulation of the ionotropic response generated in chordotonal neurons upon mechanical stimulation of *Drosophila* larvae.

5.2.4 The expression profile of *dCirl* is exclusively neuronal

dCIRL localization in the larval CNS and PNS cannot only be investigated on translational, but also on transcriptional levels. A recently established GAL4/UAS strategy was employed (Scholz et al., 2015): the *dCirl* promoter (*dCirlp*) was used to drive the expression of GAL4, which in turn initiates the transcription of the nuclear localizing reporter *GFP::nls* via binding the UAS promoter (**Figure 17A**). This way expression of the fluorophore is restricted to cells with endogenous *dCirl* transcription, which enables their identification.

In CHOs, GFP signals were detected in the nuclei of bipolar chordotonal neurons, but not in any nuclei of the support cells (**Figure 17B**). Similarly, in solitary ventral and lateral CHOs only nuclei of the sensory neurons proved positive for GFP (data not shown). Thus, the dCIRL^{N-RFP/C-Flag} expression observed in **Figure 16** is strictly of neuronal origin.

The same experimental rationale (*dCirlp-GAL4 > UAS-GFP::nls*) has shown the expression of *dCirl* in various motoneurons (Scholz et al., 2015). Based on the fact that dCIRL constitutes one of the receptors recognized by alpha-LTX, which unfolds its effects by releasing massive amounts of SVs from the presynaptic terminal, it has been assumed that dCIRL is expressed presynaptically. However, this has not been addressed experimentally thus far. Further, the question of whether dCIRL is solely expressed at the presynapse has remained unanswered.

Confocal microscopy of the VNC revealed a broad *dCirl* transcription profile in numerous cell bodies of the cortex (**Figure 17C**), though they might not necessarily be motoneurons, as also other cell types are found there. **Figure 17D** shows *GFP::nls* expression in myocytes of the larval body wall under the transcriptional control of

dCirlp and *G7*, a muscle specific driver used as positive control. Indeed, while GFP signals were detected in the nuclei of *G7 > GFP::nls*, nuclei of *dCirlp > GFP::nls* were devoid of such signals. This indicates no endogenous *dCirlp* activity in muscle cells and only leaves presynaptic motoneurons as *dCirl* expressing cells at the NMJ.

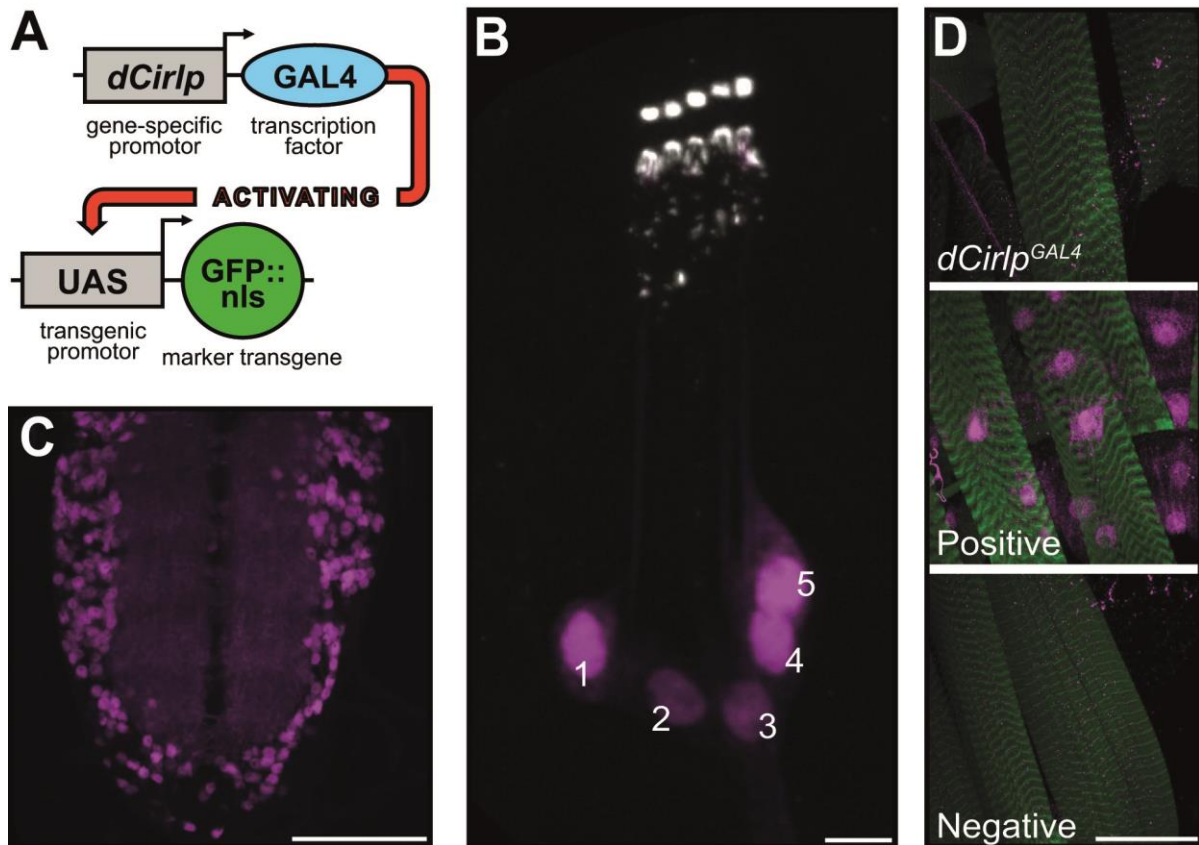


Figure 17. The expression profile of *dCirl* is exclusively neuronal. (A) Schematic illustration of the experimental strategy applied (*dCirlp-GAL4 > UAS-GFP::nls*): *GAL4* is exclusively expressed in *dCirlp* cells, where it enables *GFP::nls* expression, which in turn can be detected. (B) Confocal image of a pentascolopodial CHO stained against GFP (magenta), HRP-counterstaining in white. In CHOs, *dCirl* expression is exclusive to the bipolar choro-tonal neurons. Scale bar 5 μ m. (C) Maximal projection of confocal images of a larval VNC, GFP stained in magenta. Scale bar 50 μ m. (D) Confocal images at the level of myocyte nuclei. GFP in magenta, F-actin stained with phalloidin in green. Postsynaptic (muscular) expression of *dCirl* can be excluded due to the missing GFP expression in myocyte nuclei. Positive control: *G7-GAL4 > UAS-GFP::nls*, negative control: *w¹¹⁸ > UAS-GFP::nls*. Scale bar 50 μ m.

In summary, with *dCirl^{N-RFP/C-Flag}* an allele was created which contained the endogenous *dCirl* sequence fused to two biochemical tags. Locus-directed insertion was biochemically verified and proved to rescue behavioral phenotypes exhibited by *dCirl^{KO}* mutant larvae before.

Antibody staining of the 3xFlag tag largely failed, but anti-mRFP staining revealed broad distribution of dCIRL throughout the larval CNS, most prominently in the neuropile of the VNC. This contrasts with the expression pattern in adult *Drosophila* CNS, where dCIRL was generally absent from synapse-rich regions (Scholz, 2015). At the NMJ, dCIRL's origin is exclusively presynaptic, although an effect on the modulation of postsynaptic structures has been proposed (Scholz, 2015). Further expression was found in CHOs, where dCIRL localizes to the membrane of distal dendrites and cilia of chordotonal neurons, in close proximity to the TRP channel NOMPC. Consequently, *dCirl* is a neuronal gene expressed in both CNS and PNS with functional and regulatory implication in synaptic morphology and peripheral mechanosensation.

5.3 Analysis of dCIRL autoproteolysis

5.3.1 dCIRL^{H>A} and dCIRL^{T>A} contain a mutated GPS

Juxtamembrane autoproteolysis has been identified as a key characteristic at an early stage of aGPCR research (Gray et al., 1996; V. G. Krasnoperov et al., 1997). The GPS, where the cleavage takes place, constitutes a highly conserved motif, which is absolutely necessary, but insufficient to mediate the autoproteolytic reaction (Chang et al., 2003). Nearly a decade after its identification, the GPS was discovered to be part of a larger domain, the GAIN domain, which is sufficient to promote the cleavage reaction on its own (Arac et al., 2012).

Yet, reports about the functional relevance of GPS autoproteolysis have been conflicting. While cleavage seemed crucial for membrane trafficking of GPR126 (Liefscher et al., 2014b), no such effect was shown for GPR133 (Bohnekamp and Schöneberg, 2011). For Latrophilin-1, studies provided mixed results regarding the cell-surface transport of the uncleaved receptor (V. Krasnoperov et al., 2002b; Arac et al., 2012). Investigation of the GPS proteolysis of LAT-1 in *C. elegans* LAT-1 showed it is dispensable for receptor function *in vivo* (Prömel et al., 2012).

Methodically, these investigations were mainly based on mutating the -2 or +1 residue of the cleavage site (**Figure 18A**), removing either the nucleophile or the proton

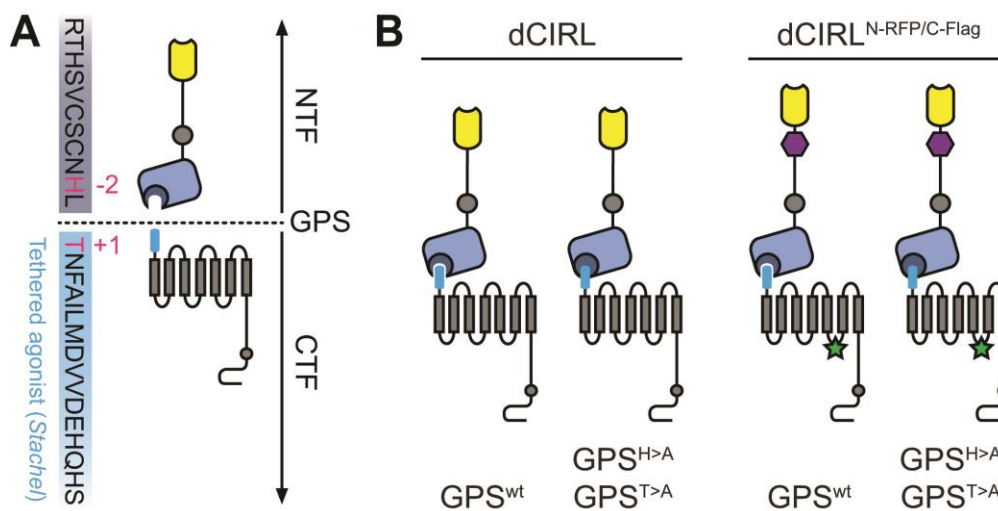


Figure 18. dCIRL^{H>A} and dCIRL^{T>A} contain a mutated GPS. (A) Illustration of dCIRL that highlights the position of the breaking point in proteolyzable aGPCRs. The *Stachel* sequence is located directly at the N-term of the C-terminal cleavage component (light blue). Residues that are crucial for proteolysis mutated in this study are marked red. (B) Depiction of the three GPS variants (wt, T>A, H>A) in wt and tagged dCIRL^{N-RFP/C-Flag} background. Cleavage-deficiency of dCIRL^{H>A} and dCIRL^{T>A} is indicated by a stuck *Stachel*.

donor and thus leaving the receptor unable to perform the autocatalytic reaction (Lin et al., 2004; Prömel et al., 2012). Following these previous examples, two GPS mutant *dCirl* alleles were engineered using site-directed mutagenesis (**Figure 18B**). The -2 (histidine) or +1 (threonine) position of the cleavage site was replaced by an alanine, respectively, creating two different proteolysis-deficient *dCirl* GPS variants, *dCirl^{H>A}* and *dCirl^{T>A}*. Note that the threonine mutated in *dCirl^{T>A}* is not only crucial for autoproteolysis, but also represents the first residue of the tethered agonist *Stachel* (Liebscher et al., 2014b), a fact that requires diligence with the interpretation of functional data. Additional to the unmodified receptor variants, in a second step the GPS mutations were inserted into the mRFP/Flag-tagged *dCirl* background for western blot and immunohistochemical analyses.

5.3.2 GPS autoproteolysis is disabled in *dCIRL^{H>A}* and *dCIRL^{T>A}*

Transgene introduction and cleavage-deficiency of *dCIRL* was verified on both genomic and protein levels.

Subsequent to the generation of transgenic animals, genomic DNA (gDNA) was isolated from adult *Drosophila*, purified, amplified and analyzed using the Sanger sequencing method (Sanger et al., 1977). This way, the exact sequence of the different GPS variants was verified. *dCirl^{T>A}* as well as *dCirl^{H>A}* cleavage sites proved to bear the introduced point mutations, thus encoding cleavage triplets H⁻²L⁻¹A⁺¹ and A⁻²L⁻¹T⁺¹ instead of wildtype H⁻²L⁻¹T⁺¹ (**Figure 19A**). This however only shows that the mutagenesis was performed reliably, but does not reveal if *dCIRL*'s autoproteolytic potential is abolished, as assumed.

For this purpose, western blot analysis of protein extracts was performed. Again using the mRFP tag to specifically detect the receptor NTF provided evidence for the abrogation of the autoproteolytic activity in both GPS mutant receptors (**Figure 19B**). While the cleaved NTF of wildtype *dCIRL* was detected at ~ 106 kDa, no such band was present in *dCirl^{T>A}* or *dCirl^{H>A}*. Instead, the mutant proteins were represented as full-length receptors at ~ 218 kDa, suggesting that they consisted of unproteolyzed and yet covalently bound NTF and CTF.

Furthermore, western blot analysis revealed substantial differences in the protein amounts detected as the protein band of full-length *dCIRL^{H>A}* appeared considerably weaker compared to *dCIRL^{T>A}*. A possible explanation for this result could well be a lower endogenous expression level of *dCirl^{H>A}*, however, there are also several limitations to this hypothesis: with a total of only five *Drosophila* heads per genotype, the variation of individual expression levels is relatively high and cannot be controlled. Moreover, Latrophilin and its homologs have proved to be essential players

involved in embryogenesis and nervous system development (Langenhan et al., 2009; Langenhan et al., 2016). Although animals of the same larval stage were utilized for all experiments, varying expression profiles of the different transgenic *dCirl* alleles during development cannot be excluded. These western blot results pose a first hint that the two GPS mutants might not have identical properties.

Further, a second band in *dCIRL^{T>A}* and *dCIRL^{H>A}* was observed at approximately 130 kDa, which is absent when the receptor is able to perform GPS autoproteolysis. Together with a ~ 75 kDa band, which is present in all three genotypes (data not shown), this additional protein band might originate from alternative cleavage of *dCIRL* by exogenous proteases as proposed before and not uncommon for the aGPCR class (Moriguchi et al., 2004; V. Krasnoperov et al., 2009; Nieberler et al., 2016), or alternative splicing events (Bjarnadóttir et al., 2007).

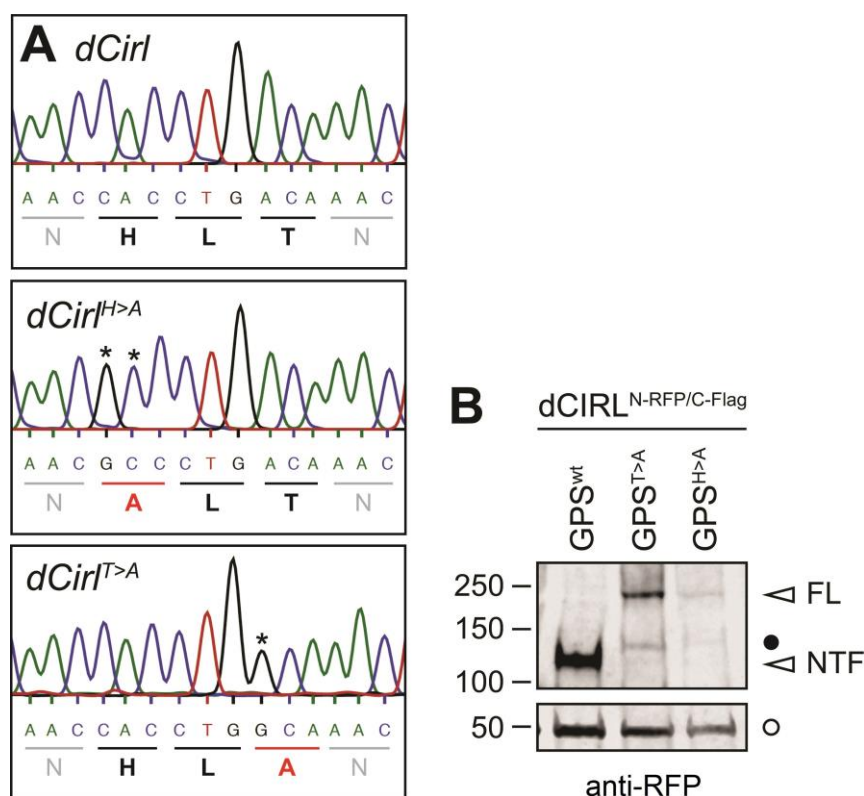


Figure 19. GPS autoproteolysis is disabled in H>A and T>A dCIRL mutants. (A) Sequencing results of gDNA extracted from transgenic adult flies. Inserted point mutations are marked with asterisks. (B) Western blot of adult fly protein extracts containing the three GPS variants in a *dCIRL^{N-RFP/C-Flag}* background probed against the mRFP tag in the NTF. GPS^{wt} displays the cleaved NTF fragment (~ 106 kDa), while the two GPS mutants show the uncleaved full-length receptor (FL) at ~ 218 kDa. Additional band at ~ 130 kDa marked with full circle, positive control with beta-tubulin at ~ 55 kDa (open circle).

5.3.3 Receptor cleavage is dispensable for dCIRL function

One major goal of this study was to examine the role of aGPCR autoproteolysis on receptor function and to understand how receptor cleavage may inflict with the physiology of CHOs. Previous studies have shown dCIRL's necessity for proper locomotion and touch sensitivity of *Drosophila* larvae (Scholz et al., 2015). Thus, the established assays were used to score the impact of GPS autoproteolysis based on the animals' ability to crawl or to sense gentle touch.

The head swinging phenotype and the reduced crawling distance measured in *dCirl^{KO}* larvae was not observed in *dCirl^{T>A}* and *dCirl^{H>A}* animals, which suggests that receptor cleavage is dispensable for proper larval locomotion (**Figure 20**).

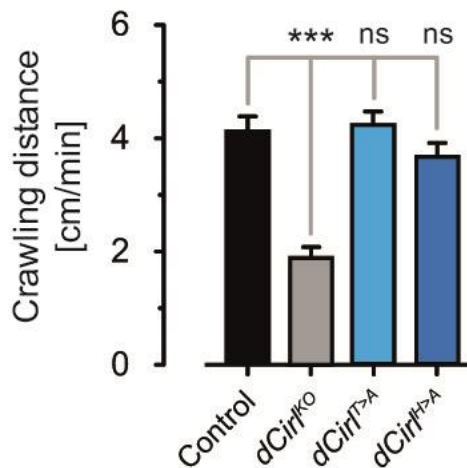


Figure 20. dCIRL autoproteolysis is dispensable for larval locomotion. Quantification of crawling distances as a read-out to test for the impact of dCIRL receptor cleavage. Both GPS mutants sufficed to rescue the phenotype displayed in *dCirl^{KO}*. n=20 per genotype. Data are presented as mean \pm SEM.

The touch sensitivity assay (TSA), however, provided different results presented in **Figure 21**. While *dCirl^{H>A}* sufficed to rescue the phenotype, the sensitivity of *dCirl^{T>A}* animals toward gentle touch was significantly reduced and comparable to values measured for *dCirl^{KO}* animals.

Figure 19B indicates that both point mutations reliably disable GPS-mediated autoproteolysis of dCIRL. Thus, behavioral differences seen in *dCirl^{T>A}* larvae may result from functional deficits, rather than the cleavage disability of the receptor itself. This is in line with the fact that the threonine at the +1 position of the GPS constitutes also the first amino acid of the putative tethered agonist *Stachel* and that mutation of this residue interferes with its agonistic activity. Thus, sensation of gentle touch seems to require an intact *Stachel* sequence, but not autoproteolysis itself. In con-

trast, larval locomotion is governed independent from both receptor cleavage and the tethered agonist, which is surprising as both processes rely on intact mechanosensation modulated by dCIRL in chordotonal neurons (Scholz et al., 2015; Scholz et al., 2017). Experiments using cell-specific expression of *dCirl^{T>A}* and *dCirl^{H>A}* in chordotonal neurons could probably help answer the question about the background of this differential behavior.

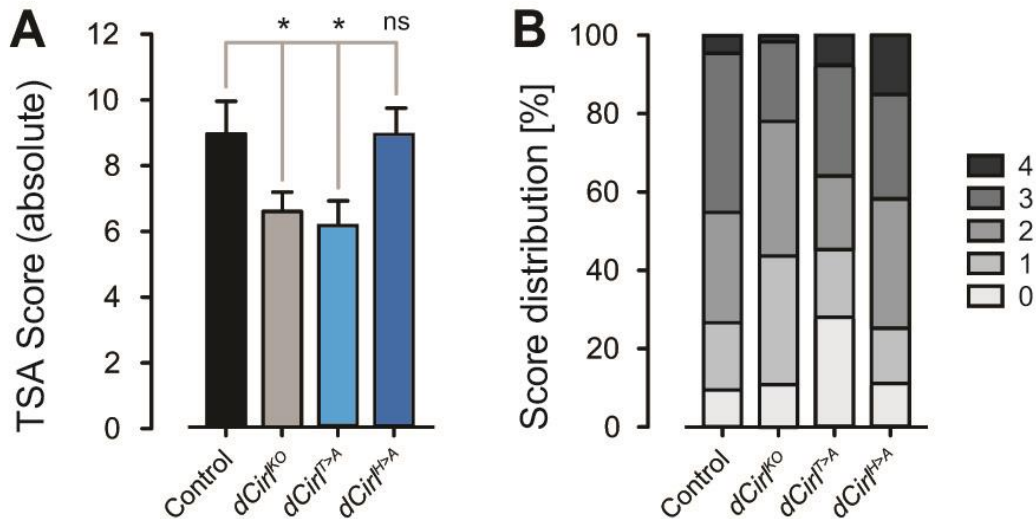


Figure 21. *dCirl^{T>A}* shows impaired sensitivity toward gentle touch. (A) Averaged results from testing the touch sensitivity paradigm displayed as sum of four-fold scoring (0-4) of individual larvae (for description of the assay and protocol see 4.4.4 on page 28). While *dCirl^{H>A}* animals behave normally, *dCirl^{T>A}* larvae show impaired touch sensitivity that is comparable to *dCirl^{KO}*. n=16 per genotype. Data are presented as mean \pm SEM. (B) Distribution of individual scores.

5.3.4 dCIRL trafficking does not rely on GPS autoproteolysis

To investigate whether GPS-mediated proteolysis affects receptor trafficking, expression levels or subcellular localization, VNCs and CHOs of transgenic animals that express cleavage-deficient mRFP/Flag-tagged dCIRL variants were analyzed utilizing microscopic techniques.

Stained with an antibody against the extracellular mRFP epitope, confocal microscopy revealed similar expression patterns of the different GPS variants in the larval VNC (**Figure 22**). The staining is most prominent in the neuropile, as already shown before, and the localization of the signal is largely unaffected by the loss of receptor autoproteolysis. However, the mRFP signal intensity of *dCirl^{H>A}* appeared mildly diminished when compared to the other genotypes suggesting a lower expression level, a fact that has already been found by western blot analysis in **Figure 19**.

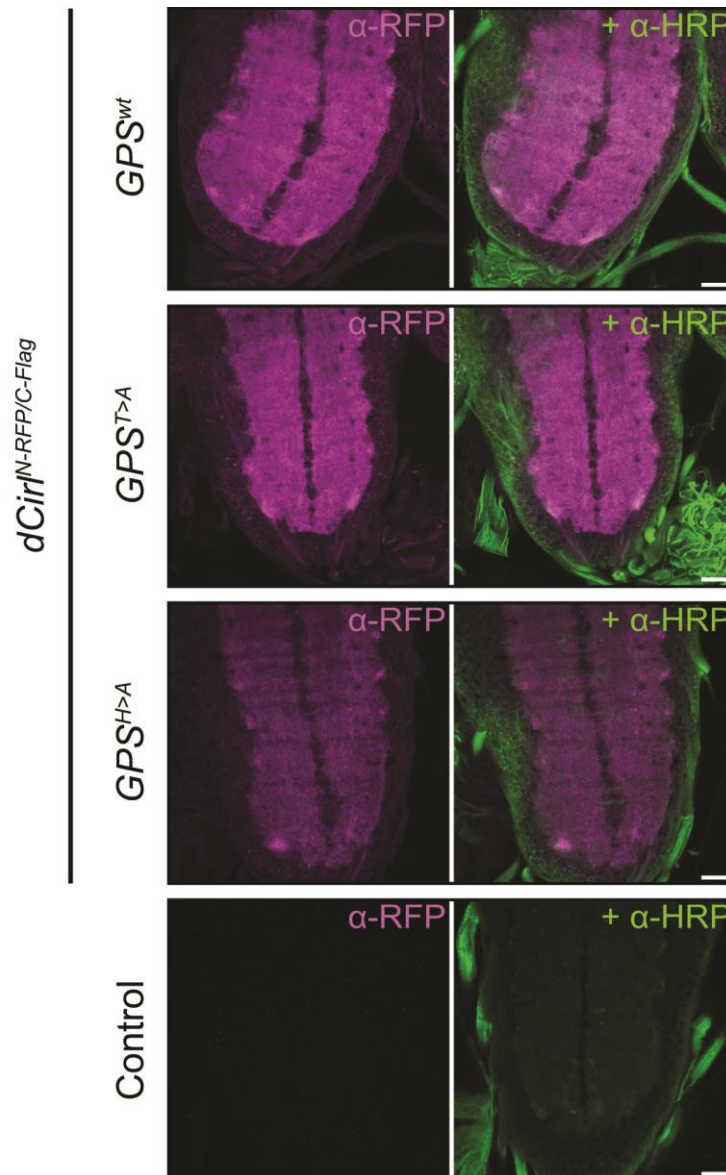


Figure 22. *dCirl* expression in the VNC is unaffected by the loss of GPS cleavage. Maximal projections of confocal images of larval VNCs show *dCirl*^{N-RFP/C-Flag} expression in wildtype and cleavage-defective GPS. mRFP is stained in magenta, counterstaining against HRP in green. Cleavage-deficient and wt dCIRL localizes similarly. Scale bar 20 μ m.

Next, the impact of GPS cleavage-deficiency on dCIRL expression and localization in chordotonal neurons of pentascolopodial organs was analyzed. Super-resolution imaging presented in **Figure 23** indicates proper protein synthesis of unproteolyzed dCIRL in CHO neurons. Similar to normally cleaved receptors, dCIRL^{T>A} and dCIRL^{H>A} are trafficked into cilia and distal dendrites, where they localize in a patchy manner alongside neuronal membranes. Compatible with findings in VNC stainings, the dCIRL^{H>A} signal seems to be reduced in CHOs, too. Although the expression

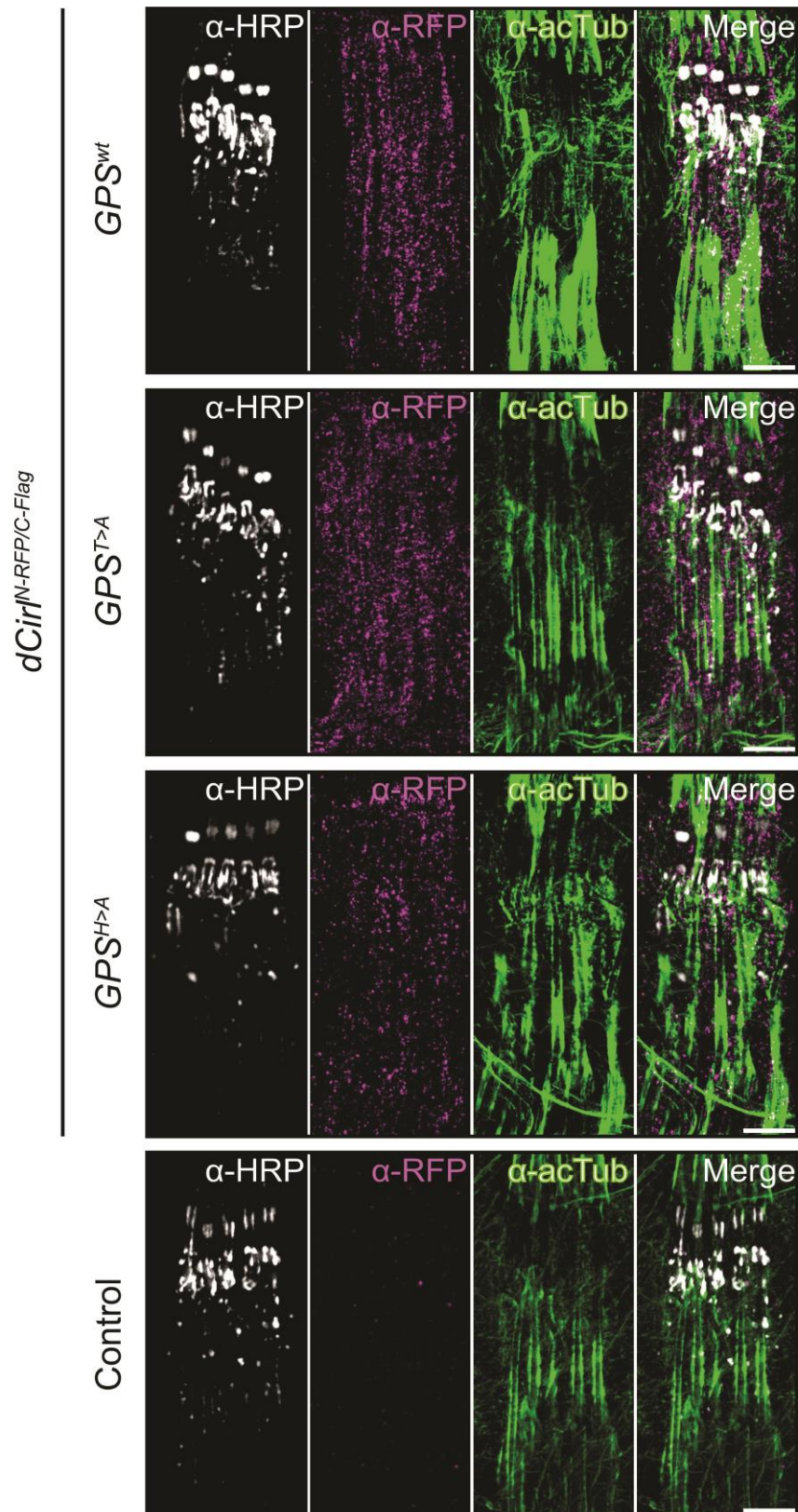


Figure 23. dCIRL trafficking in CHO neurons does not rely on intact GPS autoproteolysis. Maximal projection of SIM images showing *dCIRL^{N-RFP/C-Flag}* expression of wildtype and cleavage-defective GPS. mRFP in magenta, HRP in white, acetylated tubulin in green. The protein is trafficked into dendrites and cilia, regardless of autoproteolytic receptor cleavage. Scale bar 5 μ m.

level has not been statistically quantified, the consistency of biochemical and immunohistochemical results may hint to altered protein levels in *dCirl^{H>A}* larvae.

In summary, two previously described GPS mutations were inserted into the *dCirl* allele, creating two proteolysis-deficient receptor variants, *dCirl^{T>A}* and *dCirl^{H>A}*. Subsequent to the biochemical verification of cleavage-deficiency, *dCirl^{H>A}* proved to rescue the behavioral phenotypes exhibited by knock-out larvae, indicating unaffected receptor function. In contrast, *dCirl^{T>A}* expressing animals display decreased touch sensitivity, probably due to reduced *Stachel* activity, which, however, does not affect locomotion. Immunohistochemical analysis of GPS-mutated *dCirl* larvae showed receptor localization similar to *GPS^{wt}* animals, but seemingly lower expression levels of *dCirl^{H>A}*. This, though, does not appear to affect the function of chordotonal organs, as the behavioral phenotypes are fully rescued. Altogether, these results indicate that GPS autoproteolysis is dispensable for dCIRL function *in vivo*.

5.4 Structural analysis of extracellular dCIRL motifs

5.4.1 The IRH region of dCIRL is heavily glycosylated

To gain further insights into the structural properties of dCIRL's NTF, and particularly its adhesion domains, further *dCirl* constructs were created. The Olfactomedin-like (OLF) domain constitutes the only domain that has been identified exclusively in vertebrate Latrophilins (Langenhan et al., 2009). Biochemical analyses indicate that the OLF domain plays a pivotal role in ligand binding (Boucard et al., 2012; Jackson et al., 2015). Therefore, it is interesting to interrogate the structural correlate of dCIRL's adhesive properties and to understand if any domains in the NTF of dCIRL substitute for the absence of the OLF domain.

To this end, structural analyses of the linking region between RBL and HRM folds, where the OLF domain is located in Latrophilin-1, -2 and -3, were performed. The corresponding region in dCIRL was termed IRH ("Inter-RBL-HRM"; **Figure 24A**).

First, a *dCirl-IRH* construct for the expression of the encoded protein in HEK293T cells was engineered. Samples of the produced protein were isolated and analyzed in SDS-PAGE and western blot. dCIRL-IRH was C-terminally fused to a 6xHistidine-tag, to enable its specific immunohistochemical detection (**Figure 24B**). The detected band appears very wide and ranges between 28 and 39 kDa, which may indicate heterogeneity of proteins in the sample.

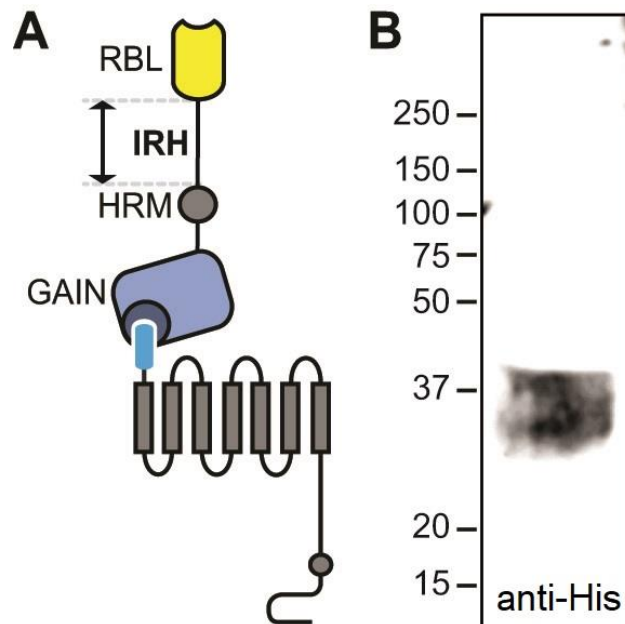


Figure 24. The IRH region is part of dCIRL's NTF. (A) Schematic representation of dCIRL's extracellular domains. The protein region comprising the OLF domain in vertebrate Latrophilins has been termed IRH. (B) Western blot analysis of dCIRL-IRH protein, which was heterologously expressed in HEK293T cells, using His antiserum.

According to online protein analysis tools (e.g. <http://protcalc.sourceforge.net/>), the molecular mass for dCIRL-IRH including the 6xHis-tag was 24.74 kDa, which differs from the protein detected in the western blot analysis.

Excessive glycosylation may explain the deviation of the experimentally determined molecular weight from its theoretical value, as glycosylation represents an abundant form of posttranslational modification. In order to test this hypothesis and the extent of potential carbohydrates linked to dCIRL-IRH, two deglycosylating enzymes were used: first, Endoglycosidase F, which cleaves high mannose and some hybrid oligosaccharides from N-linked (linked to a nitrogen atom) glycoproteins, and second PNGase F, which additionally removes some more complex N-linked oligosaccharides (Maley et al., 1989). O-linked (linked to an oxygen atom) carbohydrates remain unaltered by both enzymes.

The deglycosylated protein samples were compared on an SDS gel stained with a triphenylmethane dye (Coomassie) shown in **Figure 25**. It shows considerably more unspecific bands than **Figure 24B**, which may be explained by the fact that Coomassie stains all proteins present, which includes contaminants remaining from the cell culture medium, while the 6xHis-antibody specifically detects heterologously expressed dCIRL-IRH.

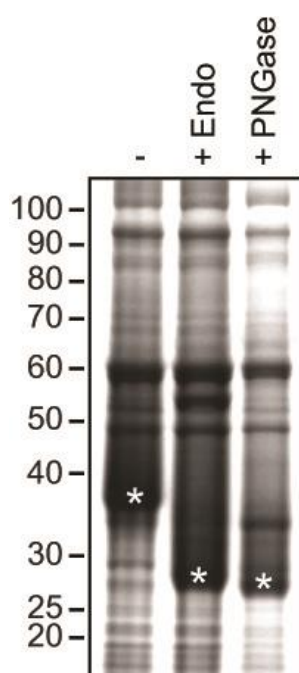


Figure 25. dCIRL-IRH is heavily glycosylated. Heterologously expressed IRH was analyzed for glycosylation. The left lane shows untreated protein stained with Coomassie, the middle and right lanes show protein after deglycosylating reactions with Endoglycosidase F and PNGase F, respectively. The blot shows unpurified protein samples, the bands that correspond to dCIRL-IRH are marked with asterisks.

The untreated IRH in the left lane indicates a molecular weight between 35 and 40 kDa, which is consistent with previous data. In contrast, the deglycosylation of samples with Endo H in the middle and PNGase F in the right lane reduces the IRH weight to ~ 27 kDa. The remaining difference in molecular mass of ~ 3 kDa may be due to the persisting saccharides, as both enzymes are incapable of removing the attached carbohydrates completely.

In sum, dCIRL-IRH seems to be heavily glycosylated. However, one has to keep in mind that the protein is expressed heterologously and that the glycosylation machineries in insects and mammals are substantially different (Rendić et al., 2007), which renders the determined molecular weight of carbohydrates linked to IRH imprecise. However, if the IRH is glycosylated in mammalian cells, it is conceivable that this is true also for endogenously expressed dCIRL-IRH.

To further investigate the properties of dCIRL-IRH as a glycoprotein and to determine its absolute molar mass, highly purified protein samples were used for a conjugate analysis using Size Exclusion Chromatography with Multi-Angle Light Scattering (SEC-MALS; **Figure 26**). This technique combines a SEC column to separate molecules strictly based on their size, and MALS, which determines the molar mass of the eluted proteins and therefore allows precise molecular weight measurements of proteins and complexes, independent of their conformation or interactions with the column.

This analysis shows a maximal molecular mass of values up to 34.18 kDa, the estimated amount of carbohydrates ranged between 0 and 2.74 kDa. As larger molecules are eluted first from the SEC column, the most glycosylated IRH molecules were analyzed first, while later portions of the eluate did not contain any carbohydrates. Strikingly, conjugate analysis revealed that the extent of glycosylation of heterologously expressed dCIRL-IRH is inconstant. This is only little surprising considering the translation of IRH peptide chains in HEK293T cells and their following glycosylation as an enduring process. Furthermore, the incomplete glycosylation might be a result of the limited capacity of glycosylating enzymes paired with a high-copy protein expression.

Interestingly, the absolute molecular weights determined from SEC-MALS analysis slightly differ from the values obtained from the deglycosylation assays (**Figure 25**). Still, both data sets can be considered compatible, as SEC-MALS conjugate analysis only provides a calculation based on the estimated number of glycosylated residues obtained from sequence predictions, which is hardly exact. In addition, even the absolute molecular weight of the theoretically constant protein share deviates up to 4 kDa, which means that measurement errors cannot be excluded.

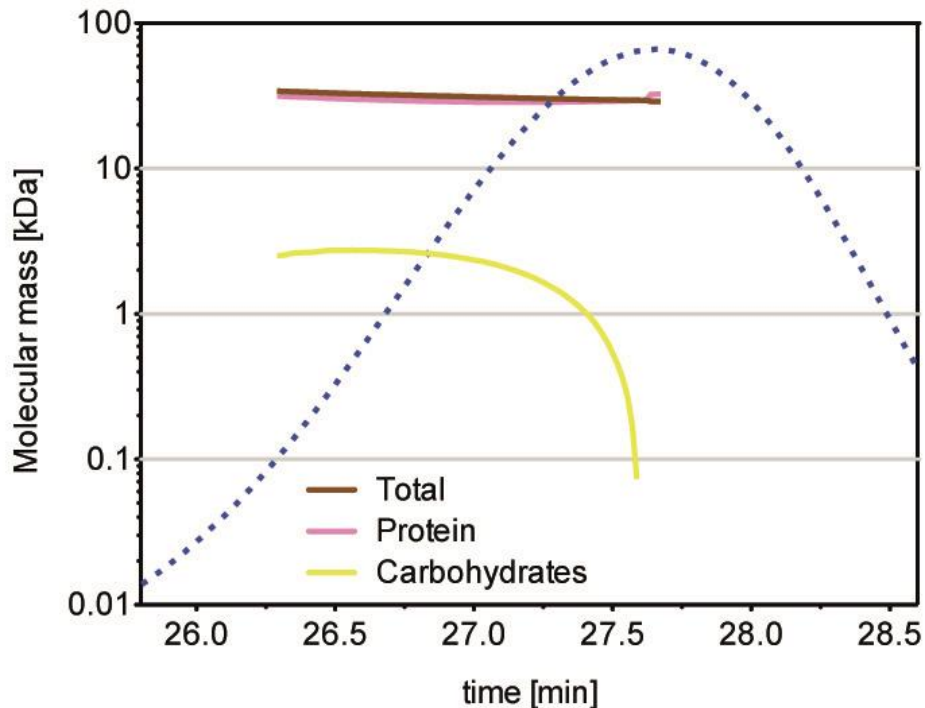


Figure 26. The extent of glycosylation of the IRH is inconstant. The composition of IRH containing samples was analyzed via SEC-MALS. The absolute amount of carbohydrates and peptides are indicated in yellow and pink, respectively; the total molecular weight of the glycoprotein is shown in red. The blue dotted curve symbolizes the relative amount of IRH molecules eluted from the column with a maximum concentration at 27.7 min. The most glycosylated IRH molecules were analyzed first, while later portions of the eluate did not contain any carbohydrates.

Taking all results into consideration, dCIRL-IRH seems to be highly glycosylated, although this has solely been tested with heterologously expressed protein so far.

5.4.2 dCIRL-IRH follows the random coil model

Like glycosylation, secondary structures contribute to local structural properties and dynamic functions of proteins. The most common types of secondary protein structures are alpha helices and beta sheets. The OLF domain in Latrophilin-3 (LPHN3-OLF), for example, consists of 20 beta sheets, which are arranged in a very compact manner and thus lend the domain its characteristic shape (Jackson et al., 2015).

For the analysis of putative secondary structures in dCIRL-IRH, circular dichroism (CD) spectrophotometry was used. This technique can provide evidence for the

presence of alpha or beta structures in a purified sample utilizing the chirality of proteins. The result of the CD analysis of IRH is shown in **Figure 27**.

Ellipticity θ forms a spectrum characteristic for dCIRL-IRH. It barely reaches positive values and exhibits a minimum peak at around 199 nm. The shape of this spectrum is ultimately determined by the amount of alpha helices or beta sheets present, as these structures introduce specific features to the CD spectrum of proteins.

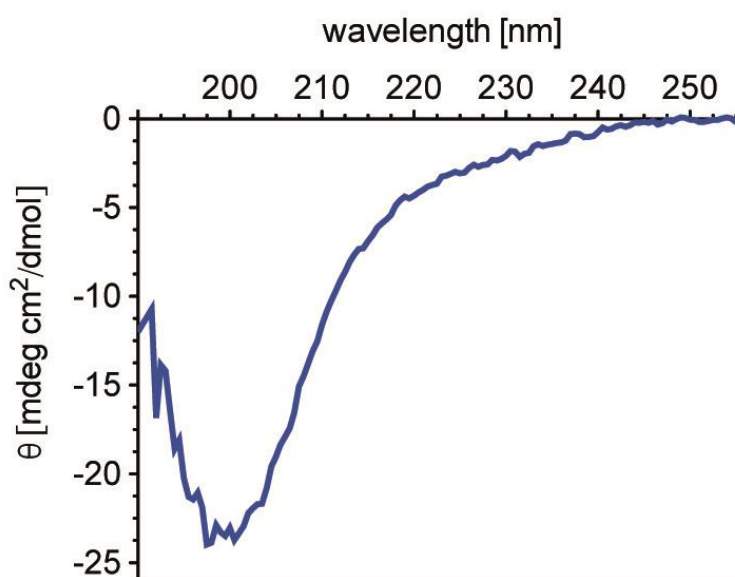


Figure 27. dCIRL-IRH follows the random coil model. Ellipticity θ is displayed as a function of the UV wavelength and forms a spectrum characteristic for dCIRL-IRH. The diagram shows averaged results from three independent experiments. Standard CD spectra are shown in Figure 8 (page 33).

Standard curves for proteins that exclusively consist of alpha helices or beta sheets, respectively, are shown in **Figure 8** (page 33). Comparison of the IRH spectrum presented in **Figure 27** with these model curves shows the resemblance of the IRH with a random coil protein structure. For the interpretation of secondary structures not the absolute θ values, but rather the shape and location of the peaks are relevant. The random coil model is based on the fact that the constant existence of preferred secondary structures within the protein cannot be proved, although this does not exclude residual or temporary conformations. However, the only fixed connections between the amino acids are the peptide bonds of adjacent residues (Smith et al., 1996).

Finally, CD spectrophotometry suggests that the IRH comprises an unstructured region within the NTF of dCIRL, which opens exciting avenues for its function and impact on cell biology to be discussed below.

5.4.3 The IRH is a large and elongated region in dCIRL's NTF

Dynamic Light Scattering (DLS) is a technique commonly employed for the experimental estimation of the size of macromolecules such as proteins. More explicitly, this method allows the calculation of the hydrodynamic radius R_h of single molecules according to the fluctuation intensity of the laser beam, which is scattered when it hits the solvated particles. The R_h value itself must not be equalized with the apparent physical radius, but offers valuable insights in the structural dimension of the molecule of interest.

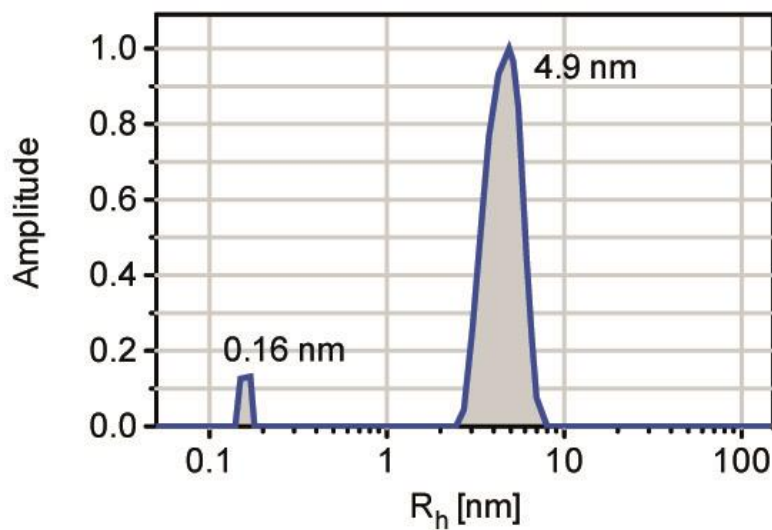


Figure 28. The IRH exhibits a large dimension. The hydrodynamic radius R_h of dCIRL-IRH was obtained from DLS experiments. The diagram shows the distribution of the data acquired in ten DLS runs.

DLS analysis of dCIRL-IRH protein samples (**Figure 28**) offers two R_h values: 4.9 and 0.16 nm, with the amplitude of the second DLS signal being depicted with respect to the 4.9 nm peak. The peak at 0.16 nm may be attributed to a contamination in the sample buffer. Thus, the value of 4.9 nm seems to correspond to dCIRL-IRH (hydrodynamic diameter of 9.8 nm). As stated above, this theoretical parameter does not represent the actual size of the molecule, but rather indicates the dimension of size and shape.

Although extensive glycosylation of the IRH may cause an increase in the R_h value, 4.9 nm may still be considered huge for a glycoprotein of a molecular mass less than 40 kDa (Erickson, 2009). In comparison, LPHN3-OLF, which exhibits a similar molecular weight as the IRH, measures only 3-4 nm in diameter (Jackson et al., 2016). Considering that OLF is a neatly packed domain, the result of a more than

twofold larger size suggests an elongated rather than a spherical, ordered structure for dCIRL-IRH, which corroborates the results from CD experiments (**Figure 27**) agreeing with a random coil protein structure.

To further confirm the hypothesis that dCIRL's IRH adopts an elongated and unstructured region, the heterologously expressed protein was analyzed via Size Exclusion Chromatography and Multi-Angle Light Scattering (SEC-MALS).

Primarily, SEC-MALS is a technique used to determine molecular weights, but as a gel filtration displays a crucial part of the experiment, it also offers a comparative structural analysis of different proteins. The employed proteins are separated according to their interaction with the gel matrix, which mainly informs about size and shape. This allows, together with the molecular weight, a comparison of their structural dimensions.

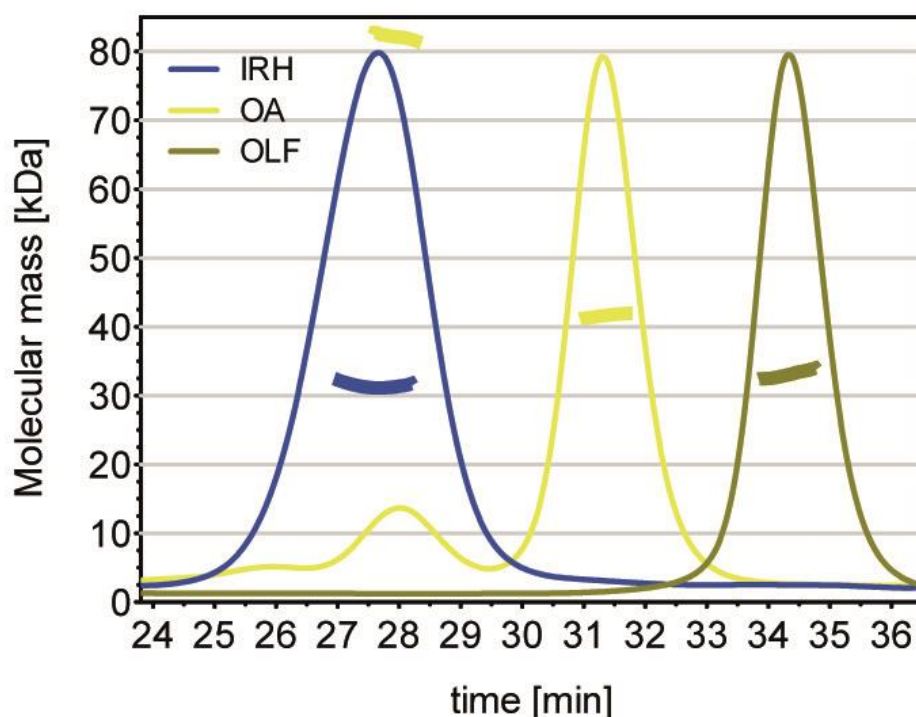


Figure 29. dCIRL-IRH is a large and elongated region in the receptor's NTF. Protein samples of dCIRL-IRH, Ovalbumin (OA) and LPHN3-OLF were analyzed via SEC-MALS to compare their structural properties. The thin curves display the elution of the proteins as a function of their retention time in the column, the thick curves mark the molecular weight of the respective protein fraction.

The results of the SEC-MALS analysis of dCIRL-IRH, Ovalbumin as a protein standard and LPHN3-OLF are presented in **Figure 29**. The thin curves in the diagram indicate the relative concentration of the respective protein in the eluate as a

function of time. As small molecules tend to interact more excessively with the gel matrix, they need more time to pass the column. LPHN3-OLF (green) is eluted last of the three proteins (maximum concentration at 34.5 min), which suggests it is the smallest of the three. The graph of Ovalbumin (yellow) shows three peaks of increasing amplitude, which is due to the fact that Ovalbumin not only exists as monomer, but also forms oligomeric complexes. Yet, the majority of Ovalbumin molecules is found in the monomeric fraction (31.5 min) rather than in dimeric (28 min) or trimeric (26 min) complexes.

The protein of major interest for this study, dCIRL-IRH (blue), reaches its maximum concentration in the eluate after 27.7 min. A larger mean variation can be noticed comparing IRH with the other analyzed proteins, suggesting that the sample consisted of less uniform molecules, probably due to an unstable extent of glycosylation as indicated by the conjugate analysis.

As a second feature in **Figure 29**, the thick curves represent the identified molecular weight of the respective eluted protein fraction, for instance a value of ~ 32 kDa for OLF and 31 kDa for IRH.

Taking a closer look at these results, various conclusions can be drawn from the SEC-MALS analysis: foremost, the experiment seems to deliver authentic values, as for example the MW of monomeric Ovalbumin (41 kDa) is – aside from a minimal measurement error – consistent with its theoretical value of 42.7 kDa. The fact that the determined MW of dimeric Ovalbumin (82 kDa) is exactly twice as high as the one of the monomer further substantiates the experiment's reliability. The dimensions of the three proteins can be categorized. Both Ovalbumin and LPHN3-OLF are densely structured: Ovalbumin adopts a serpin-like structure in an ellipsoidal shape with dimensions of approximately 7 x 4 x 5 nm (Stein et al., 1991), while OLF forms a rather spherical structure with a diameter of 3-4 nm (Jackson et al., 2016). Comparing these values, it is not surprising that Ovalbumin is eluted prior the OLF due to its increased size. dCIRL-IRH is eluted before Ovalbumin dimers, which suggests an even larger dimension despite having the least MW.

Overall, the structural analyses of the IRH indicate that this extracellular region of dCIRL is excessively glycosylated, though the precise extent of carbohydrates *in vivo* is hard to define due to heterologous expression. Furthermore, the IRH seems not to contain any fixed secondary structures but follows the random coil model. Random coils lack alpha helices or beta sheets, however, this structural configuration determines the stability and flexibility (Thornton, 1992; Smith et al., 1996) and may thus have a crucial impact on functional aspects of the receptor. Finally, the IRH seems to have a large dimension compared to other (folded) proteins with simi-

lar molecular weight such as the vertebrate equivalent OLF. These findings are in line with and also impact each other: defined secondary structures usually lead to a reduced size in proteins (Thornton, 1992), which explains why the random coil IRH appears so capacious. Further, the numerous carbohydrates linked to the protein may further enhance the dimension of the domain.

6. Discussion

The physiological function of the GAIN domain and the autoproteolytic properties of the GPS have been subject of intense discussions in the aGPCR field over the last years. This study was set out to provide visual proof of endogenous *dCirl* expression, as well as insights into the role of GPS autoproteolysis in dCIRL function *in vivo*. Furthermore, the structure of dCIRL's ECD was analyzed to contribute to the understanding of the proposed molecular signaling mechanism of dCIRL/Latrophilin.

6.1 dCIRL function in *Drosophila*'s central nervous system

A variety of aGPCRs are expressed in the nervous system throughout many different species (Strokes and Piao, 2010; Hamann et al., 2015; Langenhan et al., 2016), indicating their significance for the function of the CNS and PNS. Accordingly, previous studies revealed dCIRL and vertebrate Latrophilin localization in different neuronal tissues (V. G. Krasnoperov et al., 1996; Lelianova et al., 1997; Gehring, 2014; Scholz, 2015), consistent with findings from this study on *dCirl* expression in *Drosophila* larvae.

A property apparent in all experiments was the low signal intensity of dCIRL when expressed from the endogenous locus. Weak expression has also been observed for other aGPCRs, such as LAT-1 in *C. elegans* (Langenhan et al., 2009) or GPR126 (Waller-Evans et al., 2010), and might be one of the reasons why their microscopic visualization *in vivo* is challenging. Fortunately, signal amplification using polyclonal antibodies helped reveal broad dCIRL distribution throughout the larval VNC, where it was most prominent in the synapse-rich neuropile, but also in somata of the lateral cortex. Furthermore, utilizing super-resolution imaging, *dCirl* expression was detected at the presynaptic side of larval NMJs and at the level of distal dendrites and cilia of peripheral chordotonal neurons.

Other aGPCRs found in neural cells include members from different families: CELSR1, for example, localizes to adherens junctions in the embryonic neural plate and plays a crucial role during neural tube closure (Curtin et al., 2003; Nishimura et al., 2012). Accordingly, mutations in CELSR1 lead to severe neural tube defects (Allache et al., 2012; Robinson et al., 2012; Lei et al., 2014). Studies on the invertebrate CELSR orthologue Flamingo (FMI) revealed further involvement in the regulation of dendrite morphology and axon guidance in the CNS and PNS (Gao et al., 1999; Sweeney et al., 2002; R. C. Lee et al., 2003; Senti et al., 2003; Kimura et al., 2006). Interestingly, during VNC formation only the CTF is required for pathfinding of the pioneer axons, while follower axons require only the NTF of FMI-1 (Steimel et

al., 2010), which suggests differential signaling mechanisms of the same receptor depending on the expressing subpopulation of neurons.

Similar to CELSR, GPR56 is also involved in the regulation of neuronal migration. In the cerebral cortex, activation of GPR56 through binding ECM-bound collagen III at the pial surface results in the inhibition of neuronal migration and thus correct cortical lamination (Luo et al., 2011). In contrast, mutations in GPR56 lead to overmigration and penetration of the pial basement membrane (S. Li et al., 2008; Bahi-Buisson et al., 2010; Langenhan et al., 2016). In humans, this defect was causally linked to a disorder referred to as bilateral frontoparietal polymicrogyria (BFPP), signified by cortical malformation. Hence, patients suffer from mental retardation, language impairment, motor disability and is often associated with epilepsy (Piao et al., 2004; Piao et al., 2005; Jeong et al., 2012).

aGPCR expression is not restricted to the CNS. For example, beside localization in heart, lung and endothelia (Moriguchi et al., 2004), GPR126 expression was found in Schwann cells (Monk et al., 2009; Monk et al., 2011). These specialized glial cells form multilayered myelin sheaths around the axons of peripheral nerves, serving electrical insulation. GPR126 was shown to signal through Gas to modulate the terminal differentiation and initiation of the myelination process of these cells and is thus indispensable for myelinogenesis (Glenn and Talbot, 2013; Mogha et al., 2013; Sigoillot et al., 2016). Similar to FMI-1, domain-specific functions have been proposed for GPR126: while the NTF is necessary and sufficient for radial axon sorting, the CTF promotes Schwann cell wrapping to form myelin through second messenger cascades. This dual role was shown to depend on the mechanical stimulation of GPR126 through its endogenous ligand, Laminin-211 (Petersen et al., 2015).

Several other aGPCRs are expressed in neuronal tissues and have been assigned different functions in the nervous system (McMillan et al., 2002; Kee et al., 2004; Weston et al., 2004; Collins et al., 2006; Selimi et al., 2009; Knapp and Wolfrum, 2016). What they all have in common is the fact that they are key regulators in the early development of the nervous system, giving rise to the question whether dCIRL might also be involved in developmental processes, similarly to LAT-1 and mammalian Latrophilins (Langenhan et al., 2009; O'Sullivan et al., 2012; Anderson et al., 2017).

Earlier studies on *dCirl* expression in adult *Drosophila* revealed signal enrichment in somata-dominated regions of the fly brain, but absence of dCIRL in the synapse-rich neuropile (Gehring, 2014; Scholz, 2015). This represents an expression pattern inverse to the one found in larval VNCs.

Differences in the characteristic expression profile throughout development have been described for other aGPCRs. BAI3 levels, for instance, reach their peak during

neonatal development, but afterwards decrease to persist at low levels during adulthood. Furthermore, BAI3 distribution seems similar to the one of BAI1 and BAI2 in the adult CNS, but completely different in developmental stages (Kee et al., 2004). Similar findings have been obtained from studies on CELSR1-3, in that each homolog has its own characteristic expression profile with a distinct localization during development (Shima et al., 2002).

Differences between larval and adult *dCirl* expression patterns in the fly CNS might be due to neural reorganization during maturation, which mainly consists of programmed cell death and the addition of new, adult-specific neurons (Truman, 1990). It is conceivable that dCIRL, like vertebrate Latrophilin-1 and -3, is involved in synaptogenesis and synapse regulation, which would offer an explanation for its broad distribution throughout the larval neuropile but decreased dCIRL levels in adults. dCIRL's putative function in synaptic transmission would also be consistent with its localization to the presynaptic, neuronal side of larval NMJs as shown in 5.2.3 and 5.2.4. Interestingly, in contrast to GPR56 or FMI, loss of *dCirl* (*dCirl^{KO}*) does not lead to morphological alterations of the nervous system (Gehring, 2014; Scholz, 2015; Scholz et al., 2017). A single structural abnormality identified in *dCirl^{KO}* animals is the enlargement of the postsynaptic subsynaptic reticulum accompanied by increased Discs-large (DLG) levels (Gehring, 2014; Scholz, 2015). How dCIRL affects muscle morphology in this case has yet to be investigated.

However, *dCirl^{KO}* animals develop normally and do not show increased lethality (Scholz et al., 2015), which suggests that dCIRL plays only a minor role in the development of *Drosophila's* nervous system, if at all. This is even further corroborated by the fact that also for chordotonal neuron development and morphology, *dCirl* seems dispensable (Scholz et al., 2015), implicating that dCIRL's physiological role in *Drosophila* indeed lies beyond development.

6.2 Tethered agonism and versatile signaling modes for Latrophilin

The physiological role of dCIRL autoproteolysis at the GPS was analyzed utilizing two cleavage-deficient receptor variants, dCIRL^{T>A} and dCIRL^{H>A}, which were both tested *in vivo*. Larvae expressing the *dCirl^{T>A}* variant exhibited impaired sensitivity toward gentle touch, usually governed by dCIRL in CHOs (Scholz et al., 2015). In contrast, the behavior of *dCirl^{H>A}* animals was unaffected, leading to the conclusion that GPS proteolysis is not essential for dCIRL function in chordotonal neurons. This was further corroborated by results from electrophysiological recordings of chordotonal neurons, where dCIRL^{H>A}, but not dCIRL^{T>A} sufficed to provide wildtypic receptor currents upon mechanical stimulation (Guan, 2016; Scholz et al., 2017).

These findings could be explained by the fact that the threonine mutated in dCIRL^{T>A} also constitutes the first residue of the tethered agonist (Liebscher et al., 2014b; Stoveken et al., 2015) and that its mutation abolishes dCIRL's activation and thus mechanosensory function. After having been shown for several other aGPCRs including the *C. elegans* homolog LAT-1 (Müller et al., 2015; Liebscher and Schöneberg, 2016), these results provide the first evidence that also dCIRL activation is mediated through the tethered agonist *Stachel*.

Receptor activation is initiated through a yet to be defined interaction of the *Stachel* with the 7TM domain, which is likely induced through conformational changes of the GAIN domain and maybe the ECD (Liebscher et al., 2014b; Petersen et al., 2015; Liebscher and Schöneberg, 2016). Therefore, deletion of the NTF of GPR126 and GPR133 may lead to activation of the receptor due to exposure of the tethered agonist (Liebscher et al., 2014b). The fact that the NTF may act as an inverse agonist on CTF signaling, and that removal of the NTF induces aGPCR signaling had been uncovered earlier (Paavola et al., 2011; Yang et al., 2011). However, this study demonstrates that GPS proteolysis is not a prerequisite for *Stachel*'s agonistic effect on dCIRL, which is consistent with earlier results proving that uncleaved GPR126 and GPR133 can be activated by synthetic *Stachel* peptides (Liebscher et al., 2014b) and that autoproteolysis is dispensable for LAT-1 function in *C. elegans* embryogenesis (Prömel et al., 2012). The addition of synthetic peptides seems to induce aGPCR activation even more efficiently than the deletion of the NTF (Demberg et al., 2015), underlining the hypothesis that GPS autoproteolysis might be of minor importance for aGPCR activation through the tethered agonist.

Sequential mutagenesis of several aGPCRs revealed that the N-terminal half of the *Stachel* (including the threonine mutated in dCIRL^{T>A}) confers its agonistic activity, while the C-terminal part seems to mediate the molecular interaction with the 7TM domain (Liebscher et al., 2014b; Wilde et al., 2016). This is compatible with findings from sequence alignment studies of aGPCRs from different subfamilies, which uncovered a common genomic organization for this core region directly downstream of the GPS cleavage site (Wilde et al., 2016). Thus, it is not surprising that synthetic *Stachel* peptides are capable of cross-activation (Demberg et al., 2017), resulting in experimental problems regarding specificity of aGPCR activation *in vivo*.

Interestingly, the model of a tethered agonist that is liberated upon receptor cleavage is not exclusive to aGPCRs: protease-activated receptors (PARs) are other members of the GPCR superfamily and play a key role in the regulation of platelet aggregation (Davey and Luscher, 1967; Sambrano et al., 2001). For activation of PAR1, the serine protease thrombin cleaves the ectodomain of the receptor, which then exposes a tethered agonist in the new N-terminus (Vu et al., 1991a). The ago-

nist then structurally interacts with the 7TM domain of PAR1 to initiate intracellular signaling (Vu et al., 1991a; Vu et al., 1991b; Hammes and Coughlin, 1999).

Additional results from the study presented here suggested that membrane targeting and correct intracellular trafficking of dCIRL rely neither on autoproteolysis, nor on an intact *Stachel* sequence, which is in line with previous findings for other aGPCRs (Liebscher et al., 2014b). Further, the locomotion phenotype was fully rescued in both cleavage-deficient *dCirl* variants, suggesting that this part of dCIRL function remains unaffected by mutation of the tethered agonist. This behavior could easily be explained by the existence of more than only one possible signaling pathway of dCIRL in chordotonal neurons. Autoproteolysis- and/or *Stachel*-independent signaling, alongside the *Stachel*-dependent mechanism proposed for dCIRL by the TSA results, is not a new concept for the aGPCR class.

Studies on BAI1 showed robust signaling activity, even when the majority of its ECD (including the tethered agonist) was deleted (Stephenson et al., 2013; Kishore et al., 2016). In some assays, BAI1 was even more active when truncated (Kishore et al., 2016), suggesting a different mode of activation for this aGPCR. Similar experiments with GPR56 provided mixed results: removal of the *Stachel* region impaired receptor activity in some signaling assays, while on others it had only very little effect (Kishore et al., 2016). This might indicate that the tethered agonist is required for certain aspects of GPR56 signaling, but dispensable for others. A different study proposed that binding of a ligand to the ECD of GPR56 is directly sensed by the 7TM domain, which may lead to the regulation of its signaling activity independently from the *Stachel* sequence (Salzman et al., 2017).

Although it has been suggested that GPS autoproteolysis is not required for *Stachel*-mediated activation of some aGPCRs (Liebscher et al., 2014b; Scholz et al., 2017), several studies raise doubts that exposure of the tethered agonist is possible without NTF shedding or at least substantial structural deformation (Kishore and Hall, 2016; Kishore et al., 2016; Salzman et al., 2017), as it is buried within the hydrophobic core of the GAIN domain (Arac et al., 2012; Salzman et al., 2016). GPS proteolysis may provide the perfect mechanism to allow these structural changes leading to the release of the *Stachel* sequence, which gave rise to the hypothesis that autoproteolysis is a prerequisite for mechanical shedding of the NTF and thus *Stachel*-mediated signaling. As not all aGPCRs undergo receptor cleavage at the GPS, and as cleavage-competent aGPCR homologs may not always be completely proteolyzed (Iguchi et al., 2008; Nieberler et al., 2016), the necessity of a second signaling mode independent of proteolysis and *Stachel* exposure is widely suspected.

A different model suggests that ligand binding could elicit internal force upon the *Stachel* region leading to a conformational change in the C-terminal half of the tethered agonist granting it its full agonistic competence (Stoveken et al., 2015). This mechanism could provide aGPCR activation through the tethered agonist regardless of their autoproteolytic behavior at the GPS.

Which of these models prevails, if and how the *Stachel* is released and how it activates receptor signaling remains controversially discussed. Future studies will have to identify the yet unknown interaction with the 7TM domain and further investigate in detail the *Stachel*-dependent and -independent signaling modes for this receptor class.

6.3 Physiological function of GPS cleavage

Some receptors have been shown to critically rely on GPS autoproteolysis to ensure proper signaling, while for the function of others self-cleavage seems irrelevant (V. Krasnoperov et al., 2002b; Chang et al., 2003; Lin et al., 2004; Liebscher et al., 2014a; Nieberler et al., 2016). Polycystin-1, for example, absolutely requires GPS proteolysis in its role in renal function (Yu et al., 2007). Mouse mutants expressing cleavage-deficient Polycystin-1 showed abnormal postnatal renal development apparent in size and weight of the mice, as well as grossly enlarged cystic kidneys and reduced life expectancy (Yu et al., 2007). As knock-out mice display even more severe defects, the observed phenotype can be specifically attributed to GPS-deficiency and not to complete loss of function of Polycystin-1 (Yu et al., 2007; Kurbegovic et al., 2014; Trudel et al., 2016).

The study presented here provides the first evidence – together with additional experiments conducted with the same fly genotypes (Guan, 2016; Scholz et al., 2017) – that GPS proteolysis is not required for dCIRL's mechanosensory faculty in chordotonal neurons of *Drosophila* larvae. But why would cells perform this energetically highly unfavorable reaction? Several hypotheses and roles for GPS proteolysis in aGPCRs have been proposed over the last years.

One of the first models suggested GPS autoproteolysis as a maturation signal during biosynthesis of the aGPCR molecule in the ER (V. Krasnoperov et al., 2002b). This theory derived from the observation that GPS-mutated Latrophilin-1 did not traffic to the plasma membrane (V. Krasnoperov et al., 2002b). However, shortly after, it was shown that other aGPCR members are trafficked independently of receptor proteolysis (Qian et al., 2002; Bohnkamp and Schöneberg, 2011; Prömel et al., 2012). Further studies on Polycystin-1 indicated that its whole CTF, rather than autoproteolysis itself, may act as a cofactor that is necessary for cell surface transport of the

NTF and thus the whole receptor (Yu et al., 2007). The lack of GPS cleavage and the resulting changes in the GAIN domain could alternatively lead to disturbance of the structural integrity of the receptor molecule and consequently impairment of proper membrane trafficking. Additionally, *in vitro* analysis of characteristics of aGPCR autoproteolysis can only offer limited conclusions, as these experimental setups may not provide the regulating factors that have been shown to modify the cleavage including specific cell context or glycosylation (Qian et al., 2002; Hsiao et al., 2009).

A different role for aGPCRs could be assumed comparing GPS cleavage to the autoproteolytic processing of SEA domains in mucins. The SEA domain is a conserved, extracellular protein motif usually found in mucin-like membrane proteins (Khatri et al., 2003; Palmari-Pallag et al., 2005), and intriguingly, in two members of the aGPCR class, GPR110 and GPR116 (Hamann et al., 2015). The SEA domain autocatalytically mediates cleavage in a way that shares many characteristics with GPS autoproteolysis of aGPCRs (Wreschner et al., 2002; Levitin et al., 2005), and like NTF and CTF, the cleaved fragments remain non-covalently associated (Levitin et al., 2005; Macao et al., 2006; Johansson et al., 2009). For mucins, dissociation of the fragments was suggested to occur in response to extracellular mechanical stress to protect the expressing epithelial cell from damage (Macao et al., 2006). According to this hypothesis, loss of the extracellular part of the protein leads to modifications in signaling in order to sense the mechanical shear stress at the mucosal surface (Macao et al., 2006).

With the evolving idea of aGPCRs as mechanosensors (Scholz et al., 2016), a similar role for this class seems conceivable. Most aGPCRs possess a variety of different adhesion domains thought to engage in binding events with interaction partners that are either affixed within the ECM or anchored on nearby cell surfaces (Langenhan et al., 2013). Hence, a possible function of GPS proteolysis and the non-covalent association of NTF and CTF consists in the determination of a force threshold applied to the NTF, above which it is shed and relieved of its adhesive duties (Nieberler et al., 2016). An example from the aGPCR class corroborating this hypothesis is EMR2 expressed on the surface of mast cells. Vibratory stress leads to the dissociation of cleaved NTF and CTF, resulting in degranulation and the release of histamine (Boyden et al., 2016). Similarly, binding of the endogenous ligand CD55 causes shear stress to the ECD of the leucocyte-resident aGPCR CD97 in a circulating blood stream, which leads to NTF shedding and subsequently to a down-regulation of CD97 expression (Karpus et al., 2013).

These two examples described above could also involve exposure of the *Stachel* sequence. How GPS autoproteolysis and NTF shedding may affect the metabotropic signaling status through the tethered agonist is discussed in detail in 6.2.

NTF dissociation from the CTF does not only lead to signaling in the aGPCR-expressing cell, but the soluble NTF may additionally act as a ligand and initiate cell-non-autonomous effects. This has been shown for GPR126, where the NTF suffices to mediate normal heart development, while its CTF – although it contains its metabotropic signaling unit – is dispensable (Waller-Evans et al., 2010; Patra et al., 2013). It was shown that both endocardial cells and cardiomyocytes depend on the presence of the NTF, even though GPR126 is only expressed in endocardial cells. Further studies suggested that GPR126 may employ a paracrine mode in cardiomyocytes, presumably through shedding of the NTF (Patra et al., 2013; Musa et al., 2016). Earlier observations on Latrophilin-1 and EMR2 had indicated that their NTFs are anchored in the plasma membrane independently of the CTFs (Volynski et al., 2004; Silva and Ushkaryov, 2010; Huang et al., 2012). Moreover, single receptor fragments or complete aGPCR molecules were even shown to form homo- and heterogeneric oligomers of a yet unidentified function (Serova et al., 2010).

As described in detail above, many mechanisms have been conceived trying to explain why aGPCRs undergo autoproteolysis at the GPS. What is often disregarded is the fact that aGPCRs are further modified by other forms of proteolytic processing, such as self-cleavage of the SEA domain in GPR110 and GPR116 (see above). Furthermore, several aGPCRs are targets of classical, exogenous proteases like furin or matrix metalloproteinase MMP (Moriguchi et al., 2004; Fukuzawa and Hirose, 2006; Cork et al., 2012). Each of these additional proteolytic sites has been located to the NTF of the receptors, in most cases even N-terminal to the autoproteolytic cleavage sites of GPS and SEA domains. However, Latrophilin-1 has been shown to possess a furin cleavage site C-terminal to the GPS motif between the GAIN domain and the first transmembrane helix (V. Krasnoperov et al., 2009). Proteolytic processing at this location exhibits an efficiency of about 5% and leads to the dissociation of a soluble receptor fragment containing the NTF and a small peptide of the CTF, and thus an intact GAIN domain. It was proposed that this form of two-step processing may represent a means to regulate expression of functional transmembrane and soluble variants of Latrophilin-1 (V. Krasnoperov et al., 2009).

In line with this finding, western blot analysis of protein homogenates from fly brain suggested the presence of a second cleavage site in dCIRL (data not shown). According to the size of the protein band, its location can be estimated close to the GAIN domain, similar to Latrophilin-1. The existence of a second step of proteolytic processing in dCIRL would, of course, set some limitations to the conclusions drawn

from experiments presented here: it cannot be excluded that RFP signals in microscopic images portrayed only a dissociated fragment of the ECD containing the mRFP cassette rather than the whole NTF, even in preparations from GPS cleavage-deficient *dCirl* variants. As dCIRL localization seems not impaired by the loss of GPS autoproteolysis, two scenarios seem reasonable: first, cleaved fragments stay attached upon exogenous proteolysis, which would lead to the immunohistochemical detection of heterodi-/trimeric receptors, assuming NTF and CTF also remain associated. Second, dCIRL is shed at the putative second cleavage site, which leads to dissociation of the mRFP-containing fragment. In this scenario, the anti-mRFP staining would only detect this separated fragment, independent of dCIRL cleavage at the GPS. In order to investigate this question once and for all, a reliable intracellular tag for the investigation of dCIRL in colocalization studies is absolutely necessary.

6.4 Role of the IRH region in dCIRL's mechanosensitive function

The IRH region represents a central part of the NTF of dCIRL. It is located between the N-terminal RBL and its neighboring HRM domain ("inter-RBL-HRM"), at the exact position that is occupied by the OLF domain in vertebrate Latrophilins (Hamann et al., 2015). In Latrophilin-3, the OLF domain holds a binding site for its ligand FLRT, and is critically involved in cell adhesion and repulsion (Jackson et al., 2015; Jackson et al., 2016), consistent with an implication in its regulatory function in synapse development (O'Sullivan et al., 2012). Furthermore, transsynaptic Latrophilin-1 interaction with neurexins is mediated through the OLF domain (Boucard et al., 2012).

With the OLF domain executing crucial roles in ligand binding and neuronal function of vertebrate Latrophilins, the fact that this domain is not conserved in *Drosophila melanogaster* seems inscrutable. FLRT proteins are also not conserved in *Drosophila*, whereas neurexins are critical for the assembly of NMJs in the fly and thereby fulfil important roles similar to those in vertebrates (J. Li et al., 2007; Chen et al., 2010). However, this study provides evidence that there is no structured fold in the IRH region of dCIRL that could substitute for the OLF domain's adhesive properties. This argues against an evolutionary conservation of the Latrophilin-neurexin interaction, which may have developed only in vertebrates (Boucard et al., 2012).

Further analysis of the IRH region revealed excessive glycosylation, though the exact amount of carbohydrates *in vivo* is hard to determine due to heterologous expression of the IRH protein in HEK293 cells. Posttranslational protein modification

through glycosylation in general can account for a variety of crucial functions. Most importantly, many proteins require glycosylation for correct folding and stabilization (Varki and Gagneux, 2015; Varki, 2017), which is a prerequisite for their functioning. Additionally, protein-bound carbohydrates play a major role in the immune system, as they are involved in the regulation of antigen presentation and recognition (Hounsell and Davies, 1993; Maverakis et al., 2015). Oligosaccharides may themselves act as ligands for carbohydrate binding proteins called lectins (Varki, 2017), a motif that is also existent in dCIRL's NTF (RBL domain; see 3.2.1). Last but not least, glycosylation has also been shown to directly modulate receptor function, for instance acting as an on/off switch (Arey, 2012; Fu et al., 2014) or through regulation of proteolytic processes (Kötzler and Withers, 2016), also in the aGPCR class (Hsiao et al., 2009).

If carbohydrates in the IRH region fulfil one of these regulatory roles in dCIRL's implication in the nervous system or if they "just" promote proper folding of its ECD still awaits clarification. To address this question, the distinct amino acids bound to saccharides will have to be precisely localized and specifically altered in order to test the resulting *dCirl* mutants in functional assays.

A different and more mechanistic model sees the IRH as a rigid stalk that gives the ECD a certain length that may be needed to make dCIRL accessible for intercellular interaction partners. This is in line with additional findings from this study which propose that the IRH adopts a large and elongated configuration within dCIRL's ECD. Glycosylation has a huge effect on protein conformation, decreases its dynamics and leads to an increase in stability (H. S. Lee et al., 2015), which suggests that bound carbohydrates may even further straighten and stiffen the ECD.

Previous studies on mammalian Latrophilin-3 proposed a highly glycosylated semi-rigid linker region between the GAIN/HRM and OLF/RBL domains (O'Sullivan et al., 2014). It is comparable to the model of dCIRL-IRH as a rigid stalk, although data suggests that Latrophilin-3's stalk may contain stable secondary structures (O'Sullivan et al., 2014). The length of the Latrophilin-3 stalk is variable, but long enough to bridge the synaptic cleft, where it may interact with postsynaptic ligands such as FLRTs (O'Sullivan et al., 2014; Jackson et al., 2015).

Comparable glycosylated stalk motifs have been identified in other proteins, most of which have been shown to be involved in immunological processes (Daniels et al., 2001; Moody et al., 2001; Hartmann et al., 2012): the transmembrane chemokine CX3CL1, for example, requires its elongated and rigid mucin stalk for selective binding of leucocytes that are positive for its receptor CX3CR1 (Fong et al., 2000; Ostuni et al., 2014). Both shortening the stalk and its full deglycosylation resulted in impaired adhesion ability, most likely due to reduced accessibility of its adhesive do-

main that was located too close to the plasma membrane (Ostuni et al., 2014). It is not unlikely that the IRH region performs a similar function in dCIRL and is responsible for keeping the N-terminal domains at a certain distance from the plasma membrane to allow ligand binding.

In this context, dCIRL's mechanosensory capacity that was very recently further characterized: elongation of the ECD led to a gradual decrease of chordotonal neuron response to mechanical stimuli, suggesting impaired dCIRL signaling (Scholz et al., 2017). A substantial increase in NTF length (~ 20 nm) altered the mechanosensitive profile of the expressing neurons drastically (Scholz et al., 2017). These results demonstrated a direct connection between the length and tensile properties of dCIRL's ECD and its capacity to shape mechanosensation. It was hypothesized that the ECD of dCIRL has to maintain a defined tension or preload, accomplished by physical interaction with a ligand bound to an opposing cell or the ECM. Mechanical challenge in the form of ligand dislocation and thus force transmission may induce putative structural changes in the ECD inducing metabotropic receptor signaling (Scholz et al., 2017). In this model, elongation of the ECD length would reduce the preload of this ligand-receptor association and thus lead to impaired sensitivity for incoming mechanical stimuli, consistent with experimental findings. This hypothesis advocates that dCIRL is part of a mechanism that tunes neuronal mechanosensitivity through a cAMP-dependent modulation of ionotropic TRP channels located in close proximity in distal dendrites and cilia of CHOs (Scholz et al., 2015; Scholz et al., 2017).

Similar models have been proposed for the intracellular transmission of mechanical forces in mechanosensitive neurons, where pre-stressed components of the cytoskeleton are essential for efficient responses to external stimuli (Krieg et al., 2014; Zhang et al., 2015).

The IRH region with its elongated and highly glycosylated physique could contribute to this function of dCIRL's ECD as a pre-stressed stalk. However, if this hypothesis is transferable to vertebrate Latrophilins and thus represents a general molecular mechanism remains disputable. Future research will have to identify endogenous dCIRL ligands to gain deeper understanding in how this receptor perceives and transduces mechanical signals and if and how this affects central and peripheral neuronal functions. This will certainly help understand the molecular mechanisms underlying activation and signaling of the aGPCR class, as well as their regulation, and hopefully shed more light on the functional rationale and general purpose of aGPCR autoproteolysis.

7. References

- Adams MD, Celniker SE, Holt RA, Evans CA, Gocayne JD, Amanatides PG, Scherer SE, Li PW, Hoskins RA, Galle RF, George RA, Lewis SE, Richards S, Ashburner M, Henderson SN, Sutton GG, Wortman JR, Yandell MD, Zhang Q, Chen LX, et al. (2000). The genome sequence of *Drosophila melanogaster*. *Science* 287(5461): 2185-2195.
- Allache R, De Marco P, Merello E, Capra V, Kibar Z (2012). Role of the planar cell polarity gene CELSR1 in neural tube defects and caudal agenesis. *Birth Defects Res A Clin Mol Teratol* 94(3): 176-181.
- Anderson GR, Maxeiner S, Sando R, Tsetsenis T, Malenka RC, Südhof TC (2017). Postsynaptic adhesion GPCR latrophilin-2 mediates target recognition in entorhinal-hippocampal synapse assembly. *Journal of Cell Biology* 216(11): 3831-3846.
- Arac D, Boucard AA, Bolliger MF, Nguyen J, Soltis SM, Südhof TC, Brunger AT (2012). A novel evolutionarily conserved domain of cell-adhesion GPCRs mediates autoproteolysis. *EMBO Journal* 31(6): 1364-1378.
- Arac D, Sträter N, Seiradake E (2016). Understanding the Structural Basis of Adhesion GPCR Functions. *Handb Exp Pharmacol* 234: 67-82.
- Arakawa T, Wen J (2001). Determination of carbohydrate contents from excess light scattering. *Analytical Biochemistry* 299(2): 158-161.
- Arcos-Burgos M, Jain M, Acosta MT, Shively S, Stanescu H, Wallis D, Domene S, Velez JI, Karkera JD, Balog J, Berg K, Kleita R, Gahl WA, Roessler E, Long R, Lie J, Pineda D, Londono AC, Palacio JD, Arbelaez A, et al. (2010). A common variant of the latrophilin 3 gene, LPHN3, confers susceptibility to ADHD and predicts effectiveness of stimulant medication. *Molecular Psychiatry* 15(11): 1053-1066.
- Arey BJ. (2012). The Role of Glycosylation in Receptor Signaling. In S. Petrescu (Ed.), *Glycosylation* (pp. Ch. 12). Rijeka: InTech.
- Ashburner M, Golic K, Hawley S (2005). *Drosophila: a laboratory handbook*. Cold Spring Harbor Laboratory Press, New York.
- Ashburner M, Roote J (2007). Culture of *Drosophila*: the laboratory setup. *CSH Protoc* 2007: pdb ip34.
- Aust G, Eichler W, Laue S, Lehmann I, Heldin NE, Lotz O, Scherbaum WA, Dralle H, Hoang-Vu C (1997). CD97: a dedifferentiation marker in human thyroid carcinomas. *Cancer Research* 57(9): 1798-1806.
- Aust G, Zhu D, Van Meir EG, Xu L (2016). Adhesion GPCRs in Tumorigenesis. *Handb Exp Pharmacol* 234: 369-396.
- Bahi-Buisson N, Poirier K, Boddaert N, Fallet-Bianco C, Specchio N, Bertini E, Caglayan O, Lascelles K, Elie C, Rambaud J, Baulac M, An I, Dias P, des Portes V, Moutard ML, Soufflet C, El Maleh M, Beldjord C, Villard L, Chelly J (2010). GPR56-

related bilateral frontoparietal polymicrogyria: further evidence for an overlap with the cobblestone complex. *Brain* 133(11): 3194-3209.

Bellen HJ, Tong C, Tsuda H (2010). 100 years of *Drosophila* research and its impact on vertebrate neuroscience: a history lesson for the future. *Nature Reviews: Neuroscience* 11(7): 514-522.

Beychok S (1966). Circular dichroism of biological macromolecules. *Science* 154(3754): 1288-1299.

Bjarnadóttir TK, Geirardsdóttir K, Ingemansson M, Mirza MA, Fredriksson R, Schiöth HB (2007). Identification of novel splice variants of Adhesion G protein-coupled receptors. *Gene* 387(1-2): 38-48.

Bohnekamp J, Schöneberg T (2011). Cell adhesion receptor GPR133 couples to Gs protein. *Journal of Biological Chemistry* 286(49): 41912-41916.

Boucard AA, Ko J, Südhof TC (2012). High affinity neurexin binding to cell adhesion G-protein-coupled receptor C1RL1/latrophilin-1 produces an intercellular adhesion complex. *Journal of Biological Chemistry* 287(12): 9399-9413.

Boucard AA, Maxeiner S, Südhof TC (2014). Latrophilins function as heterophilic cell-adhesion molecules by binding to teneurins: regulation by alternative splicing. *Journal of Biological Chemistry* 289(1): 387-402.

Boussif O, Lezoualc'h F, Zanta MA, Mergny MD, Scherman D, Demeneix B, Behr JP (1995). A versatile vector for gene and oligonucleotide transfer into cells in culture and in vivo: polyethylenimine. *Proc Natl Acad Sci U S A* 92(16): 7297-7301.

Boyden SE, Desai A, Cruse G, Young ML, Bolan HC, Scott LM, Eisch AR, Long RD, Lee CC, Satorius CL, Pakstis AJ, Olivera A, Mullikin JC, Chouery E, Megarbane A, Medlej-Hashim M, Kidd KK, Kastner DL, Metcalfe DD, Komarow HD (2016). Vibratory Urticaria Associated with a Missense Variant in ADGRE2. *N Engl J Med* 374(7): 656-663.

Brand AH, Perrimon N (1993). Targeted Gene-Expression as a Means of Altering Cell Fates and Generating Dominant Phenotypes. *Development* 118(2): 401-415.

Bruxel EM, Salatino-Oliveira A, Akutagava-Martins GC, Tovo-Rodrigues L, Genro JP, Zeni CP, Polanczyk GV, Chazan R, Schmitz M, Arcos-Burgos M, Rohde LA, Hutz MH (2015). LPHN3 and attention-deficit/hyperactivity disorder: a susceptibility and pharmacogenetic study. *Genes Brain Behav* 14(5): 419-427.

Caldwell JC, Miller MM, Wing S, Soll DR, Eberl DF (2003). Dynamic analysis of larval locomotion in *Drosophila* chordotonal organ mutants. *Proc Natl Acad Sci U S A* 100(26): 16053-16058.

Chang GW, Stacey M, Kwakkenbos MJ, Hamann J, Gordon S, Lin HH (2003). Proteolytic cleavage of the EMR2 receptor requires both the extracellular stalk and the GPS motif. *FEBS Letters* 547(1-3): 145-150.

Chen K, Gracheva EO, Yu SC, Sheng Q, Richmond J, Featherstone DE (2010). Neurexin in embryonic *Drosophila* neuromuscular junctions. *PLoS One* 5(6): e11115.

Cheng LE, Song W, Looger LL, Jan LY, Jan YN (2010). The role of the TRP channel NompC in *Drosophila* larval and adult locomotion. *Neuron* 67(3): 373-380.

Collins MO, Husi H, Yu L, Brandon JM, Anderson CN, Blackstock WP, Choudhary JS, Grant SG (2006). Molecular characterization and comparison of the components and multiprotein complexes in the postsynaptic proteome. *Journal of Neurochemistry* 97 Suppl 1: 16-23.

Cork SM, Kaur B, Devi NS, Cooper L, Saltz JH, Sandberg EM, Kaluz S, Van Meir EG (2012). A proprotein convertase/MMP-14 proteolytic cascade releases a novel 40 kDa vasculostatin from tumor suppressor BAI1. *Oncogene* 31(50): 5144-5152.

Curtin JA, Quint E, Tshipouri V, Arkell RM, Cattanach B, Copp AJ, Henderson DJ, Spurr N, Stanier P, Fisher EM, Nolan PM, Steel KP, Brown SD, Gray IC, Murdoch JN (2003). Mutation of *Celsr1* disrupts planar polarity of inner ear hair cells and causes severe neural tube defects in the mouse. *Current Biology* 13(13): 1129-1133.

Daniels MA, Devine L, Miller JD, Moser JM, Lukacher AE, Altman JD, Kavathas P, Hogquist KA, Jameson SC (2001). CD8 binding to MHC class I molecules is influenced by T cell maturation and glycosylation. *Immunity* 15(6): 1051-1061.

Davey MG, Luscher EF (1967). Actions of thrombin and other coagulant and proteolytic enzymes on blood platelets. *Nature* 216(5118): 857-858.

Davletov BA, Shamotienko OG, Lelianova VG, Grishin EV, Ushkaryov YA (1996). Isolation and biochemical characterization of a Ca²⁺-independent alpha-latrotoxin-binding protein. *Journal of Biological Chemistry* 271(38): 23239-23245.

Deltcheva E, Chylinski K, Sharma CM, Gonzales K, Chao Y, Pirzada ZA, Eckert MR, Vogel J, Charpentier E (2011). CRISPR RNA maturation by trans-encoded small RNA and host factor RNase III. *Nature* 471(7340): 602-607.

Demberg LM, Rothmund S, Schöneberg T, Liebscher I (2015). Identification of the tethered peptide agonist of the adhesion G protein-coupled receptor GPR64/ADGRG2. *Biochemical and Biophysical Research Communications* 464(3): 743-747.

Demberg LM, Winkler J, Wilde C, Simon KU, Schön J, Rothmund S, Schöneberg T, Prömel S, Liebscher I (2017). Activation of Adhesion G Protein-coupled Receptors: AGONIST SPECIFICITY OF STACHEL SEQUENCE-DERIVED PEPTIDES. *Journal of Biological Chemistry* 292(11): 4383-4394.

Deyev IE, Petrenko AG (2010). Regulation of C1RL-1 proteolysis and trafficking. *Biochimie* 92(4): 418-422.

Dietzl G, Chen D, Schnorrer F, Su KC, Barinova Y, Fellner M, Gasser B, Kinsey K, Oppel S, Scheiblaue S, Couto A, Marra V, Keleman K, Dickson BJ (2007). A genome-wide transgenic RNAi library for conditional gene inactivation in *Drosophila*. *Nature* 448(7150): 151-156.

Eberl DF (1999). Feeling the vibes: chordotonal mechanisms in insect hearing. *Current Opinion in Neurobiology* 9(4): 389-393.

Eberl DF, Hardy RW, Kernan MJ (2000). Genetically similar transduction mechanisms for touch and hearing in *Drosophila*. *Journal of Neuroscience* 20(16): 5981-5988.

Erickson HP (2009). Size and shape of protein molecules at the nanometer level determined by sedimentation, gel filtration, and electron microscopy. *Biol Proced Online* 11: 32-51.

Faiz A, Donovan C, Nieuwenhuis MA, van den Berge M, Postma DS, Yao S, Park CY, Hirsch R, Fredberg JJ, Tjin G, Halayko AJ, Rempel KL, Ward JP, Lee T, Bosse Y, Nickle DC, Obeidat M, Vonk JM, Black JL, Oliver BG, et al. (2017). Latrophilin receptors: novel bronchodilator targets in asthma. *Thorax* 72(1): 74-82.

Fong AM, Erickson HP, Zachariah JP, Poon S, Schamberg NJ, Imai T, Patel DD (2000). Ultrastructure and function of the fractalkine mucin domain in CX(3)C chemokine domain presentation. *Journal of Biological Chemistry* 275(6): 3781-3786.

Fredriksson R, Lagerström MC, Lundin LG, Schiöth HB (2003). The G-protein-coupled receptors in the human genome form five main families. Phylogenetic analysis, paralogon groups, and fingerprints. *Molecular Pharmacology* 63(6): 1256-1272.

Fredriksson R, Schiöth HB (2005). The repertoire of G-protein-coupled receptors in fully sequenced genomes. *Molecular Pharmacology* 67(5): 1414-1425.

Fu HL, Valiathan RR, Payne L, Kumarasiri M, Mahasenan KV, Mobashery S, Huang P, Fridman R (2014). Glycosylation at Asn211 regulates the activation state of the discoidin domain receptor 1 (DDR1). *Journal of Biological Chemistry* 289(13): 9275-9287.

Fukuzawa T, Hirose S (2006). Multiple processing of Ig-Hepta/GPR116, a G protein-coupled receptor with immunoglobulin (Ig)-like repeats, and generation of EGF2-like fragment. *J Biochem* 140(3): 445-452.

Gao FB, Brenman JE, Jan LY, Jan YN (1999). Genes regulating dendritic outgrowth, branching, and routing in *Drosophila*. *Genes & Development* 13(19): 2549-2561.

Gehring J (2014). Functional analysis of the latrophilin homolog dCirl in *Drosophila melanogaster* (Dissertation, University of Würzburg, Würzburg, Germany).

Glenn TD, Talbot WS (2013). Analysis of Gpr126 function defines distinct mechanisms controlling the initiation and maturation of myelin. *Development* 140(15): 3167-3175.

Gong Z, Son W, Chung YD, Kim J, Shin DW, McClung CA, Lee Y, Lee HW, Chang DJ, Kaang BK, Cho H, Oh U, Hirsh J, Kernan MJ, Kim C (2004). Two interdependent TRPV channel subunits, inactive and Nanchung, mediate hearing in *Drosophila*. *Journal of Neuroscience* 24(41): 9059-9066.

Grace CR, Perrin MH, DiGruccio MR, Miller CL, Rivier JE, Vale WW, Riek R (2004). NMR structure and peptide hormone binding site of the first extracellular domain of a type B1 G protein-coupled receptor. *Proc Natl Acad Sci U S A* 101(35): 12836-12841.

Gray JX, Haino M, Roth MJ, Maguire JE, Jensen PN, Yarme A, Stetler-Stevenson MA, Siebenlist U, Kelly K (1996). CD97 is a processed, seven-transmembrane, heterodimeric receptor associated with inflammation. *Journal of Immunology* 157(12): 5438-5447.

Greenfield NJ (2006). Using circular dichroism spectra to estimate protein secondary structure. *Nat Protoc* 1(6): 2876-2890.

Groth AC (2004). Construction of Transgenic *Drosophila* by Using the Site-Specific Integrase From Phage C31. *Genetics* 166(4): 1775-1782.

Guan C (2016). Functional and genetic dissection of mechanosensory organs of *Drosophila melanogaster* (Dissertation, University of Würzburg, Würzburg, Germany).

Gustafsson MG (2000). Surpassing the lateral resolution limit by a factor of two using structured illumination microscopy. *Journal of Microscopy (Oxford)* 198(Pt 2): 82-87.

Hamann J, Aust G, Arac D, Engel FB, Formstone C, Fredriksson R, Hall RA, Harty BL, Kirchhoff C, Knapp B, Krishnan A, Liebscher I, Lin HH, Martinelli DC, Monk KR, Peeters MC, Piao X, Prömel S, Schöneberg T, Schwartz TW, et al. (2015). International Union of Basic and Clinical Pharmacology. XCIV. Adhesion G protein-coupled receptors. *Pharmacological Reviews* 67(2): 338-367.

Hamann J, Stortelers C, Kiss-Toth E, Vogel B, Eichler W, van Lier RA (1998). Characterization of the CD55 (DAF)-binding site on the seven-span transmembrane receptor CD97. *European Journal of Immunology* 28(5): 1701-1707.

Hamann J, Vogel B, van Schijndel GM, van Lier RA (1996). The seven-span transmembrane receptor CD97 has a cellular ligand (CD55, DAF). *Journal of Experimental Medicine* 184(3): 1185-1189.

Hammes SR, Coughlin SR (1999). Protease-activated receptor-1 can mediate responses to SFLLRN in thrombin-desensitized cells: evidence for a novel mechanism for preventing or terminating signaling by PAR1's tethered ligand. *Biochemistry* 38(8): 2486-2493.

Harmar AJ (2001). Family-B G-protein-coupled receptors. *Genome Biol* 2(12): REVIEWS3013.

Hartmann J, Tran TV, Kaudeer J, Oberle K, Herrmann J, Quagliano I, Abel T, Cohnen A, Gatterdam V, Jacobs A, Wollscheid B, Tampe R, Watzl C, Diefenbach A, Koch J (2012). The stalk domain and the glycosylation status of the activating natural killer cell receptor NKp30 are important for ligand binding. *Journal of Biological Chemistry* 287(37): 31527-31539.

Hassan PA, Rana S, Verma G (2015). Making sense of Brownian motion: colloid characterization by dynamic light scattering. *Langmuir* 31(1): 3-12.

Heintzmann R, Cremer C (1999). Laterally modulated excitation microscopy: Improvement of resolution by using a diffraction grating. *Proc SPIE* 3568: 185-196.

Heng BC, Aibel D, Fussenegger M (2013). An overview of the diverse roles of G-protein coupled receptors (GPCRs) in the pathophysiology of various human diseases. *Biotechnology Advances* 31(8): 1676-1694.

Hosono M, Ishikawa K, Mineki R, Murayama K, Numata C, Ogawa Y, Takayanagi Y, Nitta K (1999). Tandem repeat structure of rhamnose-binding lectin from catfish (*Silurus asotus*) eggs. *Biochimica et Biophysica Acta (BBA) - Bioenergetics* 1472(3): 668-675.

Hounsell EF, Davies MJ (1993). Role of protein glycosylation in immune regulation. *Annals of the Rheumatic Diseases* 52 Suppl 1: S22-29.

Hsiao CC, Cheng KF, Chen HY, Chou YH, Stacey M, Chang GW, Lin HH (2009). Site-specific N-glycosylation regulates the GPS auto-proteolysis of CD97. *FEBS Letters* 583(19): 3285-3290.

Huang YS, Chiang NY, Hu CH, Hsiao CC, Cheng KF, Tsai WP, Yona S, Stacey M, Gordon S, Chang GW, Lin HH (2012). Activation of myeloid cell-specific adhesion class G protein-coupled receptor EMR2 via ligation-induced translocation and interaction of receptor subunits in lipid raft microdomains. *Molecular and Cellular Biology* 32(8): 1408-1420.

Iguchi T, Sakata K, Yoshizaki K, Tago K, Mizuno N, Itoh H (2008). Orphan G protein-coupled receptor GPR56 regulates neural progenitor cell migration via a G alpha 12/13 and Rho pathway. *Journal of Biological Chemistry* 283(21): 14469-14478.

Jackson VA, del Toro D, Carrasquero M, Roversi P, Harlos K, Klein R, Seiradake E (2015). Structural basis of latrophilin-FLRT interaction. *Structure* 23(4): 774-781.

Jackson VA, Mehmood S, Chavent M, Roversi P, Carrasquero M, Del Toro D, Seyit-Bremer G, Ranaivoson FM, Comoletti D, Sansom MS, Robinson CV, Klein R, Seiradake E (2016). Super-complexes of adhesion GPCRs and neural guidance receptors. *Nat Commun* 7: 11184.

Jan LY, Jan YN (1976). L-glutamate as an excitatory transmitter at the *Drosophila* larval neuromuscular junction. *J Physiol* 262(1): 215-236.

Jeon MS, Song SH, Yun J, Kang JY, Kim HP, Han SW, Kim TY (2016). Aberrant Epigenetic Modifications of LPHN2 Function as a Potential Cisplatin-Specific Biomarker for Human Gastrointestinal Cancer. *Cancer Res Treat* 48(2): 676-686.

Jeong SJ, Luo R, Li S, Strokes N, Piao X (2012). Characterization of G protein-coupled receptor 56 protein expression in the mouse developing neocortex. *Journal of Comparative Neurology* 520(13): 2930-2940.

Johansson DG, Wallin G, Sandberg A, Macao B, Aqvist J, Hard T (2009). Protein autoproteolysis: conformational strain linked to the rate of peptide cleavage by the pH dependence of the N → O acyl shift reaction. *Journal of the American Chemical Society* 131(27): 9475-9477.

Kan Z, Jaiswal BS, Stinson J, Janakiraman V, Bhatt D, Stern HM, Yue P, Haverty PM, Bourgon R, Zheng J, Moorhead M, Chaudhuri S, Tomsho LP, Peters BA, Pujara K, Cordes S, Davis DP, Carlton VE, Yuan W, Li L, et al. (2010). Diverse somatic mutation patterns and pathway alterations in human cancers. *Nature* 466(7308): 869-873.

Karpus ON, Veninga H, Hoek RM, Flierman D, van Buul JD, Vandenakker CC, vanBavel E, Medof ME, van Lier RA, Reedquist KA, Hamann J (2013). Shear stress-dependent downregulation of the adhesion-G protein-coupled receptor CD97 on circulating leukocytes upon contact with its ligand CD55. *Journal of Immunology* 190(7): 3740-3748.

Kee HJ, Ahn KY, Choi KC, Won Song J, Heo T, Jung S, Kim JK, Bae CS, Kim KK (2004). Expression of brain-specific angiogenesis inhibitor 3 (BAI3) in normal brain and implications for BAI3 in ischemia-induced brain angiogenesis and malignant glioma. *FEBS Letters* 569(1-3): 307-316.

Keil TA (1997). Functional morphology of insect mechanoreceptors. *Microscopy Research and Technique* 39(6): 506-531.

Kernan M, Cowan D, Zuker C (1994). Genetic dissection of mechanosensory transduction: mechanoreception-defective mutations of *Drosophila*. *Neuron* 12(6): 1195-1206.

Kernan MJ (2007). Mechanotransduction and auditory transduction in *Drosophila*. *Pflugers Arch* 454(5): 703-720.

Khatri IA, Wang R, Forstner JF (2003). SEA (sea-urchin sperm protein, enterokinase and agrin)-module cleavage, association of fragments and membrane targeting of rat intestinal mucin Muc3. *Biochemical Journal* 372(Pt 1): 263-270.

Kimura H, Usui T, Tsubouchi A, Uemura T (2006). Potential dual molecular interaction of the *Drosophila* 7-pass transmembrane cadherin Flamingo in dendritic morphogenesis. *Journal of Cell Science* 119(Pt 6): 1118-1129.

Kishore A, Hall RA (2016). Versatile Signaling Activity of Adhesion GPCRs. *Handb Exp Pharmacol* 234: 127-146.

Kishore A, Purcell RH, Nassiri-Toosi Z, Hall RA (2016). Stalk-dependent and Stalk-independent Signaling by the Adhesion G Protein-coupled Receptors GPR56 (ADGRG1) and BAI1 (ADGRB1). *Journal of Biological Chemistry* 291(7): 3385-3394.

Knapp B, Wolfrum U (2016). Adhesion GPCR-Related Protein Networks. *Handb Exp Pharmacol* 234: 147-178.

Kötzler MP, Withers SG (2016). Proteolytic Cleavage Driven by Glycosylation. *Journal of Biological Chemistry* 291(1): 429-434.

Krasnoperov V, Bittner MA, Holz RW, Chepurny O, Petrenko AG (1999). Structural requirements for alpha-latrotoxin binding and alpha-latrotoxin-stimulated secretion. A study with calcium-independent receptor of alpha-latrotoxin (CIRL) deletion mutants. *Journal of Biological Chemistry* 274(6): 3590-3596.

Krasnoperov V, Bittner MA, Mo W, Buryanovsky L, Neubert TA, Holz RW, Ichtchenko K, Petrenko AG (2002a). Protein-tyrosine phosphatase-sigma is a novel member of the functional family of alpha-latrotoxin receptors. *Journal of Biological Chemistry* 277(39): 35887-35895.

Krasnoperov V, Deyev IE, Serova OV, Xu C, Lu Y, Buryanovsky L, Gabibov AG, Neubert TA, Petrenko AG (2009). Dissociation of the subunits of the calcium-independent receptor of alpha-latrotoxin as a result of two-step proteolysis. *Biochemistry* 48(14): 3230-3238.

Krasnoperov V, Lu Y, Buryanovsky L, Neubert TA, Ichtchenko K, Petrenko AG (2002b). Post-translational proteolytic processing of the calcium-independent receptor of alpha-latrotoxin (CIRL), a natural chimera of the cell adhesion protein and the G protein-coupled receptor. Role of the G protein-coupled receptor proteolysis site (GPS) motif. *Journal of Biological Chemistry* 277(48): 46518-46526.

Krasnoperov VG, Beavis R, Chepurny OG, Little AR, Plotnikov AN, Petrenko AG (1996). The calcium-independent receptor of alpha-latrotoxin is not a neurexin. *Biochemical and Biophysical Research Communications* 227(3): 868-875.

Krasnoperov VG, Bittner MA, Beavis R, Kuang Y, Salnikow KV, Chepurny OG, Little AR, Plotnikov AN, Wu D, Holz RW, Petrenko AG (1997). alpha-Latrotoxin stimulates exocytosis by the interaction with a neuronal G-protein-coupled receptor. *Neuron* 18(6): 925-937.

Kreienkamp HJ, Zitzer H, Gundelfinger ED, Richter D, Bockers TM (2000). The calcium-independent receptor for alpha-latrotoxin from human and rodent brains interacts with members of the ProSAP/SSTRIP/Shank family of multidomain proteins. *Journal of Biological Chemistry* 275(42): 32387-32390.

Krieg M, Dunn AR, Goodman MB (2014). Mechanical control of the sense of touch by beta-spectrin. *Nature Cell Biology* 16(3): 224-233.

Kurbegovic A, Kim H, Xu H, Yu S, Cruanes J, Maser RL, Boletta A, Trudel M, Qian F (2014). Novel functional complexity of polycystin-1 by GPS cleavage in vivo: role in polycystic kidney disease. *Molecular and Cellular Biology* 34(17): 3341-3353.

Lagerström MC, Schiöth HB (2008). Structural diversity of G protein-coupled receptors and significance for drug discovery. *Nature Reviews: Drug Discovery* 7(4): 339-357.

Lange M, Norton W, Coolen M, Chaminade M, Merker S, Proft F, Schmitt A, Vernier P, Lesch KP, Bally-Cuif L (2012). The ADHD-susceptibility gene lphn3.1 modulates dopaminergic neuron formation and locomotor activity during zebrafish development. *Molecular Psychiatry* 17(9): 946-954.

Langenhan T, Aust G, Hamann J (2013). Sticky signaling--adhesion class G protein-coupled receptors take the stage. *Sci Signal* 6(276): re3.

Langenhan T, Piao X, Monk KR (2016). Adhesion G protein-coupled receptors in nervous system development and disease. *Nature Reviews: Neuroscience* 17(9): 550-561.

Langenhan T, Prömel S, Mestek L, Esmaili B, Waller-Evans H, Hennig C, Kohara Y, Avery L, Vakonakis I, Schnabel R, Russ AP (2009). Latrophilin signaling links anterior-posterior tissue polarity and oriented cell divisions in the *C. elegans* embryo. *Developmental Cell* 17(4): 494-504.

Langenhan T, Russ AP (2010). Latrophilin signalling in tissue polarity and morphogenesis. *Advances in Experimental Medicine and Biology* 706: 37-48.

Lee HS, Qi Y, Im W (2015). Effects of N-glycosylation on protein conformation and dynamics: Protein Data Bank analysis and molecular dynamics simulation study. *Sci Rep* 5: 8926.

Lee RC, Clandinin TR, Lee CH, Chen PL, Meinertzhagen IA, Zipursky SL (2003). The protocadherin Flamingo is required for axon target selection in the *Drosophila* visual system. *Nature Neuroscience* 6(6): 557-563.

Lei Y, Zhu H, Yang W, Ross ME, Shaw GM, Finnell RH (2014). Identification of novel CELSR1 mutations in spina bifida. *PLoS One* 9(3): e92207.

Lelianova VG, Davletov BA, Sterling A, Rahman MA, Grishin EV, Totty NF, Ushkaryov YA (1997). Alpha-latrotoxin receptor, latrophilin, is a novel member of the secretin family of G protein-coupled receptors. *Journal of Biological Chemistry* 272(34): 21504-21508.

Levitin F, Stern O, Weiss M, Gil-Henn C, Ziv R, Prokocimer Z, Smorodinsky NI, Rubinstein DB, Wreschner DH (2005). The MUC1 SEA module is a self-cleaving domain. *Journal of Biological Chemistry* 280(39): 33374-33386.

Leyva-Diaz E, del Toro D, Menal MJ, Cambray S, Susin R, Tessier-Lavigne M, Klein R, Egea J, Lopez-Bendito G (2014). FLRT3 is a Robo1-interacting protein that determines Netrin-1 attraction in developing axons. *Current Biology* 24(5): 494-508.

Li A, Tian X, Sung SW, Somlo S (2003). Identification of two novel polycystic kidney disease-1-like genes in human and mouse genomes. *Genomics* 81(6): 596-608.

Li J, Ashley J, Budnik V, Bhat MA (2007). Crucial role of *Drosophila* neurexin in proper active zone apposition to postsynaptic densities, synaptic growth, and synaptic transmission. *Neuron* 55(5): 741-755.

Li S, Jin Z, Koirala S, Bu L, Xu L, Hynes RO, Walsh CA, Corfas G, Piao X (2008). GPR56 regulates pial basement membrane integrity and cortical lamination. *Journal of Neuroscience* 28(22): 5817-5826.

Liebscher I, Ackley B, Arac D, Ariestanti DM, Aust G, Bae BI, Bista BR, Bridges JP, Duman JG, Engel FB, Giera S, Goffinet AM, Hall RA, Hamann J, Hartmann N, Lin HH, Liu M, Luo R, Mogha A, Monk KR, et al. (2014a). New functions and signaling mechanisms for the class of adhesion G protein-coupled receptors. *Annals of the New York Academy of Sciences* 1333: 43-64.

Liebscher I, Monk KR, Schöneberg T (2015). How to wake a giant. *Oncotarget* 6(27): 23038-23039.

Liebscher I, Schön J, Petersen SC, Fischer L, Auerbach N, Demberg LM, Mogha A, Cöster M, Simon KU, Rothmund S, Monk KR, Schöneberg T (2014b). A tethered agonist within the ectodomain activates the adhesion G protein-coupled receptors GPR126 and GPR133. *Cell Rep* 9(6): 2018-2026.

Liebscher I, Schöneberg T (2016). Tethered Agonism: A Common Activation Mechanism of Adhesion GPCRs. *Handb Exp Pharmacol* 234: 111-125.

Lin HH, Chang GW, Davies JQ, Stacey M, Harris J, Gordon S (2004). Autocatalytic cleavage of the EMR2 receptor occurs at a conserved G protein-coupled receptor proteolytic site motif. *Journal of Biological Chemistry* 279(30): 31823-31832.

Lin HH, Stacey M, Yona S, Chang GW (2010). GPS proteolytic cleavage of adhesion-GPCRs. *Advances in Experimental Medicine and Biology* 706: 49-58.

Luo R, Jeong SJ, Jin Z, Strokes N, Li S, Piao X (2011). G protein-coupled receptor 56 and collagen III, a receptor-ligand pair, regulates cortical development and lamination. *Proc Natl Acad Sci U S A* 108(31): 12925-12930.

Macao B, Johansson DG, Hansson GC, Hard T (2006). Autoproteolysis coupled to protein folding in the SEA domain of the membrane-bound MUC1 mucin. *Nature Structural & Molecular Biology* 13(1): 71-76.

Maley F, Trimble RB, Tarentino AL, Plummer TH (1989). Characterization of glycoproteins and their associated oligosaccharides through the use of endoglycosidases. *Analytical Biochemistry* 180(2): 195-204.

Maretto S, Müller PS, Aricescu AR, Cho KW, Bikoff EK, Robertson EJ (2008). Ventral closure, headfold fusion and definitive endoderm migration defects in mouse embryos lacking the fibronectin leucine-rich transmembrane protein FLRT3. *Developmental Biology* 318(1): 184-193.

Martinez AF, Abe Y, Hong S, Molyneux K, Yarnell D, Lohr H, Driever W, Acosta MT, Arcos-Burgos M, Muenke M (2016). An Ultraconserved Brain-Specific Enhancer Within ADGRL3 (LPHN3) Underpins Attention-Deficit/Hyperactivity Disorder Susceptibility. *Biol Psychiatry* 80(12): 943-954.

Martinez AF, Muenke M, Arcos-Burgos M (2011). From the black widow spider to human behavior: Latrophilins, a relatively unknown class of G protein-coupled receptors, are implicated in psychiatric disorders. *Am J Med Genet B Neuropsychiatr Genet* 156B(1): 1-10.

Matsushita H, Lelianova VG, Ushkaryov YA (1999). The latrophilin family: multiply spliced G protein-coupled receptors with differential tissue distribution. *FEBS Letters* 443(3): 348-352.

Matteoli M, Haimann C, Torri-Tarelli F, Polak JM, Ceccarelli B, De Camilli P (1988). Differential effect of alpha-latrotoxin on exocytosis from small synaptic vesicles and from large dense-core vesicles containing calcitonin gene-related peptide at the frog neuromuscular junction. *Proc Natl Acad Sci U S A* 85(19): 7366-7370.

Maverakis E, Kim K, Shimoda M, Gershwin ME, Patel F, Wilken R, Raychaudhuri S, Ruhaak LR, Lebrilla CB (2015). Glycans in the immune system and The Altered Glycan Theory of Autoimmunity: a critical review. *Journal of Autoimmunity* 57: 1-13.

McMillan DR, Kayes-Wandover KM, Richardson JA, White PC (2002). Very large G protein-coupled receptor-1, the largest known cell surface protein, is highly expressed in the developing central nervous system. *Journal of Biological Chemistry* 277(1): 785-792.

Mogha A, Benesh AE, Patra C, Engel FB, Schöneberg T, Liebscher I, Monk KR (2013). Gpr126 functions in Schwann cells to control differentiation and myelination via G-protein activation. *Journal of Neuroscience* 33(46): 17976-17985.

Monk KR, Naylor SG, Glenn TD, Mercurio S, Perlin JR, Dominguez C, Moens CB, Talbot WS (2009). A G protein-coupled receptor is essential for Schwann cells to initiate myelination. *Science* 325(5946): 1402-1405.

Monk KR, Oshima K, Jors S, Heller S, Talbot WS (2011). Gpr126 is essential for peripheral nerve development and myelination in mammals. *Development* 138(13): 2673-2680.

Moody AM, Chui D, Reche PA, Priatel JJ, Marth JD, Reinherz EL (2001). Developmentally regulated glycosylation of the CD8alpha coreceptor stalk modulates ligand binding. *Cell* 107(4): 501-512.

Moriguchi T, Haraguchi K, Ueda N, Okada M, Furuya T, Akiyama T (2004). DREG, a developmentally regulated G protein-coupled receptor containing two conserved proteolytic cleavage sites. *Genes to Cells* 9(6): 549-560.

Müller A, Winkler J, Fiedler F, Sastradihardja T, Binder C, Schnabel R, Kungel J, Rothmund S, Hennig C, Schöneberg T, Prömel S (2015). Oriented Cell Division in

the *C. elegans* Embryo Is Coordinated by G-Protein Signaling Dependent on the Adhesion GPCR LAT-1. *PLoS Genetics* 11(10): e1005624.

Musa G, Engel FB, Niaudet C (2016). Heart Development, Angiogenesis, and Blood-Brain Barrier Function Is Modulated by Adhesion GPCRs. *Handb Exp Pharmacol* 234: 351-368.

Nadrowski B, Albert JT, Gopfert MC (2008). Transducer-based force generation explains active process in *Drosophila* hearing. *Current Biology* 18(18): 1365-1372.

Nakaya N, Sultana A, Lee HS, Tomarev SI (2012). Olfactomedin 1 interacts with the Nogo A receptor complex to regulate axon growth. *Journal of Biological Chemistry* 287(44): 37171-37184.

Nakaya N, Sultana A, Munasinghe J, Cheng A, Mattson MP, Tomarev SI (2013). Deletion in the N-terminal half of olfactomedin 1 modifies its interaction with synaptic proteins and causes brain dystrophy and abnormal behavior in mice. *Experimental Neurology* 250: 205-218.

Nieberler M, Kittel RJ, Petrenko AG, Lin HH, Langenhan T (2016). Control of Adhesion GPCR Function Through Proteolytic Processing. *Handb Exp Pharmacol* 234: 83-109.

Nishimura T, Honda H, Takeichi M (2012). Planar cell polarity links axes of spatial dynamics in neural-tube closure. *Cell* 149(5): 1084-1097.

Nordström KJ, Lagerström MC, Waller LM, Fredriksson R, Schiöth HB (2009). The Secretin GPCRs descended from the family of Adhesion GPCRs. *Molecular Biology and Evolution* 26(1): 71-84.

O'Sullivan ML, de Wit J, Savas JN, Comoletti D, Otto-Hitt S, Yates JR, 3rd, Ghosh A (2012). FLRT proteins are endogenous latrophilin ligands and regulate excitatory synapse development. *Neuron* 73(5): 903-910.

O'Sullivan ML, Martini F, von Daake S, Comoletti D, Ghosh A (2014). LPHN3, a presynaptic adhesion-GPCR implicated in ADHD, regulates the strength of neocortical layer 2/3 synaptic input to layer 5. *Neural Dev* 9: 7.

Okajima D, Kudo G, Yokota H (2010). Brain-specific angiogenesis inhibitor 2 (BAI2) may be activated by proteolytic processing. *J Recept Signal Transduct Res* 30(3): 143-153.

Orlova EV, Rahman MA, Gowen B, Volynski KE, Ashton AC, Manser C, van Heel M, Ushkaryov YA (2000). Structure of alpha-latrotoxin oligomers reveals that divalent cation-dependent tetramers form membrane pores. *Nature Structural Biology* 7(1): 48-53.

Orsini CA, Setlow B, DeJesus M, Galaviz S, Loesch K, Ioerger T, Wallis D (2016). Behavioral and transcriptomic profiling of mice null for *Lphn3*, a gene implicated in ADHD and addiction. *Mol Genet Genomic Med* 4(3): 322-343.

Ostuni MA, Guellec J, Hermand P, Durand P, Combadiere C, Pincet F, Deterre P (2014). CX3CL1, a chemokine finely tuned to adhesion: critical roles of the stalk glycosylation and the membrane domain. *Biol Open* 3(12): 1173-1182.

Ozeki Y, Matsui T, Suzuki M, Titani K (1991). Amino acid sequence and molecular characterization of a D-galactoside-specific lectin purified from sea urchin (*Anthocidaris crassispina*) eggs. *Biochemistry* 30(9): 2391-2394.

Paavola KJ, Sidik H, Zuchero JB, Eckart M, Talbot WS (2014). Type IV collagen is an activating ligand for the adhesion G protein-coupled receptor GPR126. *Sci Signal* 7(338): ra76.

Paavola KJ, Stephenson JR, Ritter SL, Alter SP, Hall RA (2011). The N terminus of the adhesion G protein-coupled receptor GPR56 controls receptor signaling activity. *Journal of Biological Chemistry* 286(33): 28914-28921.

Palmai-Pallag T, Khodabukus N, Kinarsky L, Leir SH, Sherman S, Hollingsworth MA, Harris A (2005). The role of the SEA (sea urchin sperm protein, enterokinase and agrin) module in cleavage of membrane-tethered mucins. *FEBS Journal* 272(11): 2901-2911.

Patra C, van Amerongen MJ, Ghosh S, Ricciardi F, Sajjad A, Novoyatleva T, Mogha A, Monk KR, Muhlfeld C, Engel FB (2013). Organ-specific function of adhesion G protein-coupled receptor GPR126 is domain-dependent. *Proc Natl Acad Sci U S A* 110(42): 16898-16903.

Petersen SC, Luo R, Liebscher I, Giera S, Jeong SJ, Mogha A, Ghidinelli M, Feltri ML, Schöneberg T, Piao X, Monk KR (2015). The adhesion GPCR GPR126 has distinct, domain-dependent functions in Schwann cell development mediated by interaction with laminin-211. *Neuron* 85(4): 755-769.

Piao X, Chang BS, Bodell A, Woods K, Benzeev B, Topcu M, Guerrini R, Goldberg-Stern H, Sztriha L, Dobyns WB, Barkovich AJ, Walsh CA (2005). Genotype-phenotype analysis of human frontoparietal polymicrogyria syndromes. *Annals of Neurology* 58(5): 680-687.

Piao X, Hill RS, Bodell A, Chang BS, Basel-Vanagaite L, Straussberg R, Dobyns WB, Qasrawi B, Winter RM, Innes AM, Voit T, Ross ME, Michaud JL, Descarie JC, Barkovich AJ, Walsh CA (2004). G protein-coupled receptor-dependent development of human frontal cortex. *Science* 303(5666): 2033-2036.

Pierce KL, Premont RT, Lefkowitz RJ (2002). Seven-transmembrane receptors. *Nature Reviews: Molecular Cell Biology* 3(9): 639-650.

Ponting CP, Hofmann K, Bork P (1999). A latrophilin/CL-1-like GPS domain in polycystin-1. *Current Biology* 9(16): R585-588.

Prömel S, Frickenhaus M, Hughes S, Mestek L, Staunton D, Woollard A, Vakonakis I, Schöneberg T, Schnabel R, Russ AP, Langenhan T (2012). The GPS motif is a molecular switch for bimodal activities of adhesion class G protein-coupled receptors. *Cell Rep* 2(2): 321-331.

Prömel S, Langenhan T, Arac D (2013). Matching structure with function: the GAIN domain of adhesion-GPCR and PKD1-like proteins. *Trends in Pharmacological Sciences* 34(8): 470-478.

Qian F, Boletta A, Bhunia AK, Xu H, Liu L, Ahrabi AK, Watnick TJ, Zhou F, Germino GG (2002). Cleavage of polycystin-1 requires the receptor for egg jelly domain and is disrupted by human autosomal-dominant polycystic kidney disease 1-associated mutations. *Proc Natl Acad Sci U S A* 99(26): 16981-16986.

Rahman MA, Ashton AC, Meunier FA, Davletov BA, Dolly JO, Ushkaryov YA (1999). Norepinephrine exocytosis stimulated by alpha-latrotoxin requires both external and stored Ca²⁺ and is mediated by latrophilin, G proteins and phospholipase C. *Philos Trans R Soc Lond B Biol Sci* 354(1381): 379-386.

Reiners J, van Wijk E, Marker T, Zimmermann U, Jürgens K, te Brinke H, Overlack N, Roepman R, Knipper M, Kremer H, Wolfrum U (2005). Scaffold protein harmonin (USH1C) provides molecular links between Usher syndrome type 1 and type 2. *Human Molecular Genetics* 14(24): 3933-3943.

Rendić D, Wilson IBH, Paschinger K (2007). The Glycosylation Capacity of Insect Cells. *Croatica chemica acta* 81(1): 7-21.

Robinson A, Escuin S, Doudney K, Vekemans M, Stevenson RE, Greene ND, Copp AJ, Stanier P (2012). Mutations in the planar cell polarity genes CELSR1 and SCRIB are associated with the severe neural tube defect craniorachischisis. *Human Mutation* 33(2): 440-447.

Salzman GS, Ackerman SD, Ding C, Koide A, Leon K, Luo R, Stoveken HM, Fernandez CG, Tall GG, Piao X, Monk KR, Koide S, Arac D (2016). Structural Basis for Regulation of GPR56/ADGRG1 by Its Alternatively Spliced Extracellular Domains. *Neuron* 91(6): 1292-1304.

Salzman GS, Zhang S, Gupta A, Koide A, Koide S, Arac D (2017). Stachel-independent modulation of GPR56/ADGRG1 signaling by synthetic ligands directed to its extracellular region. *Proc Natl Acad Sci U S A* 114(38): 10095-10100.

Sambrano GR, Weiss EJ, Zheng YW, Huang W, Coughlin SR (2001). Role of thrombin signalling in platelets in haemostasis and thrombosis. *Nature* 413(6851): 74-78.

Sanger F, Nicklen S, Coulson AR (1977). DNA sequencing with chain-terminating inhibitors. *Proc Natl Acad Sci U S A* 74(12): 5463-5467.

Scholz N (2015). Genetic analyses of sensory and motoneuron physiology in *Drosophila melanogaster* (Dissertation, University of Würzburg, Würzburg, Germany).

Scholz N, Gehring J, Guan C, Ljaschenko D, Fischer R, Lakshmanan V, Kittel RJ, Langenhan T (2015). The adhesion GPCR latrophilin/CIRL shapes mechanosensation. *Cell Rep* 11(6): 866-874.

Scholz N, Guan C, Nieberler M, Grotemeyer A, Maiellaro I, Gao S, Beck S, Pawlak M, Sauer M, Asan E, Rothmund S, Winkler J, Prömel S, Nagel G, Langenhan T, Kittel RJ (2017). Mechano-dependent signaling by Latrophilin/CIRL quenches cAMP in proprioceptive neurons. *Elife* 6.

Scholz N, Monk KR, Kittel RJ, Langenhan T (2016). Adhesion GPCRs as a Putative Class of Metabotropic Mechanosensors. *Handb Exp Pharmacol* 234: 221-247.

Seiradake E, del Toro D, Nagel D, Cop F, Hartl R, Ruff T, Seyit-Bremer G, Harlos K, Border EC, Acker-Palmer A, Jones EY, Klein R (2014). FLRT structure: balancing repulsion and cell adhesion in cortical and vascular development. *Neuron* 84(2): 370-385.

Selimi F, Cristea IM, Heller E, Chait BT, Heintz N (2009). Proteomic studies of a single CNS synapse type: the parallel fiber/purkinje cell synapse. *PLoS Biology* 7(4): e83.

Senti KA, Usui T, Boucke K, Greber U, Uemura T, Dickson BJ (2003). Flamingo regulates R8 axon-axon and axon-target interactions in the Drosophila visual system. *Current Biology* 13(10): 828-832.

Serova OV, Popova NV, Deev IE, Petrenko AG (2008). [Identification of proteins in complexes with alpha-latrotoxin receptors]. *Bioorg Khim* 34(6): 747-753.

Serova OV, Popova NV, Petrenko AG, Deyev IE (2010). Association of the subunits of the calcium-independent receptor of alpha-latrotoxin. *Biochemical and Biophysical Research Communications* 402(4): 658-662.

Shi N, Li CX, Cui XB, Tomarev SI, Chen SY (2017). Olfactomedin 2 Regulates Smooth Muscle Phenotypic Modulation and Vascular Remodeling Through Mediating Runt-Related Transcription Factor 2 Binding to Serum Response Factor. *Arterioscler Thromb Vasc Biol* 37(3): 446-454.

Shima Y, Copeland NG, Gilbert DJ, Jenkins NA, Chisaka O, Takeichi M, Uemura T (2002). Differential expression of the seven-pass transmembrane cadherin genes *Celsr1-3* and distribution of the *Celsr2* protein during mouse development. *Developmental Dynamics* 223(3): 321-332.

Sigoillot SM, Monk KR, Piao X, Selimi F, Harty BL (2016). Adhesion GPCRs as Novel Actors in Neural and Glial Cell Functions: From Synaptogenesis to Myelination. *Handb Exp Pharmacol* 234: 275-298.

Silva JP, Lelianova V, Hopkins C, Volynski KE, Ushkaryov Y (2009). Functional cross-interaction of the fragments produced by the cleavage of distinct adhesion G-protein-coupled receptors. *Journal of Biological Chemistry* 284(10): 6495-6506.

Silva JP, Lelianova VG, Ermolyuk YS, Vysokov N, Hitchen PG, Berninghausen O, Rahman MA, Zangrandi A, Fidalgo S, Tonevitsky AG, Dell A, Volynski KE, Ushkaryov YA (2011). Latrophilin 1 and its endogenous ligand Lasso/teneurin-2 form a high-affinity transsynaptic receptor pair with signaling capabilities. *Proc Natl Acad Sci U S A* 108(29): 12113-12118.

Silva JP, Ushkaryov YA (2010). The latrophilins, "split-personality" receptors. *Advances in Experimental Medicine and Biology* 706: 59-75.

Smith LJ, Fiebig KM, Schwalbe H, Dobson CM (1996). The concept of a random coil. Residual structure in peptides and denatured proteins. *Fold Des* 1(5): R95-106.

Snyder DA, Rivers AM, Yokoe H, Menco BP, Anholt RR (1991). Olfactomedin: purification, characterization, and localization of a novel olfactory glycoprotein. *Biochemistry* 30(38): 9143-9153.

Steimel A, Wong L, Najarro EH, Ackley BD, Garriga G, Hutter H (2010). The Flamingo ortholog FMI-1 controls pioneer-dependent navigation of follower axons in *C. elegans*. *Development* 137(21): 3663-3673.

Stein PE, Leslie AG, Finch JT, Carrell RW (1991). Crystal structure of uncleaved ovalbumin at 1.95 Å resolution. *Journal of Molecular Biology* 221(3): 941-959.

Stephenson JR, Paavola KJ, Schaefer SA, Kaur B, Van Meir EG, Hall RA (2013). Brain-specific angiogenesis inhibitor-1 signaling, regulation, and enrichment in the postsynaptic density. *Journal of Biological Chemistry* 288(31): 22248-22256.

Sternberg N, Hamilton D (1981). Bacteriophage P1 site-specific recombination. I. Recombination between loxP sites. *Journal of Molecular Biology* 150(4): 467-486.

Stoveken HM, Hajduczuk AG, Xu L, Tall GG (2015). Adhesion G protein-coupled receptors are activated by exposure of a cryptic tethered agonist. *Proc Natl Acad Sci U S A* 112(19): 6194-6199.

Strokes N, Piao X (2010). Adhesion-GPCRs in the CNS. *Advances in Experimental Medicine and Biology* 706: 87-97.

Sultana A, Nakaya N, Dong L, Abu-Asab M, Qian H, Tomarev SI (2014). Deletion of olfactomedin 2 induces changes in the AMPA receptor complex and impairs visual, olfactory, and motor functions in mice. *Experimental Neurology* 261: 802-811.

Sumbayev VV, Goncalves Silva I, Blackburn J, Gibbs BF, Yasinska IM, Garrett MD, Tonevitsky AG, Ushkaryov YA (2016). Expression of functional neuronal receptor latrophilin 1 in human acute myeloid leukaemia cells. *Oncotarget* 7(29): 45575-45583.

Sweeney NT, Li W, Gao FB (2002). Genetic manipulation of single neurons in vivo reveals specific roles of flamingo in neuronal morphogenesis. *Developmental Biology* 247(1): 76-88.

Thornton JM (1992). Lessons from analyzing protein structures. *Current Opinion in Structural Biology* 2: 888-894.

Towner RA, Jensen RL, Colman H, Vaillant B, Smith N, Casteel R, Saunders D, Gillespie DL, Silasi-Mansat R, Lupu F, Giles CB, Wren JD (2013). ELTD1, a potential new biomarker for gliomas. *Neurosurgery* 72(1): 77-90; discussion 91.

Trudel M, Yao Q, Qian F (2016). The Role of G-Protein-Coupled Receptor Proteolysis Site Cleavage of Polycystin-1 in Renal Physiology and Polycystic Kidney Disease. *Cells* 5(1).

Truman JW (1990). Metamorphosis of the central nervous system of *Drosophila*. *Journal of Neurobiology* 21(7): 1072-1084.

Tymiak AA, Norman JA, Bolgar M, DiDonato GC, Lee H, Parker WL, Lo LC, Berova N, Nakanishi K, Haber E, et al. (1993). Physicochemical characterization of a ouabain isomer isolated from bovine hypothalamus. *Proc Natl Acad Sci U S A* 90(17): 8189-8193.

Ushkaryov YA, Petrenko AG, Geppert M, Südhof TC (1992). Neurexins: synaptic cell surface proteins related to the alpha-latrotoxin receptor and laminin. *Science* 257(5066): 50-56.

Vakonakis I, Langenhan T, Prömel S, Russ A, Campbell ID (2008). Solution structure and sugar-binding mechanism of mouse latrophilin-1 RBL: a 7TM receptor-attached lectin-like domain. *Structure* 16(6): 944-953.

van der Voet M, Harich B, Franke B, Schenck A (2016). ADHD-associated dopamine transporter, latrophilin and neurofibromin share a dopamine-related locomotor signature in *Drosophila*. *Molecular Psychiatry* 21(4): 565-573.

Varki A (2017). Biological roles of glycans. *Glycobiology* 27(1): 3-49.

Varki A, Gagneux P. (2015). Biological Functions of Glycans. In rd, A. Varki, R. D. Cummings, J. D. Esko, P. Stanley, G. W. Hart, M. Aebi, A. G. Darvill, T. Kinoshita, N. H. Packer, J. H. Prestegard, R. L. Schnaar, & P. H. Seeberger (Eds.), *Essentials of Glycobiology* (pp. 77-88). Cold Spring Harbor (NY).

Volynski KE, Silva JP, Lelianova VG, Atiqur Rahman M, Hopkins C, Ushkaryov YA (2004). Latrophilin fragments behave as independent proteins that associate and signal on binding of LTX(N4C). *EMBO Journal* 23(22): 4423-4433.

Vu TK, Hung DT, Wheaton VI, Coughlin SR (1991a). Molecular cloning of a functional thrombin receptor reveals a novel proteolytic mechanism of receptor activation. *Cell* 64(6): 1057-1068.

Vu TK, Wheaton VI, Hung DT, Charo I, Coughlin SR (1991b). Domains specifying thrombin-receptor interaction. *Nature* 353(6345): 674-677.

Vysokov NV, Silva JP, Lelianova VG, Ho C, Djamgoz MB, Tonevitsky AG, Ushkaryov YA (2016). The Mechanism of Regulated Release of Lasso/Teneurin-2. *Front Mol Neurosci* 9: 59.

Waller-Evans H, Prömel S, Langenhan T, Dixon J, Zahn D, Colledge WH, Doran J, Carlton MB, Davies B, Aparicio SA, Grosse J, Russ AP (2010). The orphan adhesion-GPCR GPR126 is required for embryonic development in the mouse. *PLoS One* 5(11): e14047.

Ward Y, Lake R, Yin JJ, Heger CD, Raffeld M, Goldsmith PK, Merino M, Kelly K (2011). LPA receptor heterodimerizes with CD97 to amplify LPA-initiated RHO-dependent signaling and invasion in prostate cancer cells. *Cancer Research* 71(23): 7301-7311.

Wei W, Hackmann K, Xu H, Germino G, Qian F (2007). Characterization of cis-autoproteolysis of polycystin-1, the product of human polycystic kidney disease 1 gene. *Journal of Biological Chemistry* 282(30): 21729-21737.

Weston MD, Luijendijk MW, Humphrey KD, Möller C, Kimberling WJ (2004). Mutations in the VLGR1 gene implicate G-protein signaling in the pathogenesis of Usher syndrome type II. *American Journal of Human Genetics* 74(2): 357-366.

Wilde C, Fischer L, Lede V, Kirchberger J, Rothmund S, Schöneberg T, Liebscher I (2016). The constitutive activity of the adhesion GPCR GPR114/ADGRG5 is mediated by its tethered agonist. *FASEB Journal* 30(2): 666-673.

Winkler J, Prömel S (2016). The adhesion GPCR latrophilin - a novel signaling cascade in oriented cell division and anterior-posterior polarity. *Worm* 5(2): e1170274.

Wolpert L, Tickle C (2011). Principles of Development. Oxford University Press.

Wreschner DH, McGuckin MA, Williams SJ, Baruch A, Yoeli M, Ziv R, Okun L, Zaretsky J, Smorodinsky N, Keydar I, Neophytou P, Stacey M, Lin HH, Gordon S (2002). Generation of ligand-receptor alliances by "SEA" module-mediated cleavage of membrane-associated mucin proteins. *Protein Science* 11(3): 698-706.

Wyatt PJ (1993). Light scattering and the absolute characterization of macromolecules. *Analytica Chimica Acta* 272(1): 1-40.

Xu L, Begum S, Barry M, Crowley D, Yang L, Bronson RT, Hynes RO (2010). GPR56 plays varying roles in endogenous cancer progression. *Clinical & Experimental Metastasis* 27(4): 241-249.

Yan Z, Zhang W, He Y, Gorczyca D, Xiang Y, Cheng LE, Meltzer S, Jan LY, Jan YN (2013). Drosophila NOMPC is a mechanotransduction channel subunit for gentle-touch sensation. *Nature* 493(7431): 221-225.

Yang L, Chen G, Mohanty S, Scott G, Fazal F, Rahman A, Begum S, Hynes RO, Xu L (2011). GPR56 Regulates VEGF production and angiogenesis during melanoma progression. *Cancer Research* 71(16): 5558-5568.

Yu S, Hackmann K, Gao J, He X, Piontek K, Garcia-Gonzalez MA, Menezes LF, Xu H, Germino GG, Zuo J, Qian F (2007). Essential role of cleavage of Polycystin-1 at G protein-coupled receptor proteolytic site for kidney tubular structure. *Proc Natl Acad Sci U S A* 104(47): 18688-18693.

Zhang W, Cheng LE, Kittelmann M, Li J, Petkovic M, Cheng T, Jin P, Guo Z, Gopfert MC, Jan LY, Jan YN (2015). Ankyrin Repeats Convey Force to Gate the NOMPC Mechanotransduction Channel. *Cell* 162(6): 1391-1403.

Ziegler J, Pody R, Coutinho de Souza P, Evans B, Saunders D, Smith N, Mallory S, Njoku C, Dong Y, Chen H, Dong J, Lerner M, Mian O, Tummala S, Battiste J, Fung KM, Wren JD, Towner RA (2017). ELTD1, an effective anti-angiogenic target for gliomas: preclinical assessment in mouse GL261 and human G55 xenograft glioma models. *Neuro Oncol* 19(2): 175-185.

8. Appendix

8.1 Abbreviations

7TM	Seven transmembrane
α -LTX	α -latrotoxin
A488	Alexa Fluor 488
ADHD	Attention deficit hyperactivity disorder
ADPKD	Autosomal dominant polycystic kidney disease
aGPCR	Adhesion G protein-coupled receptor
attB	Attachment site (bacterial)
attP	Attachment site (phagal)
BFPP	Bilateral frontoparietal polymicrogyria
BSA	Bovine serum albumin
cAMP	Cyclic adenosine monophosphate
CD	Circular dichroism
cDNA	Complementary DNA
CHO	Chordotonal organ
CIRL	Calcium-independent receptor of α -latrotoxin
CNS	Central nervous system
CTF	C-terminal fragment
Cy3	Cyanine Dye 3
Cy5	Cyanine Dye 5
<i>dCirl</i>	Drosophila calcium-independent receptor of α -latrotoxin (allele)
dCIRL	Drosophila calcium-independent receptor of α -latrotoxin (protein)
<i>dCirlp</i>	Drosophila calcium-independent receptor of α -latrotoxin promoter
dH ₂ O	Distilled water
DLG	Discs-large
DLS	Dynamic light scattering
DMEM	Dulbecco's Modified Eagle Medium
DNA	Deoxyribonucleic acid
DRI	Differential refractive index
ECD	Extracellular domain
ECM	Extracellular matrix
e.g.	Exempli gratia (for example)
Endo H	Endo- β -N-acetylglucosaminidase H
ER	Endoplasmic reticulum
FBS	Fetal bovine serum

FLRT	Fibronectin leucin-rich repeat transmembrane
FMI	Flamingo
GAIN	GPCR autoproteolysis inducing
gDNA	Genomic DNA
GFP	Green fluorescent protein
GPCR	G protein-coupled receptor
GPS	G protein-coupled receptor proteolytic site
HEK	Human embryonic kidney
HL-3	Hemolymph-like solution
HRM	Hormone receptor motif
HRP	Horseradish peroxidase
IAV	Inactive
ICD	Intracellular domain
IRH	Inter-RBL-HRM
kb	Kilo base pair
kDa	Kilo Dalton
KO	Knock-out
LPHN	Latrophilin
MALS	Multi-angle laser scattering
MMP	Matrix metalloproteinase
MOPS	3-(<i>N</i> -morpholino)-propane sulfonic acid
mRFP	Monomeric red fluorescent protein
MW	Molecular weight
NaCl	Sodium chloride
NGS	Normal goat serum
nls	Nuclear localization sequence
NMJ	Neuromuscular junction
NOMPC	No mechanoreceptor potential C
ns	Non-significant
NTF	N-terminal fragment
OA	Ovalbumin
OLF	Olfactomedin
PAGE	Polyacrylamide gel electrophoresis
PAR	Protease-activated receptor
PBS	Phosphate buffered saline
PCR	Polymerase chain reaction
PEI	Polyethyleneimine
PFA	Paraformaldehyde

PKD	Polycystic kidney disease
PNGase F	Peptide N-glycosidase F
PNS	Peripheral nervous system
RBL	Rhamnose-binding lectin
R_h	Hydrodynamic radius
RIPA	Radio immunoprecipitation assay
rpm	Rounds per minute
SDS	Sodium dodecyl sulfate
SEA	Sea urchin sperm protein, enterokinase, and agrin
SEC	Size exclusion chromatography
SEM	Standard error of the mean
SIM	Structured illumination microscopy
TRP	Transient receptor potential
TSA	Touch sensitivity assay
UAS	Upstream activating sequence
UV	Ultraviolet
VLGR-1	Very large G protein-coupled receptor 1
VNC	Ventral nerve cord
wt	Wildtype

8.2 List of Figures

Figure 1. Adhesion GPCR families	5
Figure 2. Molecular architecture of aGPCRs	6
Figure 3. Mechanism of the autoproteolytic reaction at the GPS	8
Figure 4. Latrophilin and its homologs	10
Figure 5. Crystal structure of vertebrate Latrophilin domains.....	12
Figure 6. dCIRL function in <i>Drosophila</i> chordotonal organs.....	16
Figure 7. <i>Drosophila</i> life cycle.....	17
Figure 8. Standard CD spectra	33
Figure 9. The <i>dCirl</i> cloning toolkit allows easier molecular modification	36
Figure 10. dCIRL ^{N-RFP/C-Flag} is marked with immunohistochemical tags.....	37
Figure 11. <i>dCirl</i> ^{N-RFP/C-Flag} is expressed in <i>Drosophila</i>	38
Figure 12. The locomotion phenotype is rescued in <i>dCirl</i> ^{N-RFP/C-Flag} larvae	39
Figure 13. <i>dCirl</i> ^{N-RFP/C-Flag} larvae exhibit normal sensitivity toward gentle touch.....	40
Figure 14. <i>dCirl</i> is expressed throughout the larval ventral nerve cord	41
Figure 15. <i>dCirl</i> is expressed in neuromuscular junctions	42
Figure 16. dCIRL localizes to ciliary and dendritic compartments of chordotonal neurons.....	43
Figure 17. The expression profile of <i>dCirl</i> is exclusively neuronal	45
Figure 18. dCIRL ^{H>A} and dCIRL ^{T>A} contain a mutated GPS	47
Figure 19. GPS autoproteolysis is disabled in H>A and T>A dCIRL mutants	49
Figure 20. dCIRL autoproteolysis is dispensable for larval locomotion	50
Figure 21. <i>dCirl</i> ^{T>A} shows impaired sensitivity toward gentle touch	51
Figure 22. <i>dCirl</i> expression in the VNC is unaffected by the loss of GPS cleavage	52
Figure 23. dCIRL trafficking in CHO neurons does not rely on intact GPS autoproteolysis.....	53
Figure 24. The IRH region is part of dCIRL's NTF	55
Figure 25. dCIRL-IRH is heavily glycosylated.....	56
Figure 26. The extent of glycosylation of the IRH is inconstant	58
Figure 27. dCIRL-IRH follows the random coil model	59
Figure 28. The IRH exhibits a large dimension	60
Figure 29. dCIRL-IRH is a large and elongated region in the receptor's NTF.....	61

8.3 Publications

Scholz N[#], Guan C[#], **Nieberler M[#]**, Grotemeyer A[#], Maiellaro I, Gao S, Beck S, Pawlak M, Sauer M, Asan E, Rothmund S, Winkler J, Prömel S, Nagel G, Langenhan T^{*}, Kittel RJ^{*} (2017) Mechano-dependent signaling by Latrophilin/CIRL quenches cAMP in proprioceptive neurons. *eLife* 6: e28360.

Nieberler M, Kittel RJ, Petrenko AG, Lin H-H^{*}, Langenhan T^{*} (2016) Control of Adhesion GPCR Function Through Proteolytic Processing. *Handbook of Experimental Pharmacology* 234: 83-109.

[#] *equal contribution*

^{*} *correspondence*

8.4 Acknowledgements

First, I would like to thank Tobias Langenhan for an excellent introduction into the world of neurobiological research, which I couldn't have imagined better. I am highly grateful for his amazing supervision and support, but also for the freedom he granted me during my work and the numerous opportunities he offered me. Further gratitude goes to Robert Kittel for the secondary supervision and fruitful advice in the interpretation of my data.

Furthermore, I am thankful to Nicole Scholz for always finding the right words, scientifically and personally, for becoming a friend, and for her critical remarks regarding this thesis. Many thanks also to Nadine Ehmann, Jennifer Gehring, Chonglin Guan, Steffen Altrichter and all the other colleagues from the Department of Neurophysiology who contributed to this work.

For technical training and assistance, I would like to thank Uta Strobel and Claudia Wirth, but most of all Maria Oppmann, for her introduction into the field of molecular biology, for her reliability and for her open ear.

I am very grateful to Elena Seiradake for kindly hosting me in her laboratories in the Department of Biochemistry at the University of Oxford, for her supervision, and for her indispensable support with structural questions. Thanks also go to Maria Carrasquero and Verity Jackson for their assistance during my time in Oxford.

Further thanks to Markus Sauer and his colleagues, who gave me the opportunity to perform super-resolution microscopy in the Department of Biotechnology and Biophysics.

I wish to thank Anna-Leena Sirén for her expertise and for being part of my thesis committee.

Special gratitude has to be expressed to the Graduate School of Life Sciences and to the Elite Network of Bavaria for both financial and non-financial aid. I would like to thank all members and fellow students of the International Doctorate Program "Receptor Dynamics: Emerging Paradigms for Novel Drugs" for broadening my scientific horizons and for many unforgettable memories from our retreats abroad.

Probably most importantly, I need to thank Stephan and my parents for their constant love, their patience and support throughout this journey.

8.5 Curriculum vitae

Matthias Nieberler

born [REDACTED]

Education

- 12/2017 Approbation (License to Practice)
- 10/2010- Studies in Human Medicine, Julius-Maximilians-Universität Würzburg
11/2017 and Columbia University, New York City
- Practical Year:
- Internal Medicine: University Hospital, Würzburg
 - Surgery: Klinikum Würzburg Mitte (Location Juliusspital)
 - Psychiatry: University Hospital, Würzburg and New York State Psychiatric Institute, Columbia University, New York City
- 09/2001- Gymnasium Veitshöchheim
06/2010 Degree: Allgemeine Hochschulreife

Awards & Scholarships

- 03/2017 PROMOS Scholarship by the German Academic Exchange Service (Travel Scholarship for Practical Year in New York City)
- 10/2015 Best Poster Award, EUREKA! International Symposium of the Graduate School of Life Sciences, Würzburg
- 10/2014- Scholarship in the International Doctorate Program "Receptor
04/2018 Dynamics: Emerging Paradigms for Novel Drugs" by the Elite Network of Bavaria
- 12/2014- Medical Doctoral Research Scholarship by the Faculty for Medicine
04/2018 and the Graduate School of Life Sciences, University of Würzburg
- 06/2010 Award for Best Abitur Achievements, Gymnasium Veitshöchheim

Research Experience

- 08/2015 One-month Research Stay in the group of Assoc. Prof. Dr. Elena Seiradake at the Department of Biochemistry, University of Oxford
- 10/2013-06/2016 Experimental Research in the group of Prof. Dr. Tobias Langenhan, D.Phil. (Oxon) at the Department of Neurophysiology, Julius-Maximilians-Universität Würzburg
- 04/2012-06/2016 Student Assistant in the Institute for Anatomy and Cell Biology (-2013) and the Institute of Physiology, Julius-Maximilians-Universität Würzburg

Conference Contributions

- 06/2016 8th International Adhesion GPCR Workshop in Leipzig (Talk: "Impact of GPS autoproteolysis on the physiological function of the Adhesion GPCR CIRL/Latrophilin")
- 11/2015 Annual Meeting of the Israeli Society of Biochemistry and Molecular Biology in Tel Aviv (Poster: "Sub-cellular localisation of the Adhesion GPCR Latrophilin/CIRL in mechanosensory chordotonal organs in Drosophila")
- 10/2015 EUREKA! International Symposium of the Graduate School of Life Sciences in Würzburg (Poster: "Sub-cellular localisation of the Adhesion GPCR Latrophilin/CIRL in mechanosensory chordotonal organs in Drosophila")
- 03/2015 94th Annual Meeting of the German Physiological Society in Magdeburg (Poster: "The physiological role of autoproteolysis of the Adhesion GPCR CIRL/Latrophilin")

Würzburg, April 18th, 2018

8.6 Affidavit

I hereby confirm that my thesis entitled **The physiological role of autoproteolysis of the Adhesion GPCR Latrophilin/dCIRL** is the result of my own work. I did not receive any help or support from commercial consultants. All sources and / or materials applied are listed and specified in the thesis.

Furthermore, I confirm that this thesis has not yet been submitted as part of another examination process neither in identical nor in similar form.

Place, Date

Signature

Hiermit erkläre ich an Eides statt, die Dissertation **Die physiologische Bedeutung der Autoproteolyse des Adhäsions-GPCR Latrophilin/dCIRL** eigenständig, d.h. insbesondere selbstständig und ohne Hilfe eines kommerziellen Promotionsberaters, angefertigt und keine anderen als die von mir angegebenen Quellen und Hilfsmittel verwendet zu haben.

Ich erkläre außerdem, dass die Dissertation weder in gleicher noch in ähnlicher Form bereits in einem anderen Prüfungsverfahren vorgelegen hat.

Ort, Datum

Unterschrift